# "CFD ANALYSIS OF INCLINED JET IMPINGEMENT MICRO-CHANNEL HEAT SINK USING NANOFLUIDS"

## MAJOR PROJECT-II

*In partial fulfillment of the requirement of the degree of*

**MASTERS OF TECHNOLOGY**
**IN**
**THERMAL ENGINEERING**


Submitted by:
**PRAKASH SINGH**
**(Roll No. : 2K17/THE/08)**

Under the guidance of
**Dr. M. ZUNAID**
**Asst. Professor**




**DEPARTMENT OF MECHANICAL ENGINEERING**
**DELHI TECHNOLOGICAL UNIVERSITY**
(Formerly Delhi College of Engineering)
Bawana Road, Delhi-110042


**(2017-2019)**

# CANDIDATE'S DECLARATION

I, Prakash Singh, 2K17/THE/08 student of M.Tech (Thermal Engineering), hereby declare that the project Dissertation title "CFD analysis of inclined jet impingement micro-channel heat sink using nanofluids" which is submitted by me to the Department of Mechanical Engineering, Delhi Technological University, Delhi in partial fulfillment of the requirement for the award of the degree of Master of Technology, is original and not copied from any source without proper citation. This work has not previously formed the basis for the award of any Degree, Diploma Associateship, Fellowship or other similar title or recognition.

Place: Delhi **PRAKASH SINGH**

Date:

# CERTIFICATE

**DELHI TECHNOLOGICAL UNIVERSITY**

(Formerly DELHI COLLEGE OF ENGINEERING)

Date:-_____

This is to certify that report entitled **"CFD analysis of inclined jet impingement micro-channel heat sink using nanofluids"** by **MR. PRAKASH SINGH** is the requirement of the partial fulfillment for the award of Degree of **Master of Technology (M.Tech)** in **Thermal Engineering** at **Delhi Technological University, New Delhi.** This work was completed under my supervision and guidance. He has completed his work with utmost sincerity and diligence.

**Dr. M. ZUNAID**

**Asst. Professor**

**Department of Mechanical Engineering**

**DELHI TECHNOLOGICAL UNIVERSITY, DELHI**

# ACKNOWLEDGEMENT

To achieve success in any work, guidance plays an important role. It makes us put right amount of energy in the right direction and at right time to obtain the desired result. Express my sincere gratitude to my guide, **Dr. M. ZUNAID,** Asst. Professor, Mechanical Engineering Department for giving valuable guidance during the course of this work, for his ever encouraging and timely moral support. His enormous knowledge always helped me unconditionally to solve various problems.

I am greatly thankful to **Dr. VIPIN**, Professor and Head, Mechanical Engineering Department, Delhi Technological University, for his encouragement and inspiration for execution of this work. I express my feelings of thanks to the entire faculty and staff, Department of Mechanical Engineering, Delhi Technological University for their help, inspiration and moral support, which went a long way in the successful completion of my report work.

**PRAKASH SINGH**

**(2K17/THE/08)**

# ABSTRACT

In this study, the inclined jet impingement micro-channel heat sink is used for electronic cooling applications. This study focuses on analysis of 3D micro-channel heat sink. Different types of nanofluids were used for the study. The fluid flow and heat transfer characteristics has been simulated using computational fluid dynamics in rectangular micro-jet impingement. The bulk mean temperature of nanofluid at the outlet and the average interface temperature have been analyzed. The geometry of the micro-jet impingement heat sink was constructed using SOLID WORKS design software and the simulation was performed on ANSYS FLUENT solver.

In the present study, focus is put on increasing the heat transfer using the nanofluid. The jets used were placed at an inclination of 45 degree from the top surface of the impingement heat sink. The study is simulated using 6, 10, 14, 18 jets with diameters i.e. 0.1 mm. Copper was used as the solid material and nanofluid(water as base fluid) was used as a cooling fluid (working fluid). The results obtained were compared with the results of base fluid. The results showed that 1% $TiO_2$ in water gave maximum bulk mean temperature at outlet which denoted that it had the maximum temperature change.

# CONTENT

# LIST OF TABLES

# LIST OF FIGURES

# NOMENCLATURE

| | |
|---|---|
| $A_{cs}$ | Base area, $mm^2$ |
| $A_n$ | Area of nozzle, $mm^2$ |
| $C_p$ | Specific Heat, J/kg-K |
| $(C_p)_f$ | Specific Heat of fluid, J/kg-K |
| $(C_p)_{nf}$ | Specific Heat of nanofluid, J/kg-K |
| $(C_p)_f$ | Specific Heat of fluid, J/kg-K |
| $(C_p)_s$ | Specific Heat of nanoparticle, J/kg-K |
| $D_h$ | Hydraulic diameter, mm |
| $d_n$ | Nozzle diameter, mm |
| g | Acceleration due to gravity, $m/s^2$ |
| $H_c$ | Height of the Channel, mm |
| k | Thermal conductivity, W/m-K |
| $k_f$ | Thermal conductivity of fluid, W/m-K |
| $k_{nf}$ | Thermal conductivity of nanofluid, W/m-K |
| $k_s$ | Thermal conductivity of solid, W/m-K |
| $l_x$ | Length of the heat sink, mm |
| $l_y$ | Width of the heat sink, mm |
| $l_n$ | Vertical height of the micro-jet nozzle, mm |
| $n_x$ | Number of jets |
| p | Pressure in the fluid, Pa |
| q | Heat flux, $W/m^2$ |
| $\dot{q}$ | Heat generated per unit volume, $W/m^3$ |
| $S_n$ | Inter-Jet spacing, mm |
| t | Time, s |
| $t_s$ | Thickness of solid substrate, mm |

| | |
|---|---|
| $T_{avg}$ | Average temperature of fluid-solid interface, K |
| $T_f$ | Temperature of the fluid, K |
| $T_o$ | Bulk mean temperature at outlet, K |
| $T_s$ | Temperature of solid, K |
| u | Velocity of fluid in x-direction, m/s |
| v | Velocity of fluid in y-direction, m/s |
| w | Velocity of fluid in z-direction, m/s |
| Re | Reynolds number |
| $\mu$ | Dynamic viscosity, Pa-s |
| $\mu_f$ | Dynamic viscosity of fluid, Pa-s |
| $\mu_{nf}$ | Dynamic viscosity of nanofluid, Pa-s |
| $\chi$ | % Volume fraction |
| $\rho$ | Density of fluid, kg/ $m^3$ |
| $\rho_f$ | Density of fluid, kg/ $m^3$ |
| $\rho_{nf}$ | Density of nanofluid, kg/ $m^3$ |
| $\rho_s$ | Density of nanoparticle, kg/ $m^3$ |
| x,y,z Cartesian coordinates | |

# CHAPTER 1

# INTRODUCTION

## 1.1 General

Computational fluid dynamics (CFD) is one the three methods to solve the fluid dynamics problems. The flow behavior of liquids and gases are given by partial differential equations. These equations represent the conservation of mass, energy and momentum. Computational fluid dynamics utilizes different schemes and discretization techniques to solve fluid flows problems. Computers with high processing power are being used to simulate situation that exists in reality. CFD is mostly based on approximate solution of Navier-Stokes equation. Navier-Stokes equation is derived by applying conservation of momentum to fluid motion. The assumptions involved in above equation, the stress in the fluid is the sum of a pressure term and a diffusing viscous term. No one till date has given exact solution to Navier-Stokes equation. These equations when solved give correlation between the velocity, pressure, temperature, and density of a moving fluid.

When the processing power of computers was not good enough to solve large problems, analytical and experimental methods were used to solve fluid dynamics problems.. Analytical methods were used to solve the cases of one-dimensional, 1D and 2D geometry, 1D flow, and steady flow. However, experimental methods were quite expensive. It demanded a lot of resources such as data monitoring. Advent of supercomputers made life easier because it decreased the time of computing and solve complex problems in less time. Today, with a small investment, good computer with high processing power can be bought to run complex problems. The results can be obtained quickly can connecting several computers in parallel.

CFD is more economical than experiments. The problems and experiments that were difficult to perform because of limited resources are now possible. Introduction of modern computer technology has increased the popularity of CFD because solving of fluid dynamics equations has become easy and efficient.

There are three methods for solving fluid flow problem. Experiment comes first because it imitates the real phenomenon. Analytical method comes second because of different

assumptions involved during the solution of problems. CFD is last because it involves numerical, modeling, user, rounding off, machine errors, and application uncertainties. CFD analyst has to fully understand the logic of the problem and correctly interpret the results.

Now, in the present day main focus is on High-Performance Computing (HPC), with the help of HPC complex simulations (flow with high mach no.) are possible. It would require extreme conditions for a wind tunnel to imitate extreme environment. For high Mach number flow, CFD is the only viable tool to imitate the flow behavior.

## 1.2 Applications of CFD

### 1.2.1 Aerospace

CFD is now days used in many aerospace applications such as predicting component performance, optimizing and modifying the shape of aircraft, studying uncommon situation like aircraft stall, turbulence etc.

### 1.2.2 Automotive

CFD is used in automotive to model and optimize the car's aerodynamics thus reducing its drag. CFD also helps in proper optimization of the down force. It is used in engine so as to decrease knocking tendency, by properly simulating the combustion process against different engine parameters. It is also used in other fields like chassis design, auxiliary systems, engine components, etc.

### 1.2.3 Biomedical

CFD is used to design and simulate the blood flow in the heart vessels, inhalers etc. The blood flow analysis consists of circulation of blood in coronary artery and heart valves. In nasal airflow analysis, airflow takes place in human nose. CFD plays a major role in decision making, it provides the guidance and direction to provide medical alterations if needed.

### 1.2.4 Chemical Engineering

Applications of CFD in the field of chemical engineering are vast and surplus such as petrochemicals, pollution control, fertilizers, food processing, waste treatment recycle, etc.

### 1.2.5 Power Generation

In the field of power sector CFD finds applications in the analysis of economizer, super-heaters, pulverized coal combustion, low $NO_x$ burner design and in other areas so as to improve the performance of the plant.

### 1.2.6 Electronic Systems

Increase in demand for smaller, reliable and more powerful electronic equipment has lead to the use of CFD. It is used to simulate the heat transfer via conduction, convection and it also used to find out area of maximum temperature so as to overcome complex thermal problems related to their cooling.

## 1.3 Steps

- Divide the fluid volume (surface) into manageable chunks (gridding)
- The governing equations to be simplified at the required condition
- Set up the boundary conditions
- Initialize of grid values
- Simplify the equation through the step grid at the required set point.

## 1.4 Advantages

1. Cost reduction:
    - Use of physical experiments and tests to get data is expensive.
    - Costs of CFD simulation is less compared to experiments and is likely to decrease as processing power increases.
2. Quick design variations:
    - CFD simulations can be executed in a short spell.
    - Various engineering data can be introduced as early as in the designing.
3. Enables to simulate different conditions:
    - Various fluid flow and heat transfer processes can be easily simulated but cannot be easily tested.
    - CFD has the ability to theoretically simulate any physical condition.
    - CFD allows great control over the simulation of different physical processes.

- CFD has the ability to isolate specific phenomena for study.

4. Complete information:
    - Experiments only permit data to be extracted from locations where sensors and gauges are placed but CFD allows us to put probe on any location and get data about that particular location.
    - CFD allows us to interpret performance of any location through a set of thermal and flow parameters.
5. It helps to simulate the multiphase, reacting flows, vortex shredding, turbulence and other difficulties problems.

## 1.5 Disadvantages

1. Errors may occur due to improper flow models or improper boundary conditions.
2. Interpolation errors may occur due to little computing values per cell.
3. Error may also occur due to simplified boundary conditions.
4. Large computation time for large models.
5. The costs may rise due to wrong consulting compared to experiments.
6. The initial setup cost of computation is high.

## 1.6 CFD Code

CFD code uses a different category in various applications. This code can be applied in the generation tool with an associate CFD analysis.

•**CFD commercial code**: STARCD, FLUENT, CFX, CFDESIGN, FLUIDYN etc.

• **CFD research code:** COOLFLUID, CFDSHIP IOWA etc.

• **CFD public code:** WINPIPED, HYDRO etc**.**

## 1.7 CFD Process

The CFD process can be divided into three stages:

1. Pre-processing
2. Solving
3. Post-processing

Above stages are shown in Figure 1.1.

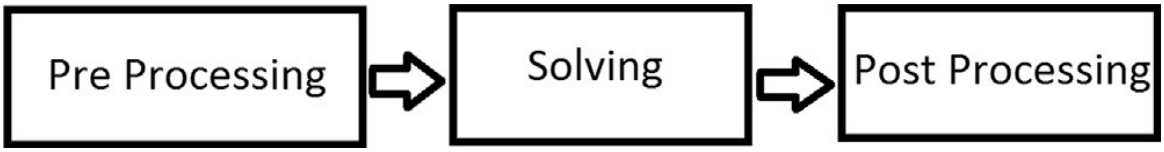


Figure 1.1 Computational fluid dynamics process

All the three stages are interdependent. It takes about 90% of effort in meshing (preprocessing) stage. The next stage (solving stage), the governing equations of flow is solved with the help of computer. If any error occurs in the meshing stage then it propagate to the solving stage, this error will produce wrong results because the governing equations are now solved for the wrong cells. The last stage after solving the governing equation is post-processing. Contours, plots, animation and different colorful pictures can be obtained. The results obtained after post-processing are used for product design, development. Results are validated by comparing it with the experimental data. In the absence of experimental data, the grid convergence study is used to judge the authenticity of the results. In this case, the mesh has to be refined three or four times. Every time after meshing it is solve again and compared with the previous results, until the solution has converged (never changing results).

In Post-processing, path lines, flow contours, vector plots, cylinders can be created which improves the way of displaying results. In unsteady flows, such as for direct numerical simulation (DNS) and large eddy simulation (LES) is also shown sometimes..

## 1.8 Numerical Discretization

There are several methods available for discretization. ANSYS FLUENT and ANSYS CFX both use FVM (Finite Volume Method). FVM has certain advantage over other methods. This scheme is robust. The other popular methods used are FDM and FEM.

### 1.8.1 Finite Difference Method

FDM is the simplest method of all. Initially, mathematicians had only derived simple formulas to calculate derivatives and then with the advance of time, methods improved and

CFD became more advanced. The foundation of FDM is derivative. The derivative of a function gives the slope of that function. A function of velocity 'u' in x-direction, the derivative of 'u' with respect to 'x' can be written as:

$$\frac{\partial u}{\partial x} = \frac{u_{i+1} - u_i}{\Delta x} \quad (1.1)$$

The subscripts 'i' and 'i + 1' are the points on which 'u' values are being calculated. Here, Δx is grid spacing. This method of calculating the first derivative is termed as forward difference method (FDM).

### 1.8.2 Finite Volume Method

The Finite volume method (FVM) is widely used because it has various advantages over FDM. The FVM can be used for any grid structure, i.e. clustered or non-clustered structured or unstructured etc. It is also used in the cases where there is discontinuity in the fluid flow.

In the FVM, the computational domain is divided into several number of control volume s. The values are calculated at cell centers. The values of fluxes at the cell interface are determined through interpolation using the values at the cell centers. An algebraic equation is obtained for each control volume, and thus a number of equations are then solved using numerical technique. The FVM and geometric volume definition are two different things.

The major disadvantage of using FVM method is that higher-order schemes are quite difficult to solve in three dimensions. It happens due to the approximations made i.e., interpolation between the cell centers and the interfaces and the integration of all surfaces.

## 1.9 Background Information

Decrease in the size of electronic systems has led to integration of more components in an electronic system. According to Moore's law (Moore 1965), "the number of transistors integrated on a chip doubles every 2 years". The number of integrated transistors on a chip has been increased from 10000 in 1967 to more than 2 billion in 2014. The direct consequences of Moore's law were increased performance and reduced size of a microprocessor. Due to decrease in the size of the electronics the power density have increased drastically. This led to increase in heat fluxes and thus needed better heat

dissipation system. Now, heat dissipation required in microelectronics has come to hundreds of $W/cm^2$. It will surely continue to rise in future. High heat flux in the microelectronic devices makes it difficult to cool. It is one of the major challenges regarding the dense packaging of the microelectronics devices. This problem has to be resolved in order to further decrease the size of microchips. Therefore, new technologies should be developed for better thermal management and to promote the miniaturization process.

Micro-channels have become quite important in scientific community and industry and have received a lot of attention form them. One of the pioneer works in this field was done by Tuckerman and Pease. They showed that micro-channels had very effective cooling potential. Thus, micro-channels can be used to increase the heat dissipation. The heat exchangers coupled with micro-channels have now become compact, lightweight and thermally efficient (due to high surface area to volume ratio). Microchips will work properly only if there is proper heat dissipation and the surface temperature of the microchip is within the permissible limits. Multiphase flows such as nanofluids or boiling heat transfer can maintain the required temperature of such systems. The latent heat associated with phase change has heat transferring capability. Sensible heat transfer option is used for cooling when heat capacity of the based fluid is high or there are some auxiliary devices attached to it. The use of nano-particles in the base fluid increases the effective thermal conductivity of the resulting nanofluid. It allows us to design a compact heat exchange device. Nanofluid removes more heat when compared to single phase base liquid used as a coolant.

Increasing the density of the microelectronics was one of the first motivations for micro-channel work. The application of micro-channels are not only limited to electronics. There are several areas of science and engineering that utilize micro-channels. Micro-channel heat exchangers can significantly decrease the refrigerant charge compared to conventional sized heat exchangers for the same heat transfer performance and effectiveness. It also helps to overcome space constraints and provides great design flexibility. Few other application areas of micro-channels are: micro fluids devices, chemical processing industry, fuel cells, bio applications etc.

Instead of all the advantages of the micro-channels, the understanding of the mechanics behind the fluid flow behavior and thermal transport mechanism is far from satisfactory. Therefore, the proper understanding of the micro-channels could only be achieved by conducting more studies focusing on the understanding of governing phenomena.

The science and practice of achieving approximate numerical solutions using a digital computer are known as Computational Mechanics. When this approach is applied in the field of problems concerned with thermal and fluid problems, it is generally termed as (CFD) Computational Fluid Dynamics. Thus, Computational fluid dynamics (CFD) is a branch of continuum mechanics which deals with fluid flow and heat transfer problems and its numerical simulation.

The Navier-Stokes equation is the basic fundamental of almost all CFD problems. The Euler equation is achieved by removing the viscous term from the Navier-Stokes equation. Euler equation is also the momentum conservation equation. The full potential of the equation can be obtained by eliminating the terms describing vorticity. Navier-Stokes equation is a non-linear partial differential equation and it is fundamental of any fluid flow problem. It has no exact solution. It can only be solved by approximate method. The equation is converted to algebraic form by FVM before it becomes solvable. In this process of solving the Navier-Stokes equation many errors are introduced. Two-dimensional (2D) methods were developed using flow over a cylinder by taking airfoil as reference selection. These calculations were the basis for solving modern CFD problems. The increase in processing power led to development of three-dimensional (3-D) methods. Los Alamos National Lab was first place to model fluid flow governed by the Navier-Stokes equation using computers. Francis H. Harlow, one of the pioneers of CFD led this group. They developed various types of numerical methods like Particle-in-cell method, Fluid-in-cell method, Vorticity stream function method, Marker-and-cell method to simulate transient two-dimensional fluid flows.

Today, different types of codes have been developed. They are being used in different field i.e. high-speed trains, racing yachts, submarines, helicopters, surface ship, and also in jet impingement and micro-channel cooling technology.

Nowadays to remove large amount heat and reduce high temperature in the channel flow, a hybrid technology of micro-channel and jet impingement cooling is field of research. Researchers are trying to harness the two cooling technologies. Jet impingement offers high thermal management. It also helps to reduce hot spots in electronic system. It offers more uniform temperature over the entire surface.

## 1.10 Objectives

The characteristics of fluid flows can be investigated by modelling single-phase fluid flow or multiphase flow. Different types of models are available to solve multiphase flow. The flow here has been assumed to be fully developed. Different parameter such as Reynolds number, substrate material, channel geometry and working fluid has an effect on heat transfer and flow behaviour and thus affecting the performance of jet impingement.

Optimum values of some of the important parameters have been used during the study, and further steps have also been taken to improve the model. Jet impingement has been proposed to achieve high temperature uniformity and manage hot spots.

The main objectives of the work are mentioned below:

- Prepare the jet impingement model by using Cad software.
- Measure fluid flow characteristics and heat transfer.
- Study effects of jet impingement on heat transfer and on the performance of cooling during fluid flow.
- To improve cooling characteristics apply the optimum characteristics during studies.

# CHAPTER 2

# LITERATURE REVIEW

In this chapter we take a look at the previous research paper that focused on micro-channel, jet impingement and nanofluid under different conditions. Heat transfer and fluid flow characteristics through jet impingement and micro-channel has been studied in these research papers. It contains several experiments and numerical modeling of electronic chips. Most of the papers in this study optimize the results obtained.

The performance of heat exchanger depends on heat flow parameters which uses various kinds of technologies such as jet impingement and micro-channel heat sink. We can review this work in the following three parts:

- Micro-channel
- Jet impingement
- Nanofluid in micro-channel

## 2.1 Experimental and numerical studies on the micro-channel heat sink

Temperature control is a critical factor in the design of electronic equipment because miniaturization of components in the electronic industries which causes hindrance in heat dissipation. Increase in demand for high system performance and reliability also intensifies the needs for better thermal management.

L.T. Yeh[3] reviewed different heat transfer technologies used in electronic equipment. He laid an emphasis on design of electronics equipment. Electronic equipments should have proper thermal design for proper heat dissipation. According to him no single design could be adopted universally. In this study, different ways of cooling the electronics equipments such as air cooling, liquid cooling, jet impingement, micro-channel cooling, heat pipe etc. were reviewed. The performance of the micro-channel using porous media was better than micro-channels, but the pressure drop in porous micro-channel was much large.

Chein & Chen [40] proposed a numerical study on micro-channel heat sink. They simulated for different inlet and outlet arrangements. The governing equations of heat transfer and fluid flow are solved using FVM approach. Results such as heat transfer,

pressure drop and temperature distribution obtained were different for different arrangements. They concluded that highest temperature occur at the edge of the micro-channel and lowest temperature at the plate occurs at the entry side.

Knight et al.[2] represented the multi-objective optimization technique, the prey-predator algorithm was applied to micro-channels to find optimum values of the heat sink parameters.. This scheme used for solving these equations displays the thermal resistance and pressure drop. The total pressure drop was calculated by estimating the power requirement to move the fluid inside the micro-channel. Pressure drop showed the hydraulic resistance of the system. They performed the simulation on MATLAB and obtained thermal resistance and power to be 0.134133 ohm and 2.79344 W.

B.W. & maha [4] presented that liquid jet impingement increases both heat and mass transfer. A thin hydrodynamic and thermal boundary layer in formed just beneath the liquid jet striking the surface. In wall jet or parallel flow zone the flow is forced to accelerate. The thickness of both the hydrodynamic and thermal boundary layers in the stagnation region is very less. Stagnation zone exists just under the jet. Heat and mass transfer coefficients are very high here. Liquid jet impingement has high heat transfer coefficient, thus it becomes great cooling option for high heat fluxes.

Peng et al. [6] presented an experimental investigation on micro-channels with different geometric configurations of hydraulic diameter of 0.133–0.367 mm. The experiment was performed on water as working fluid. This study was carried on both laminar and turbulent flows. It was clear from the results that geometric configuration of the micro-channels had significant impact on heat transfer and flow characteristics. It was also noted that the laminar heat transfer was dependent upon the aspect ratio.

Mala et al.[7] described that complicated geometry resulted in complicated heat transfer equations, thus, making it difficult to solve. They implemented Computational Fluid Dynamics (CFD) models to study the thermal and hydraulic performance of micro-channel heat. They also found that the conventional form of Navier-Stokes equation is still valid in the micro-channels. They considered the flow through micro-channel as laminar.

Fedorov et al. [10] developed a three-dimensional (3D) model of micro-channel heat sink to investigate the conjugate heat transfer. They used an incompressible laminar Navier-Stokes equation to find the solution. At the inlet, they observed large temperature gradients and the wall temperature near the inlet was not uniform. Thus, they concluded that the thermal–properties are temperature dependent. It was also found that poiseuille flow assumptions were not always valid and thus proper care should be taken before use.

Ambatipudi et al.[11] developed a silicon based model for numerical analysis of conjugate heat transfer. Micro-channel used had channel height of 1 μm, channel width of 25 μm, and channel length of 25 mm. the effect of channel aspect ratio, Reynolds number on hydraulic and thermal performance were obtained by solving the governing equations. They found that nusselt number is large near the entrance region. It was high because of the developing boundary layer. They concluded that as the number channels and channel depth were increased so did the local nusselt number.

Qu et al. [12-13] developed a silicon based model for numerical analysis of 3-D heat transfer. Micro-channel used had channel height of 180 μm, channel width of 57 μm, had performed numerical investigations on rectangular micro-channel using water as base fluid. A code was developed using FDM and SIMPLE algorithm. It was used to solve the governing equations. There was good agreement between the numerical predictions and experimental data. Thus, they validated the use of conventional Navier–Stokes equations for micro-channels. They concluded that a linear approximation could be assumed for the temperature rise in the flow direction.

Toh et al.[14] investigated 3-D fluid flow distribution, heat transfer in micro-channel. It was done assuming the flow to be laminar and steady. They calculated thermal resistances and frictional losses and then compared them with experimental data. The friction factor and the thermal resistance as well as the thermal resistance drop predicted matched with the experimental data. The results also indicated that as the Reynolds number decreased so did the viscosity and thus, decreased the frictional losses.

Garimella et al.[15] reviewed papers on micro-channel. A number of numerical and experimental analysis were reported related to fluid flow and heat transfer. These analysis

were carried in mini and micro-channels and microtubes. It was reported that there was difference in fluid flow and heat transfer characteristics when compared with conventional channels. The paper also focused upon the factors that directly and indirectly affect the heat transfer. They concluded that phase change process would be much more effective way for heat dissipation and there was need for extensive investigation in that field.

Liu et al.[16-17] performed numerical analysis of convective heat transfer in micro-channel. The performance of micro-channels was quite similar to that of conventional channels. They performed analysis on rectangular micro-channels which showed that the conventional correlation was good for the laminar flow. This was true for 244 μm to 974 μm of hydraulic diameter. The thermal and hydrodynamic features of laminar Newtonian compressible flows in the range of hydraulic diameter from 15 μm to 401 μm could be predicted correctly by the conventional models. They compared the results with the data available in the open literature. The theoretical models included the one-dimensional (1D) models with following assumptions:- uniform heat flux, constant heat transfer coefficient, etc. These models were not compatible with the experiments.

Foli K et al.[19] presented the optimization of micro heat exchangers with the help of multi-objective evolutionary algorithms. The study showed that the thermal properties of the fluid in the micro-channel depended on fluid flow conditions and geometric parameters of micro-channel. Two approaches were defined to determine the geometric parameters of the micro-channels. First, combines the usage of multi-objective genetic algorithm in combination with Computational Fluid Dynamics. Second, involves Computational Fluid Dynamics (CFD) analysis with an analytical method of calculating the optimal geometric parameters of micro heat exchangers.

Husain et al.[22] presented numerical analysis and optimization technique for a rectangular micro-channel heat sink. It was made of silicon. The flow was considered as laminar and FVM was applied to solve the governing equations. The surrogate method was implemented to optimize the obtained result. Micro-channel depth and fin width were the variables used to construct surrogate. The different surrogates gave different results.

## 2.2 Experimental and numerical studies on jet impingement heat sink:

Recently, the challenges faced by decreasing the size of electronic circuits is heat-flux dissipation, it has encouraged researchers to develop new cooling techniques. The air cooling techniques have reached their limits, the liquid cooling through a micro-channel heat sink has provided brilliant solutions to high heat-flux at micro level.

Tuckerman et al.[1] were the first to examine liquid flow in micro-channel heat sinks. They experimented on three micro-channels with channel widths 50, 55 and 56 μm, and channel heights 287, 302 and 320 μm. Heat flux of 790 W/cm$^2$ was found to be removed by one of the heat sinks. The results showed that there existed non-uniform temperature distribution over the heated surface. It finally decreases the life of the electronic equipments. Jet impingement cooling could be used for high hot spots management in electronics. It also helps in providing uniform temperature distribution over the entire chip surface. They developed a new concept of micro-cooling for researchers.

Wu et al.[8] experimentally examined micro impinging jet heat transfer characteristics. They planted a MEMS sensor chip for better heat transfer measurements. This arrangement allowed 2-D surface temperature measurement. It was shown that higher cooling efficiency occurred at lower driving pressure. It was concluded that micro-jet impingement is more efficient than macro-jet impingement.

Lee et al.[9] presented analysis on micro-channels and jet impingement cooling. It was concluded that micro-channel with dimensions smaller than 70 mm × 70 mm is preferable for cooling by micro-channel heated transfer. A large target plate with jet impingement showed better cooling than micro-channel. A detailed comparative analysis of the two method are presented in this paper. If choice was to be made between the two then cooling as well as economic aspects had to be seen. .

Fabbri et al.[18] tested impinging jet arrays for electronics cooling. Jet cooling has high heat transfer rates. Ten different jet arrays were used with working fluid as water and FC40. The impinging water temperature was 23.1 $^0$C and the average surface temperature reported was 73.9 $^0$C.

Sung et al.[20] proposed a hybrid cooling scheme. It combined the cooling benefits of the micro-channel and jet impingement. They showed that there exists low temperature and small temperature gradients across the surface of slotted jet impingement in the micro-channels.

Luo et al.[21] performed an experimental and numerical analysis on the cooling systems attached to light emitting diodes (LEDs). In this study, 2 × 2 LED chip array of size 1 mm × 1 mm was embedded in a 15 mm × 15 mm substrate. It was reported that array reached a temperature of 72 $^0$C within 2 min and it kept rising. After the micro-channel cooling system was employed then the maximum temperature rise in the chip was 36.7 $^0$C. The environmental temperature was considered as 28 $^0$C. The numerical results obtained showed a flow rate of 3.2 mL/s, heat transfer coefficient of 5523 W/m$^2$-K and pressure drop of about 1368 Pa.

Michna et al.[24] investigated a single-phase water micro-jet impingement on a 80 m square heated surface. They investigated the pressure drop and average heat transfer coefficient. The numerical simulation was carried to find out heat transfer and pressure drop. The study revealed that there was higher pressure-loss than the available correlations for orifice tubes under Re ≤ 500. It was observed that heat transfer coefficients obtained were than that predicted by correlations. Heat transfer was significantly affected by Reynolds number, Prandtl number, and the area ratio (total area of jets divided by the surface area).

Paz et al. [26] carried out a numerical investigation of turbine blades cooled by multi-micro-jet impingement. It was found, as H/D ratio increased from 1.58 to 3, the overall heat transfer coefficient decreased.

Husain et al.[25,28-29] and Samad et al.[23] proposed optimization models for both micro-scale and conventional thermal fluid systems. A lot of literature is available on macro-scale air jet impingement cooling. A few reports are available on micro-scale multiple liquid-jet impingements. The literature about optimization techniques used in heat-flux management of electronics are also less. The flow is considered as laminar and the allowed flow-rates and pressure-drops are relatively small.

## 2.3 Nanofluid with micro-channel

Peterson et al.[30] conducted an experimental investigation to examine thermal conductivity. They examined the effect of temperature and volume fraction on thermal conductivity. Nanoparticles of copper oxide and aluminum oxide of size 29 and 36 nm were blended with distilled water. It was done in different volume fraction of 2, 4, 6 and 10% and this was calculated at a temperature ranging from 27.5 to 34.7 °C. The results indicated that the thermal conductivity of the suspensions was affected by the nanoparticle material, volume fraction and diameter. The nanofluid containing 6% of CuO nanoparticle in distilled water increased the thermal conductivity of the nanofluid by 1.52 times than that of pure distilled water. The nanofluid containing 10% of $Al_2O_3$ nanoparticle in distilled water increased the thermal conductivity of the nanofluid by 1.3 times than that of pure distilled water.

Kondaraju et al.[31] developed an Eulerian–Lagrangian based direct numerical simulations (DNS) model. A two-way coupling was done to investigate the effective thermal conductivity of nanofluids.. The model also took into account the various forces acting on the nanoparticles. Cu nanoparticle of size 100 nm with water as base fluid and $Al_2O_3$ nanoparticle of size 80 nm with water as base fluid were simulated at different volume fractions. The effective thermal conductivity of nanofluid was calculated. They concluded that the effective thermal conductivity of nanofluids depend on particle thermal conductivity and forces acting on nanoparticle.

Wie et al.[32] worked on a model to predict large enhancement of thermal conductivity of nanofluids, the study of Brownian motion, the mutual interaction of spherical nanoparticles. The model investigates the relationship between the enhanced thermal conductivity and nanoparticle size, volume fraction and temperature, nanolayer thickness, the interaction of adjacent nanoparticles.

Wen et al. [39] prepared an experimental system which consisted of flow loop, heating unit, cooling unit, measuring unit and a control unit. They used $Al_2O_3$ as nanoparticles and de-ionized water as base fluid. This study was performed in the laminar regime to check the effects of using nanofluids on convective heat transfer. They found out that it was beneficial

to use nanofluid as it increased the convective heat transfer rate. They further tried to explain the reason behind this increase in the heat transfer and gave two reasons. Enhancement of the effective thermal conductivity and particle migration which decreases the thickness of the thermal boundary layer thus increases the heat transfer.

Yang et al. [40] performed an experiment on convective heat transfer using graphite as nanoparticle. They measured convective heat transfer coefficient in a horizontal tube heat exchanger under laminar flow for different concentration of graphite nanoparticles dispersed in base fluid. The results obtained showed an increase in convective heat transfer coefficient but it was less than that predicted by correlations. They suggested that further investigation was required to develop proper heat transfer correlation.

## 2.4 Summarizing remarks

As these case studies illustrate, There are a lot of different numerical solutions to the Navier-Stokes equations, they have been implemented successfully on the simple micro-channels as well as in jet impingement models with different thermo physical properties and designing parameters like Reynolds number, jet diameter, mass flow rate, Number of jets and type of cooling fluid. The recent challenges caused due to decrease in the size of ultra-large scale integrated (ULSI) circuits of power electronics always needs improvement in heat dissipation. Hence, the current thesis work is directed towards addressing improvement in heat transfer by performing a thermal and fluid flow analysis in an inclined jet impingement model with different nanofluids.

# CHAPTER 3

# METHODOLOGY/MODEL DESCRIPTION

## 3.1 Model Description

The analysis was performed on the fluid flow domain and solid domain. Heat flux was taken through the bottom of the solid substrate. In order to provide a cooling effect, the micro-jet impingement was used. Water and nanofluids were taken as a cooling fluid where mass flow rate (0.000122 kg/s) and heat flux (50000 $W/m^2$) were kept constant. The nozzle is inclined at $45^0$ from the base of upper surface of the fluid. The fluid domain has working or cooling fluid and the solid domain is made of copper. The micro-channel dimensions are taken as 12 mm × 12 mm × 0.8 mm ($l_x$ = 12 mm, $l_y$ = 12 mm, $t_s$ = 0.8 mm). The depth of the fluid domain which interacts with solid material is 0.3 mm.

## 3.2 Numerical Scheme

These equations were discovered by the Claude Navier and George Stokes. The basic assumption that are taken into account is fluid particle deforms under shear stress. The equations of motion of the fluid particle are given by:

1. Conservation of mass
2. Conservation of momentum
3. Conservation of energy

### 3.2.1 Conservation of mass

The mass conservation equation is given in equation 3.1. It is also known as the continuity equation. It is given by:

$$\frac{\partial \rho}{\partial t} + \nabla \cdot (\rho \vec{U}) = 0 \tag{3.1}$$

Where,

$\vec{U} = [u, v, w]$

### 3.2.2 Conservation of momentum

The conservation of momentum is given in equation 3.2, 3.3, 3.4. It is based on Newton's second law. Momentum conservation equations constitute of pressure, body and viscous forces. These equations are:

In the x-direction,

$$\frac{\partial(\rho u)}{\partial t}+\frac{u\partial(\rho u)}{\partial x}+\frac{v\partial(\rho u)}{\partial y}+\frac{w\partial(\rho u)}{\partial z}=\frac{-\partial p}{\partial x}+\mu\nabla^{2}(u)+\rho g_{x} \quad (3.2)$$

In the y-direction,

$$\frac{\partial(\rho v)}{\partial t}+\frac{u\partial(\rho v)}{\partial x}+\frac{v\partial(\rho v)}{\partial y}+\frac{w\partial(\rho v)}{\partial z}=\frac{-\partial p}{\partial y}+\mu\nabla^{2}(v)+\rho g_{y} \quad (3.3)$$

In the z-direction,

$$\frac{\partial(\rho w)}{\partial t}+\frac{u\partial(\rho w)}{\partial x}+\frac{v\partial(\rho w)}{\partial y}+\frac{w\partial(\rho w)}{\partial z}=\frac{-\partial p}{\partial z}+\mu\nabla^{2}(w)+\rho g_{z} \quad (3.4)$$

### 3.2.3 Conservation of energy

It is also called the First Law of Thermodynamics. The energy equation is based on the principle of conservation of energy. It can be written as:

$$\frac{\partial(\rho E)}{\partial t}=\rho\dot{q}+\frac{\partial}{\partial x}\left(k\frac{\partial T}{\partial x}\right)+\frac{\partial}{\partial y}\left(k\frac{\partial T}{\partial y}\right)+\frac{\partial}{\partial z}\left(\frac{\partial T}{\partial z}\right) \quad (3.5)$$

In CFD the above non-linear partial differential equations are discretized and then solved algebraically. The different approaches used to solve these equations are finite difference method (FDM), finite volume method (FVM), and finite element method (FEM). These equations can be modified according to the requirements. It can be done by assuming flow to be inviscid, incompressible, or compressible and steady or unsteady as per requirement. The viscous terms are omitted from the Navier-Stokes equation for an inviscid flow field. The equation left is called Euler equations.

## 3.3 Nanofluid Properties

There are various properties which are involved in calculating the heat transfer rate of the nanofluid. They are heat capacity, viscosity, thermal conductivity and thermal expansion coefficient. Density of the nanofluid can be expressed as:

$$_{nf}=(1-\chi)\times\square_{f}+\chi\times\square_{s} \quad (3.6)$$

Xuan and Roetzel [35] proposed the basis of single phase model. The solid particles in nanofluid are less than 100 nm and can be treated as fluid while solving the governing equations in CFD, it makes the flow either single phase or multiphase. In multiphase still the basic assumption made is that the solid particles are treated as fluid. These particles thus can be approximated as fluid. There are different modeling approaches present in CFD FLUENT such as euler-granular model, dense discrete phase model, discrete element

method. A particular method is chosen depending on the volume concentration of particle in the fluid. There exists no-slip condition between the dispersed micro particles and the base fluid. There is thermal equilibrium between the nanoparticles and base fluid. The nanofluid is considered as a single phase fluid [35,36]. The governing equations of energy and motion for the base fluid can also be used with nanofluids. However, one should keep in mind that while applying the governing equations to the nanofluids, one needs to use the properties corresponding to the nanofluids. There are various properties which are involved in calculating the heat transfer rate of the nanofluid. They are heat capacity, viscosity, thermal conductivity and thermal expansion coefficient. The properties mentioned above can be expressed as properties of nanoparticles and base fluid. The models which are available in literature [37,38] are used to calculate heat capacity $(\rho C_p)_{nf}$ of the nanofluid.

It can be expressed [37] as:

$$(C_p)_{nf} = (1-\chi)\times(C_p)_f + \chi\times(C_p)_s \tag{3.7}$$

Viscosity of the nanofluid with volume fraction ($\chi$<0.05) can be expressed as:

$$\mu_{nf} = \frac{\mu_f}{(1-\chi)^{2.5}} \tag{3.8}$$

The thermal conductivity of the nanofluid is a function of thermal conductivity of nanoparticle material, volume fraction, surface area, shape of the nanoparticles suspended in the liquid, distribution of the dispersed particles and the thermal conductivity of base fluid., Hamilton and Crosser [33] developed the model which has ratio of thermal conductivity of two phases.

It is expressed as:

$$\frac{k_{nf}}{k_f} = \frac{k_s + (n-1)\times k_f - (n-1)\times\chi\times(k_f - k_s)}{k_s + (n-1)\times k_f + \chi\times(k_f - k_s)} \tag{3.9}$$

Here ‘n’ is empirical shape factor defined in the terms of sphericity as:

$$n = \frac{3}{\varphi}$$

(For spherical particles $\varphi = 1$)

## 3.4 Assumptions

Following assumption are made due to the complexity of 3d heat sink:

1. Fully developed flow through the micro-channel and steady-state condition.
2. Water uniformly flows in the fluid domain.
3. No slip condition in domain and adiabatic condition.
4. Temperature is assumed to be constant on a solid domain.
5. Nanofluid is assumed as a volume fraction of water.
6. Thermo-physical properties are not the function of temperature.
7. All the properties are taken at 300K.
8. The molecular weight of the nanofluid is assumed to be equal to the fluid.

## 3.5 Description of problem

A copper-based substrate with 6 micro-jets impingement has been used, as shown in figure 3.1. The micro-jet nozzles were designed to be placed on the cover plate. The cover plate is also made of copper which acts as support for nozzles and creates a boundary for fluid domain. Fluid domain was created which consist of only fluid and acts as a control volume for fluid flow analysis. The fluid from micro-jets strikes the heated solid surface and thus turns the flow in radial direction. It removes heat while flowing towards outlet. The dimensions of the jet impingement heat sink is shown in Fig. 3.1 is 12mm×12 mm×0.8mm. The total thickness of the heat sink plate is 800 μm, 6 micro-jets are designed on cover plate. The parameters that affect the performance of the jet impingement heat sink are:

- The thickness of the solid substrate base ($t_s$)
- Micro-jet nozzle diameter ($d_n$)
- The vertical height of the micro-jet nozzle ($l_n$)
- Interjet spacing ($S_n$)
- Height of the fluid domain ($H_c$)

The geometric parameters, $l_n$, $t_s$, $d_n$, $S_n$ are kept constant throughout the analysis.

## 3.6 Geometry of the micro-jet impingement heat sink

In this computational fluid dynamics problem, the model of the heat sink was created using SOLIDWORKS and then it was imported to ANSYS FLUENT for further meshing and CFD simulations. First, the heat sink was made in SOLIDWORKS as per the dimensions given in table and was named as solid part while fluid channel was created of the same

dimensions as of the rectangular slot along the length and the width of heat sink for proper mating but channel height was different and it was given the name of fluid.

The mesh was generated using Curvature on option. The mesh was created as a structured mesh and for checking the solutions the mesh was made finer and the solutions obtained were mesh independent. After meshing, names were given to different surface according to their functions. Named selections are considered as boundary conditions.

## Problem: Inclined 6 jet model

**Table 3.1: Dimensions of 6 micro-jet heat sink**

| $A_{cs}$ ($mm^2$) | $H_c$ (mm) | $t_s$ (mm) | $d_n$ (mm) | $l_n$ (mm) | $S_n$ (mm) |
|---|---|---|---|---|---|
| 12 X 12 | 0.3 | 0.8 | 0.1 | 0.5 | 3 |

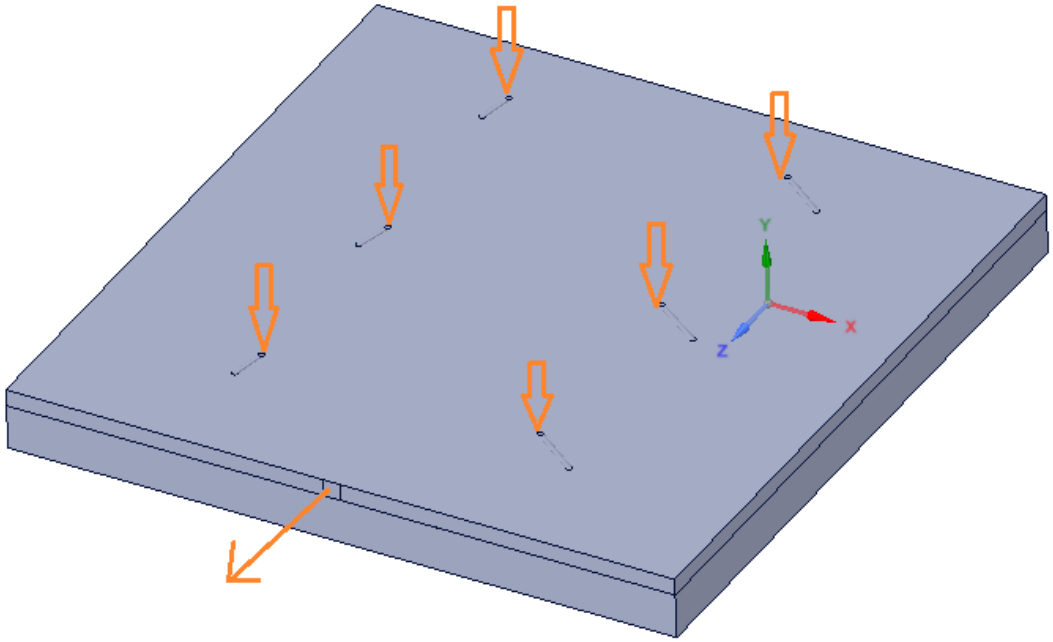


Figure 3.1: Geometry of the 6 micro-jet impingement heat sink

## Problem: Inclined 10 jet model

**Table 3.2: Dimensions of 10 micro-jet heat sink**

| $A_{cs}$ ($mm^2$) | $H_c$ (mm) | $t_s$ (mm) | $d_n$ (mm) | $l_n$ (mm) | $S_n$ (mm) |
|---|---|---|---|---|---|
| 12 X 12 | 0.3 | 0.8 | 0.1 | 0.5 | 2 |

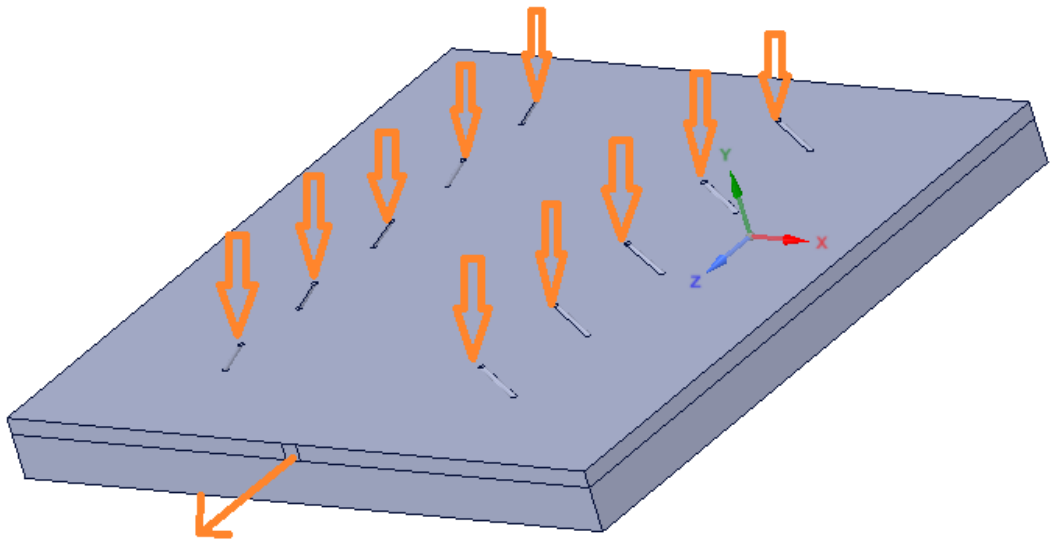


Figure 3.2: Geometry of the 10 micro-jet impingement heat sink

## Problem: Inclined 14 jet model

**Table 3.3: Dimensions of 14 micro-jet heat sink**

| $A_{cs}$ ($mm^2$) | $H_c$ (mm) | $t_s$ (mm) | $d_n$ (mm) | $l_n$ (mm) | $S_n$ (mm) |
|---|---|---|---|---|---|
| 12 X 12 | 0.3 | 0.8 | 0.1 | 0.5 | 2 |

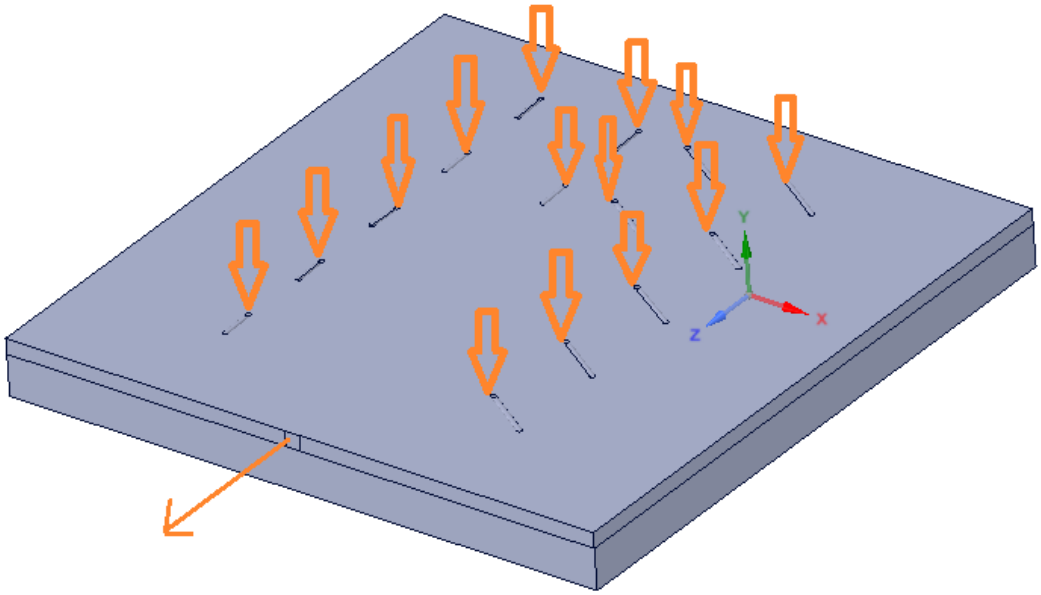


Figure 3.3: Geometry of the 14 micro-jet impingement heat sink

## Problem: Inclined 18 jet model

### Table 3.4: Dimensions of 18 micro-jet heat sink

| $A_{cs}$ ($mm^2$) | $H_c$ (mm) | $t_s$ (mm) | $d_n$ (mm) | $l_n$ (mm) | $S_n$ (mm) |
|---|---|---|---|---|---|

| | | | | | |
|---|---|---|---|---|---|
| 12 X 12 | 0.3 | 0.8 | 0.1 | 0.5 | 2 |

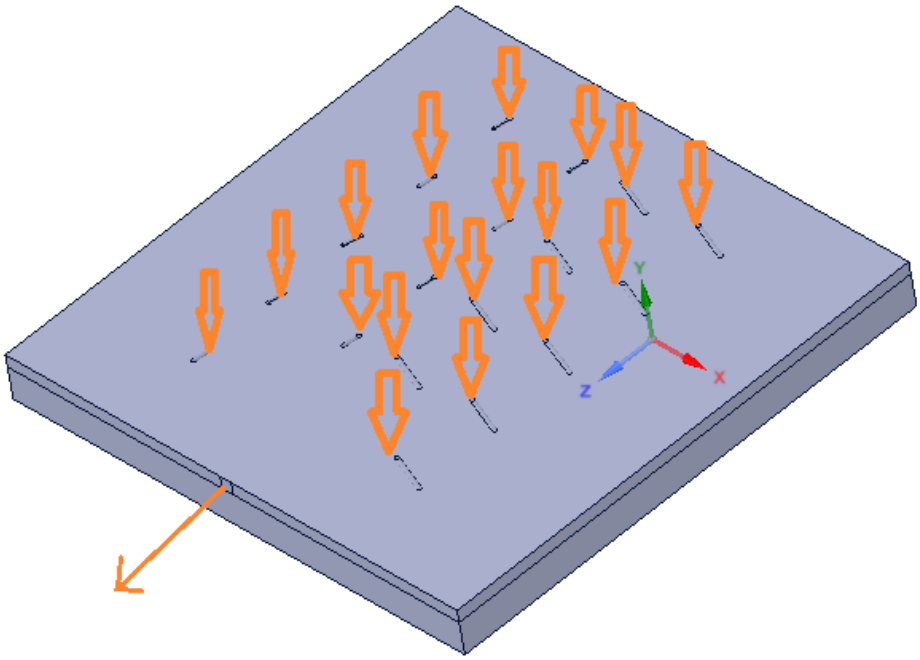


Figure 3.4: Geometry of the 18 micro-jet impingement heat sink

## 3.7 Set up details

Before giving the boundary conditions two domains were created in the ANSYS FLUENT set up. Two domains were created, one domain was given the name as fluid while the other domain was assigned the name as solid domain. The fluid channel constructed in SOLIDWORKS was given the name fluid domain while the heat sink constructed in SOLIDWORKS was given the name solid domain.

After making the domains, the boundary conditions were created in the solid domain and the fluid domain. Inlet, outlet and adiabatic boundary conditions were given in the fluid domain whereas the heat flux was given to bottom wall and adiabatic boundary conditions were given to remaining walls of the solid domain.

**Table 3.5: Zone Specification**

| | |
|---|---|
| Front wall of heat sink | Wall |
| Top wall of heat sink | Wall |

| | |
|---|---|
| Back wall of heat sink | Wall |
| Bottom wall of heat sink | Input heat flux |
| Right wall of heat sink | Wall |
| Left wall of heat sink | Wall |
| Channel entry | Mass flow inlet |
| Channel exit | Constant Pressure Outlet |
| Default face | Wall |

# CHAPTER 4

# SIMULATION RESULTS

In this study, the results of different nanofluids have been compared. Water is mixed with nano-particles of aluminum oxide ($Al_2O_3$) and titanium oxide ($TiO_2$) infractions of 0.1%, 0.5% and 1% at mass flow rate of 0.000062, 0.000122, 0.000182 kg/s.

Results showed that as the concentration of nanoparticles in the base fluid was increased, the average temperature of the plate and bvulk mean temperature at the outlet also

increased keeping mass flow rate constant. As, mass flow rate was increased, the results showed decrease in the average temperature of the plate and bulk mean temperature at the outlet when concentration was kept constant. The simulation carried out on nanofluid gave better results than water.

After simulation, nanofluid (water+0.1%$TiO_2$) obtained temperature difference of 13.914 K, nanofluid (water+0.5%$TiO_2$) obtained temperature difference of 14.11 K, nanofluid (water+1%$TiO_2$) obtained temperature difference of 14.376 K, through micro-channel for mass flow rate of 0.000122 kg/s. On further simulation, nanofluid (water+0.1%$Al_2O_3$) obtained temperature difference of 13.911 K, nanofluid (water+0.5%$Al_2O_3$) obtained temperature difference of 14.095 K, nanofluid (water+1%$Al_2O_3$) obtained temperature difference of 14.325 K in micro-channel for mass flow rate of 0.000122kg/s.

Table 4.1-4.24 shows average temperature of the plate ($T_s$) and bulk mean temperature at the outlet ($T_o$) for different concetration of nanoparticles in the base fluid and mass flow rate. The results are compared and inference has been drawn.

Final conclusion drawn from above results tell us that the nanofluid give better heat transfer than water. It also characterized impingement data under various fluid flows in micro-channel.

**Table 4.1: Simulation result of nanofluids (Water + $TiO_2$) for 6 jet with $\dot{m}$ = 0.000062 kg/s:**

| Nanofluid Properties | | | | | Simulations | |
|---|---|---|---|---|---|---|
| **Fluid** | **Density ($kg/m^3$)** | **Specific Heat (J/kg-K)** | **Thermal Conductivity (W/m-K)** | **Viscosity (Pa-s)** | **Mean Interface Temperature (K)** | **Bulk Mean Outlet Temperature (K)** |
| Water | 996.6 | 4183 | 0.5979 | 0.0008542 | 331.753 | 327.423 |

| | | | | | | |
|---|---|---|---|---|---|---|
| Water + 0.1% $TiO_2$ | 999.760 | 4168.559 | 0.5994 | 0.0008563 | 331.787 | 327.515 |
| Water + 0.5% $TiO_2$ | 1012.402 | 4111.698 | 0.6052 | 0.0008649 | 332.108 | 327.902 |
| Water + 1% $TiO_2$ | 1028.204 | 4042.588 | 0.6126 | 0.0008759 | 332.575 | 328.423 |

**Table 4.2: Simulation result of nanofluids (Water + $Al_2O_3$) for 6 jet with $\dot{m}$ = 0.000062 kg/s:**

| **Nanofluid Properties** | | | | | **Simulations** | |
|---|---|---|---|---|---|---|
| **Fluid** | **Density ($kg/m^3$)** | **Specific Heat (J/kg-K)** | **Thermal Conductivity (W/m-K)** | **Viscosity (Pa-s)** | **Mean Interface Temperature (K)** | **Outlet Temperature (K)** |
| Water + 0.1% $Al_2O_3$ | 999.573 | 4169.425 | 0.5996 | 0.0008563 | 331.779 | 327.51 |
| Water + 0.5% $Al_2O_3$ | 1011.467 | 4115.922 | 0.6064 | 0.0008649 | 332.069 | 327.874 |
| Water + 1% $Al_2O_3$ | 1026.334 | 4050.787 | 0.6151 | 0.0008759 | 332.435 | 328.331 |

**Table 4.3: Simulation result of nanofluids (Water + $TiO_2$) for 6 jet with $\dot{m}$ = 0.000122 kg/s:**

| **Nanofluid Properties** | | | | | **Simulations** | |
|---|---|---|---|---|---|---|
| **Fluid** | **Density ($kg/m^3$)** | **Specific Heat (J/kg-K)** | **Thermal Conductivity (W/m-K)** | **Viscosity (Pa-s)** | **Mean Interface Temperature (K)** | **Bulk Mean Outlet Temperature (K)** |
| Water | 996.6 | 4183 | 0.5979 | 0.0008542 | 318.096 | 313.863 |
| Water + 0.1% $TiO_2$ | 999.760 | 4168.559 | 0.5994 | 0.0008563 | 318.02 | 313.914 |

| | | | | | | |
|---|---|---|---|---|---|---|
| Water + 0.5% $TiO_2$ | 1012.402 | 4111.698 | 0.6052 | 0.0008649 | 318.259 | 314.11 |
| Water + 1% $TiO_2$ | 1028.204 | 4042.588 | 0.6126 | 0.0008759 | 318.375 | 314.376 |

**Table 4.4: Simulation result of nanofluids (Water + $Al_2O_3$) for 6 jet with $\dot{m}$ = 0.000122 kg/s:**

| **Nanofluid Properties** | | | | | **Simulations** | |
|---|---|---|---|---|---|---|
| **Fluid** | **Density ($kg/m^3$)** | **Specific Heat (J/kg-K)** | **Thermal Conductivity (W/m-K)** | **Viscosity (Pa-s)** | **Mean Interface Temperature (K)** | **Outlet Temperature (K)** |
| Water + 0.1% $Al_2O_3$ | 999.573 | 4169.425 | 0.5996 | 0.0008563 | 318.1 | 313.911 |
| Water + 0.5% $Al_2O_3$ | 1011.467 | 4115.922 | 0.6064 | 0.0008649 | 318.238 | 314.095 |
| Water + 1% $Al_2O_3$ | 1026.334 | 4050.787 | 0.6151 | 0.0008759 | 318.411 | 314.325 |

**Table 4.5: Simulation result of nanofluids (Water + $TiO_2$) for 6 jet with $\dot{m}$ = 0.000182 kg/s:**

| **Nanofluid Properties** | | | | | **Simulations** | |
|---|---|---|---|---|---|---|
| **Fluid** | **Density ($kg/m^3$)** | **Specific Heat (J/kg-K)** | **Thermal Conductivity (W/m-K)** | **Viscosity (Pa-s)** | **Mean Interface Temperature (K)** | **Outlet Temperature (K)** |
| Water + 0.1% $TiO_2$ | 999.760 | 4168.559 | 0.5994 | 0.0008563 | 312.943 | 309.342 |
| Water + 0.5% $TiO_2$ | 1012.402 | 4111.698 | 0.6052 | 0.0008649 | 313.156 | 309.457 |
| Water + 1% $TiO_2$ | 1028.204 | 4042.588 | 0.6126 | 0.0008759 | 313.21 | 309.633 |

**Table 4.6: Simulation result of nanofluids (Water + $Al_2O_3$) for 6 jet with $\dot{m}$ = 0.000182 kg/s:**

| Nanofluid Properties | | | | | Simulations | |
|---|---|---|---|---|---|---|
| **Fluid** | **Density ($kg/m^3$)** | **Specific Heat (J/kg-K)** | **Thermal Conductivity (W/m-K)** | **Viscosity (Pa-s)** | **Mean Interface Temperature (K)** | **Outlet Temperature (K)** |
| Water + 0.1% $Al_2O_3$ | 999.573 | 4169.425 | 0.5996 | 0.0008563 | 313.042 | 309.326 |
| Water + 0.5% $Al_2O_3$ | 1011.467 | 4115.922 | 0.6064 | 0.0008649 | 313.139 | 309.447 |
| Water + 1% $Al_2O_3$ | 1026.334 | 4050.787 | 0.6151 | 0.0008759 | 313.261 | 309.6 |

**Table 4.7: Simulation result of nanofluids (Water + $TiO_2$) for 10 jet with $\dot{m}$ = 0.000062 kg/s:**

| Nanofluid Properties | | | | | Simulations | |
|---|---|---|---|---|---|---|
| **Fluid** | **Density ($kg/m^3$)** | **Specific Heat (J/kg-K)** | **Thermal Conductivity (W/m-K)** | **Viscosity (Pa-s)** | **Mean Interface Temperature (K)** | **Outlet Temperature (K)** |
| Water | 996.6 | 4183 | 0.5979 | 0.0008542 | 332.743 | 327.580 |
| Water + 0.1% $TiO_2$ | 999.760 | 4168.559 | 0.5994 | 0.0008563 | 332.639 | 327.662 |
| Water + 0.5% $TiO_2$ | 1012.402 | 4111.698 | 0.6052 | 0.0008649 | 332.954 | 328.048 |
| Water + 1% $TiO_2$ | 1028.204 | 4042.588 | 0.6126 | 0.0008759 | 333.348 | 328.531 |

**Table 4.8: Simulation result of nanofluids (Water + $Al_2O_3$) for 10 jet with $\dot{m}$ = 0.000062 kg/s:**

| Nanofluid Properties | | | | | Simulations | |
|---|---|---|---|---|---|---|
| **Fluid** | **Density ($kg/m^3$)** | **Specific Heat (J/kg-K)** | **Thermal Conductivity (W/m-K)** | **Viscosity (Pa-s)** | **Mean Interface Temperature (K)** | **Outlet Temperature (K)** |
| Water + 0.1% $Al_2O_3$ | 999.573 | 4169.425 | 0.5996 | 0.0008563 | 332.631 | 327.656 |
| Water + 0.5% $Al_2O_3$ | 1011.467 | 4115.922 | 0.6064 | 0.0008649 | 332.814 | 328.019 |
| Water + 1% $Al_2O_3$ | 1026.334 | 4050.787 | 0.6151 | 0.0008759 | 333.268 | 328.474 |

**Table 4.9: Simulation result of nanofluids (Water + $TiO_2$) for 10 jet with $\dot{m}$ = 0.000122 kg/s:**

| Nanofluid Properties | | | | | Simulations | |
|---|---|---|---|---|---|---|
| **Fluid** | **Density ($kg/m^3$)** | **Specific Heat (J/kg-K)** | **Thermal Conductivity (W/m-K)** | **Viscosity (Pa-s)** | **Mean Interface Temperature (K)** | **Outlet Temperature (K)** |
| Water + 0.1% $TiO_2$ | 999.760 | 4168.559 | 0.5994 | 0.0008563 | 318.575 | 313.963 |
| Water + 0.5% $TiO_2$ | 1012.402 | 4111.698 | 0.6052 | 0.0008649 | 318.73 | 314.17 |
| Water + 1% $TiO_2$ | 1028.204 | 4042.588 | 0.6126 | 0.0008759 | 318.926 | 314.407 |

**Table 4.10: Simulation result of nanofluids (Water + $Al_2O_3$) for 10 jet with $\dot{m}$ = 0.000122 kg/s:**

| Nanofluid Properties | Simulations |
|---|---|

| Fluid | Density ($kg/m^3$) | Specific Heat (J/kg-K) | Thermal Conductivity (W/m-K) | Viscosity (Pa-s) | Mean Interface Temperature (K) | Outlet Temperature (K) |
|---|---|---|---|---|---|---|
| Water + 0.1% $Al_2O_3$ | 999.573 | 4169.425 | 0.5996 | 0.0008563 | 318.57 | 313.96 |
| Water + 0.5% $Al_2O_3$ | 1011.467 | 4115.922 | 0.6064 | 0.0008649 | 318.706 | 314.145 |
| Water + 1% $Al_2O_3$ | 1026.334 | 4050.787 | 0.6151 | 0.0008759 | 318.878 | 314.378 |

**Table 4.11: Simulation result of nanofluids (Water + $TiO_2$) for 10 jet with $\dot{m}$ = 0.000182 kg/s:**

| Nanofluid Properties | | | | | Simulations | |
|---|---|---|---|---|---|---|
| Fluid | Density ($kg/m^3$) | Specific Heat (J/kg-K) | Thermal Conductivity (W/m-K) | Viscosity (Pa-s) | Mean Interface Temperature (K) | Outlet Temperature (K) |
| Water + 0.1% $TiO_2$ | 999.760 | 4168.559 | 0.5994 | 0.0008563 | 313.411 | 309.375 |
| Water + 0.5% $TiO_2$ | 1012.402 | 4111.698 | 0.6052 | 0.0008649 | 313.516 | 309.513 |
| Water + 1% $TiO_2$ | 1028.204 | 4042.588 | 0.6126 | 0.0008759 | 313.646 | 309.678 |

**Table 4.12: Simulation result of nanofluids (Water + $Al_2O_3$) for 10 jet with $\dot{m}$ = 0.000182 kg/s:**

| Nanofluid Properties | | | | | Simulations | |
|---|---|---|---|---|---|---|
| Fluid | Density ($kg/m^3$) | Specific Heat (J/kg-K) | Thermal Conductivity (W/m-K) | Viscosity (Pa-s) | Mean Interface Temperature | Outlet Temperature (K) |

| | | | | | (K) | |
|---|---|---|---|---|---|---|
| Water + 0.1% $Al_2O_3$ | 999.573 | 4169.425 | 0.5996 | 0.0008563 | 313.407 | 309.36 |
| Water + 0.5% $Al_2O_3$ | 1011.467 | 4115.922 | 0.6064 | 0.0008649 | 313.498 | 309.471 |
| Water + 1% $Al_2O_3$ | 1026.334 | 4050.787 | 0.6151 | 0.0008759 | 313.61 | 309.626 |

**Table 4.13: Simulation result of Nanofluids (Water + $TiO_2$) for 14 jet with $\dot{m}$ = 0.000062 kg/s:**

| **Nanofluid Properties** | | | | | **Simulations** | |
|---|---|---|---|---|---|---|
| **Fluid** | **Density ($kg/m^3$)** | **Specific Heat (J/kg-K)** | **Thermal Conductivity (W/m-K)** | **Viscosity (Pa-s)** | **Mean Interface Temperature (K)** | **Outlet Temperature (K)** |
| Water | 996.6 | 4183 | 0.5979 | 0.0008542 | 331.919 | 327.693 |
| Water + 0.1% $TiO_2$ | 999.760 | 4168.559 | 0.5994 | 0.0008563 | 331.826 | 327.779 |
| Water + 0.5% $TiO_2$ | 1012.402 | 4111.698 | 0.6052 | 0.0008649 | 332.134 | 328.163 |
| Water + 1% $TiO_2$ | 1028.204 | 4042.588 | 0.6126 | 0.0008759 | 332.134 | 328.643 |

**Table 4.14: Simulation result of Nanofluids (Water + $Al_2O_3$) for 14 jet with $\dot{m}$ = 0.000062 kg/s:**

| **Nanofluid Properties** | | | | | **Simulations** | |
|---|---|---|---|---|---|---|
| **Fluid** | **Density ($kg/m^3$)** | **Specific Heat (J/kg-K)** | **Thermal Conductivity (W/m-K)** | **Viscosity (Pa-s)** | **Mean Interface Temperature** | **Outlet Temperature (K)** |

| | | | | | (K) | |
|---|---|---|---|---|---|---|
| Water + 0.1% $Al_2O_3$ | 999.573 | 4169.425 | 0.5996 | 0.0008563 | 331.818 | 327.774 |
| Water + 0.5% $Al_2O_3$ | 1011.467 | 4115.922 | 0.6064 | 0.0008649 | 332.095 | 328.134 |
| Water + 1% $Al_2O_3$ | 1026.334 | 4050.787 | 0.6151 | 0.0008759 | 332.444 | 328.585 |

**Table 4.15: Simulation result of Nanofluids (Water + $TiO_2$) for 14 jet with $\acute{m}$ = 0.000122 kg/s:**

| Nanofluid Properties | | | | | Simulations | |
|---|---|---|---|---|---|---|
| **Fluid** | **Density ($kg/m^3$)** | **Specific Heat (J/kg-K)** | **Thermal Conductivity (W/m-K)** | **Viscosity (Pa-s)** | **Mean Interface Temperature (K)** | **Outlet Temperature (K)** |
| Water + 0.1% $TiO_2$ | 999.760 | 4168.559 | 0.5994 | 0.0008563 | 318.299 | 314.119 |
| Water + 0.5% $TiO_2$ | 1012.402 | 4111.698 | 0.6052 | 0.0008649 | 318.445 | 314.315 |
| Water + 1% $TiO_2$ | 1028.204 | 4042.588 | 0.6126 | 0.0008759 | 318.628 | 314.559 |

**Table 4.16: Simulation result of Nanofluids (Water + $Al_2O_3$) for 14 jet with $\acute{m}$ = 0.000122 kg/s:**

| Nanofluid Properties | | | | | Simulations | |
|---|---|---|---|---|---|---|
| **Fluid** | **Density ($kg/m^3$)** | **Specific Heat (J/kg-K)** | **Thermal Conductivity (W/m-K)** | **Viscosity (Pa-s)** | **Mean Interface Temperature (K)** | **Outlet Temperature (K)** |
| Water + 0.1% $Al_2O_3$ | 999.573 | 4169.425 | 0.5996 | 0.0008563 | 318.294 | 314.116 |

| | | | | | | |
|---|---|---|---|---|---|---|
| Water + 0.5% $Al_2O_3$ | 1011.467 | 4115.922 | 0.6064 | 0.0008649 | 318.421 | 314.3 |
| Water + 1% $Al_2O_3$ | 1026.334 | 4050.787 | 0.6151 | 0.0008759 | 318.58 | 314.53 |

**Table 4.17: Simulation result of Nanofluids (Water + $TiO_2$) for 14 jet with $\dot{m}$ = 0.000182 kg/s:**

| Nanofluid Properties | | | | | Simulations | |
|---|---|---|---|---|---|---|
| **Fluid** | **Density ($kg/m^3$)** | **Specific Heat (J/kg-K)** | **Thermal Conductivity (W/m-K)** | **Viscosity (Pa-s)** | **Mean Interface Temperature (K)** | **Outlet Temperature (K)** |
| Water + 0.1% $TiO_2$ | 999.760 | 4168.559 | 0.5994 | 0.0008563 | 313.316 | 309.448 |
| Water + 0.5% $TiO_2$ | 1012.402 | 4111.698 | 0.6052 | 0.0008649 | 313.433 | 309.581 |
| Water + 1% $TiO_2$ | 1028.204 | 4042.588 | 0.6126 | 0.0008759 | 313.538 | 309.744 |

**Table 4.18: Simulation result of Nanofluids (Water + $Al_2O_3$) for 14 jet with $\dot{m}$ = 0.000182 kg/s**

| Nanofluid Properties | | | | | Simulations | |
|---|---|---|---|---|---|---|
| **Fluid** | **Density ($kg/m^3$)** | **Specific Heat (J/kg-K)** | **Thermal Conductivity (W/m-K)** | **Viscosity (Pa-s)** | **Mean Interface Temperature (K)** | **Outlet Temperature (K)** |
| Water + 0.1% $Al_2O_3$ | 999.573 | 4169.425 | 0.5996 | 0.0008563 | 313.313 | 309.446 |
| Water + 0.5% $Al_2O_3$ | 1011.467 | 4115.922 | 0.6064 | 0.0008649 | 313.396 | 309.570 |

| | | | | | | |
|---|---|---|---|---|---|---|
| Water + 1% $Al_2O_3$ | 1026.334 | 4050.787 | 0.6151 | 0.0008759 | 313.501 | 309.725 |

**Table 4.19: Simulation result of Nanofluids (Water + $TiO_2$) for 18 jet with $\acute{m}$ = 0.000062 kg/s:**

| Nanofluid Properties | | | | | Simulations | |
|---|---|---|---|---|---|---|
| **Fluid** | **Density ($kg/m^3$)** | **Specific Heat (J/kg-K)** | **Thermal Conductivity (W/m-K)** | **Viscosity (Pa-s)** | **Mean Interface Temperature (K)** | **Outlet Temperature (K)** |
| Water | 996.6 | 4183 | 0.5979 | 0.0008542 | 333.315 | 327.935 |
| Water + 0.1% $TiO_2$ | 999.760 | 4168.559 | 0.5994 | 0.0008563 | 333.149 | 328.017 |
| Water + 0.5% $TiO_2$ | 1012.402 | 4111.698 | 0.6052 | 0.0008649 | 333.468 | 328.401 |
| Water + 1% $TiO_2$ | 1028.204 | 4042.588 | 0.6126 | 0.0008759 | 333.868 | 328.881 |

**Table 4.20: Simulation result of Nanofluids (Water + $Al_2O_3$) for 18 jet with $\acute{m}$ = 0.000062 kg/s:**

| Nanofluid Properties | | | | | Simulations | |
|---|---|---|---|---|---|---|
| **Fluid** | **Density ($kg/m^3$)** | **Specific Heat (J/kg-K)** | **Thermal Conductivity (W/m-K)** | **Viscosity (Pa-s)** | **Mean Interface Temperature (K)** | **Outlet Temperature (K)** |
| Water + 0.1% $Al_2O_3$ | 999.573 | 4169.425 | 0.5996 | 0.0008563 | 333.141 | 328.011 |
| Water + 0.5% $Al_2O_3$ | 1011.467 | 4115.922 | 0.6064 | 0.0008649 | 333.426 | 328.371 |
| Water + | 1026.334 | 4050.787 | 0.6151 | 0.0008759 | 333.786 | 328.822 |

| | | | | | | |
|---|---|---|---|---|---|---|
| 1% $Al_2O_3$ | | | | | | |

**Table 4.21: Simulation result of Nanofluids (Water + $TiO_2$) for 18 jet with $\dot{m}$ = 0.000122 kg/s:**

| Nanofluid Properties | | | | | Simulations | |
|---|---|---|---|---|---|---|
| **Fluid** | **Density ($kg/m^3$)** | **Specific Heat (J/kg-K)** | **Thermal Conductivity (W/m-K)** | **Viscosity (Pa-s)** | **Mean Interface Temperature (K)** | **Outlet Temperature (K)** |
| Water + 0.1% $TiO_2$ | 999.760 | 4168.559 | 0.5994 | 0.0008563 | 319.044 | 314.288 |
| Water + 0.5% $TiO_2$ | 1012.402 | 4111.698 | 0.6052 | 0.0008649 | 319.196 | 314.484 |
| Water + 1% $TiO_2$ | 1028.204 | 4042.588 | 0.6126 | 0.0008759 | 319.388 | 314.730 |

**Table 4.22: Simulation result of Nanofluids (Water + $Al_2O_3$) for 18 jet with $\dot{m}$ = 0.000122 kg/s:**

| Nanofluid Properties | | | | | Simulations | |
|---|---|---|---|---|---|---|
| **Fluid** | **Density ($kg/m^3$)** | **Specific Heat (J/kg-K)** | **Thermal Conductivity (W/m-K)** | **Viscosity (Pa-s)** | **Mean Interface Temperature (K)** | **Outlet Temperature (K)** |
| Water + 0.1% $Al_2O_3$ | 999.573 | 4169.425 | 0.5996 | 0.0008563 | 333.141 | 328.011 |
| Water + 0.5% $Al_2O_3$ | 1011.467 | 4115.922 | 0.6064 | 0.0008649 | 333.426 | 328.371 |
| Water + 1% $Al_2O_3$ | 1026.334 | 4050.787 | 0.6151 | 0.0008759 | 333.786 | 328.822 |

**Table 4.23 Simulation result of Nanofluids (Water + $TiO_2$) for 18 jet with $\dot{m}$ = 0.000182 kg/s:**

| Nanofluid Properties | | | | | Simulations | |
|---|---|---|---|---|---|---|
| **Fluid** | **Density ($kg/m^3$)** | **Specific Heat (J/kg-K)** | **Thermal Conductivity (W/m-K)** | **Viscosity (Pa-s)** | **Mean Interface Temperature (K)** | **Outlet Temperature (K)** |
| Water + 0.1% $TiO_2$ | 999.760 | 4168.559 | 0.5994 | 0.0008563 | 313.82 | 309.568 |
| Water + 0.5% $TiO_2$ | 1012.402 | 4111.698 | 0.6052 | 0.0008649 | 313.924 | 309.701 |
| Water + 1% $TiO_2$ | 1028.204 | 4042.588 | 0.6126 | 0.0008759 | 314.055 | 309.867 |

**Table 4.24: Simulation result of Nanofluids (Water + $Al_2O_3$) for 18 jet with $\dot{m}$ = 0.000182 kg/s:**

| Nanofluid Properties | | | | | Simulations | |
|---|---|---|---|---|---|---|
| **Fluid** | **Density ($kg/m^3$)** | **Specific Heat (J/kg-K)** | **Thermal Conductivity (W/m-K)** | **Viscosity (Pa-s)** | **Mean Interface Temperature (K)** | **Outlet Temperature (K)** |
| Water + 0.1% $Al_2O_3$ | 999.573 | 4169.425 | 0.5996 | 0.0008563 | 313.816 | 309.566 |
| Water + 0.5% $Al_2O_3$ | 1011.467 | 4115.922 | 0.6064 | 0.0008649 | 313.905 | 309.691 |
| Water + 1% $Al_2O_3$ | 1026.334 | 4050.787 | 0.6151 | 0.0008759 | 314.017 | 309.848 |

## 4.1 Results for 6 micro jet impingement heat sink for 0.1%, 0.5%, 1% $TiO_2$ with $\dot{m}$ = 0.000062 kg/s

After simulation, nanofluid (water + 0.1% $TiO_2$) obtained temperature difference of 27.515 K, nanofluid (water + 0.5% $TiO_2$) obtained temperature difference of 27.902 K, nanofluid (water + 1% $TiO_2$) obtained temperature difference of 28.423 K through micro-channel. Figure 4.1, 4.2, 4.3 shows the maximum temperature of 332.452 K, 332.776 K, 333.252 K on the plate for concentration of 0.1%, 0.5%, 1% $TiO_2$ (nanoparticle) in water. The bulk mean temperature at the outlet for concentration of 0.1%, 0.5%, 1% $TiO_2$ was found to be 327.515 K, 327.902 K, 328.423 K. It was seen that both the average temperature of the plate and bulk mean temperature of nanofluid at the outlet increased with increase in concentration of the nanoparticles.

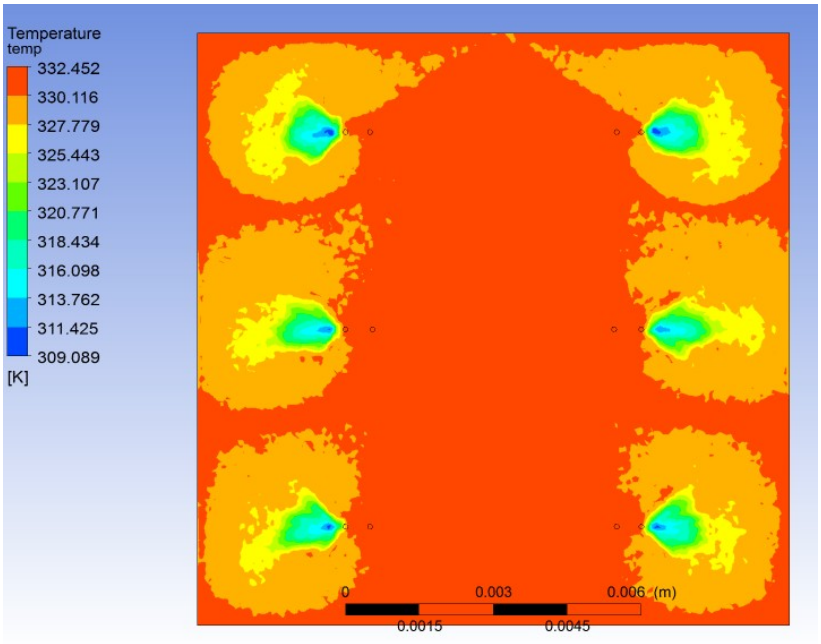


Figure 4.1: Temperature contour at solid-fluid interface across the channel for 6 jet for 0.1% $TiO_2$ ( $\dot{m}$ = 0.000062 kg/s)

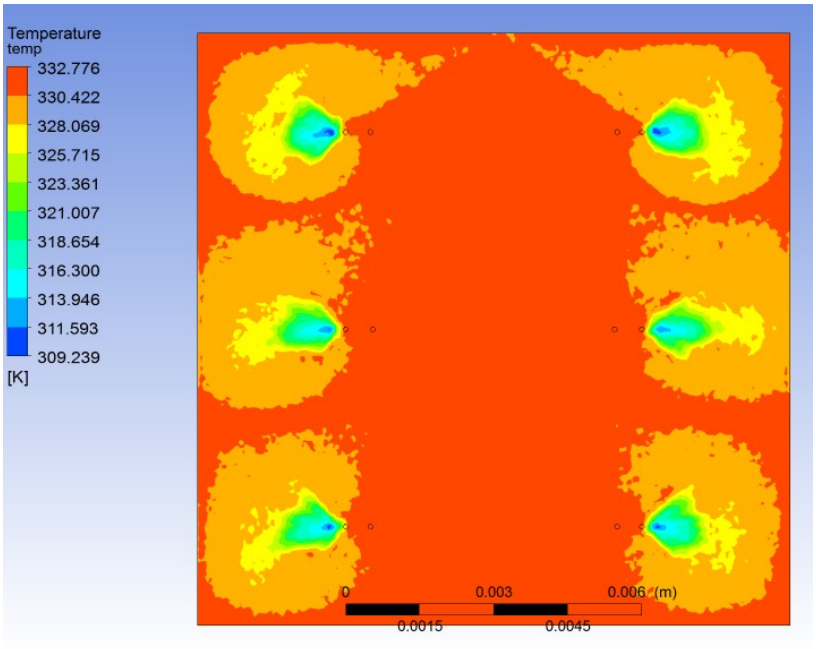


Figure 4.2: Temperature contour at solid-fluid interface across the channel for 6 jet 0.5% TiO ( $\acute{m}$ = 0.000062 kg/s)

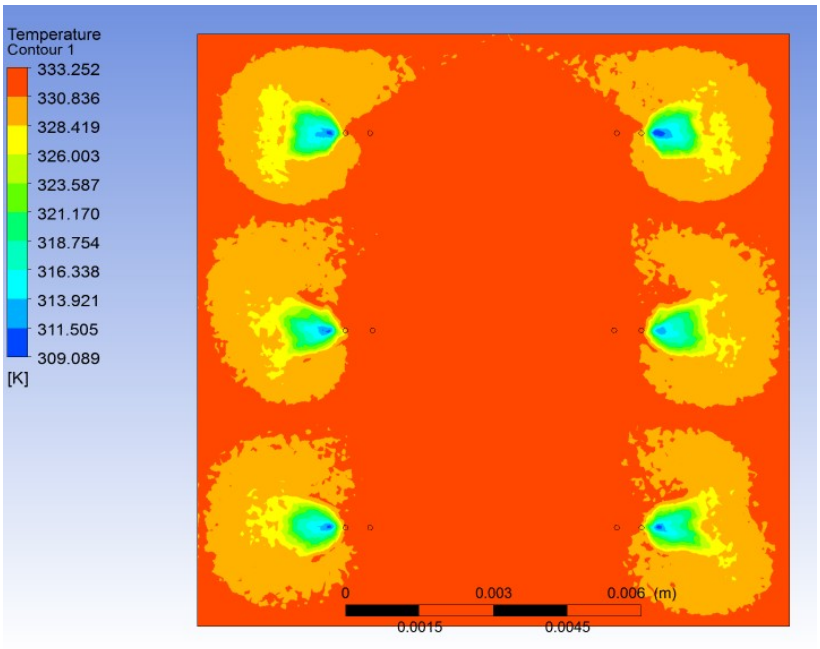


Figure 4.3: Temperature contour at solid-fluid interface across the channel for 6 jet 1% $TiO_2$ ( $\acute{m}$ = 0.000062 kg/s)

## 4.2 Results for 6 micro jet impingement heat sink for 0.1%, 0.5%, 1% $TiO_2$ with $\dot{m}$ = 0.000122 kg/s

After simulation, nanofluid (water + 0.1%$TiO_2$) obtained temperature difference of 13.914 K, nanofluid (water + 0.5% $TiO_2$) obtained temperature difference of 14.11 K, nanofluid (water + 1% $TiO_2$) obtained temperature difference of 14.376 K through micro-channel.

The maximum temperature of 318.656 K (Figure 4.4), 318.818 K (Figure 4.5), 318.972 K (Figure 4.6), was seen on the plate for arrangement with concentration of 0.1%, 0.5%, 1% $TiO_2$ (nanoparticle) in water. The bulk mean temperature at the outlet for concentration of 0.1%, 0.5%, 1% $TiO_2$ was found to be 313.914 K, 314.11 K, 314.376 K. It was seen that both the average temperature of the plate and bulk mean temperature of nanofluid at the outlet increased with increase in concentration of the nanoparticles. Results also showed that as mass flow rate of nanofluid was increased, the outlet fluid temperature and average surface temperature decreased.

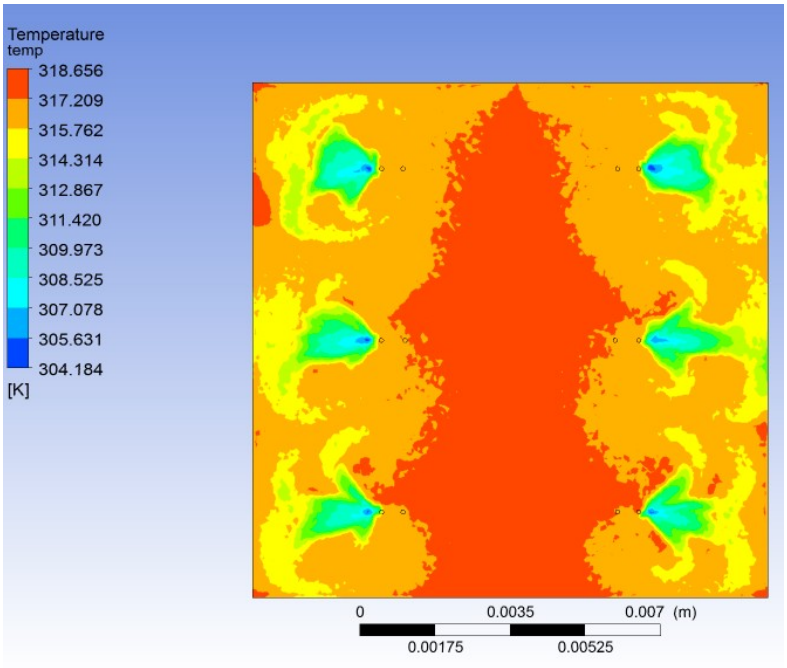


Figure 4.4: Temperature contour at solid-fluid interface across the channel for 6 jet 0.1% $TiO_2$ ¿ = 0.000122 kg/s)

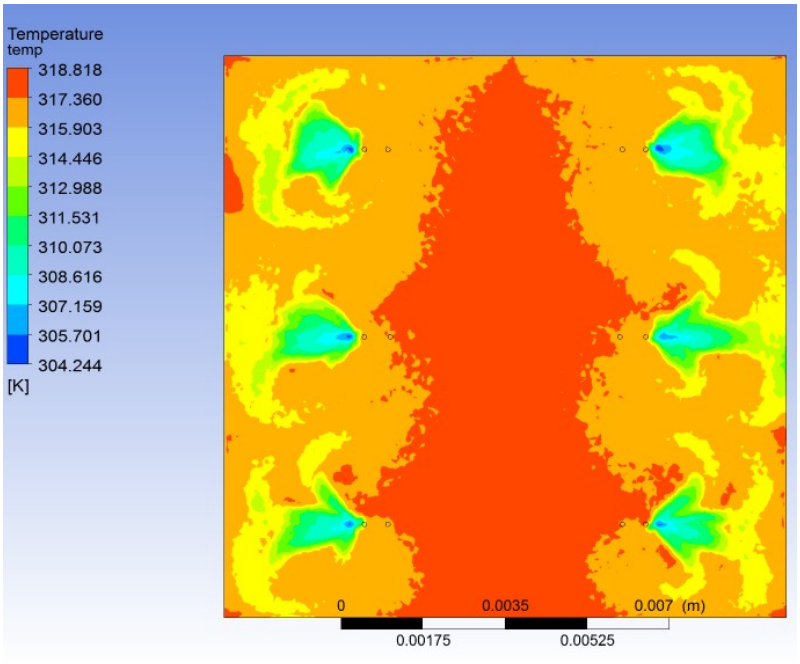


Figure 4.5: Temperature contour at solid-fluid interface across the channel for 6 jet 0.5% $TiO_2$ ($\dot{m}$ = 0.000122 kg/s)

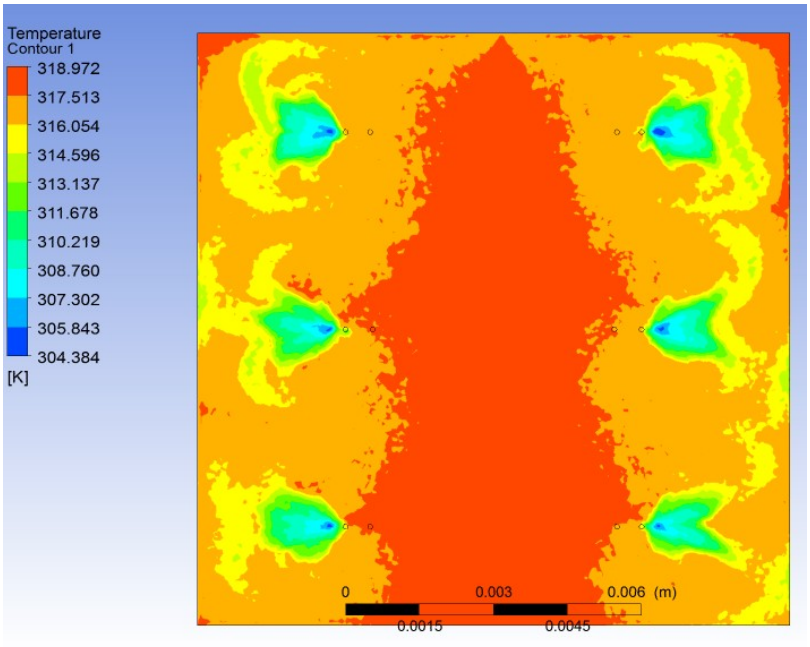

Figure 4.6: Temperature contour at solid-fluid interface across the channel for 6 jet 1% $TiO_2$ ($\acute{m}$ = 0.000122 kg/s)

## 4.3 Results for 6 micro jet impingement heat sink for 0.1%, 0.5%, 1% $TiO_2$ with $\acute{m}$ = 0.000182 kg/s

After simulation, nanofluid (water + 0.1% $TiO_2$) obtained temperature difference of 9.027 K, nanofluid (water + 0.5% $TiO_2$) obtained temperature difference of 9.457 K, nanofluid (water + 1% $TiO_2$) obtained temperature difference of 9.633 K through micro-channel.

Figure 4.7, 4.8, 4.9 shows the maximum temperature of 310.818 K, 313.675 K, 313.756 K for concentration of 0.1%, 0.5%, 1% $TiO_2$ (nanoparticle) in water. The bulk mean temperature of the nanofluid at the outlet for concentration of 0.1%, 0.5%, 1% $TiO_2$ was found to be 309.027 K, 309.457 K, 309.633 K respectively. It was observed that as the mass flow rate increased the average temperature and the maximum temperature of the plate decreased, the bulk mean temperature of the nanofluid at the outlet also decreased.

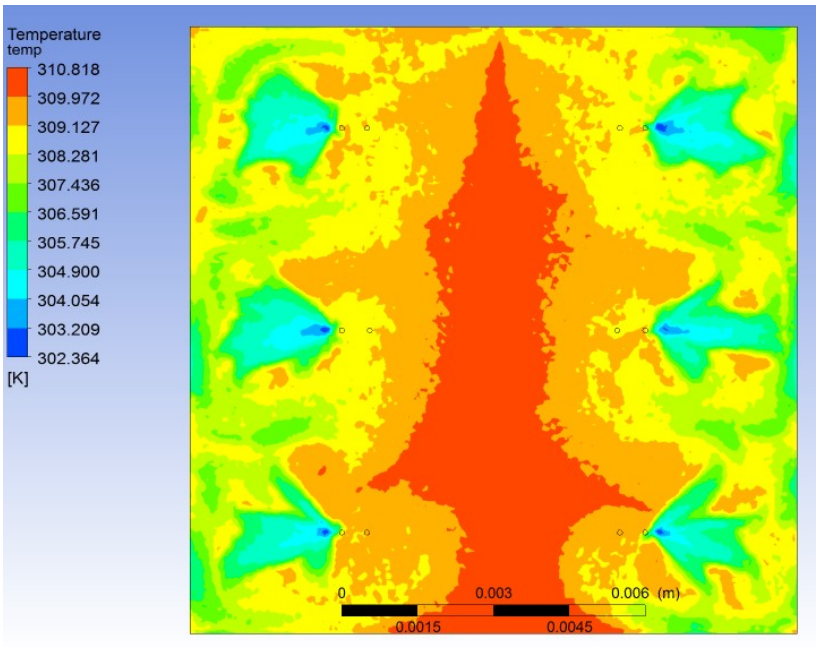


Figure 4.7: Temperature contour at solid-fluid interface across the channel for 6 jet for 0.1% $TiO_2$ ¿ = 0.000182 kg/s)

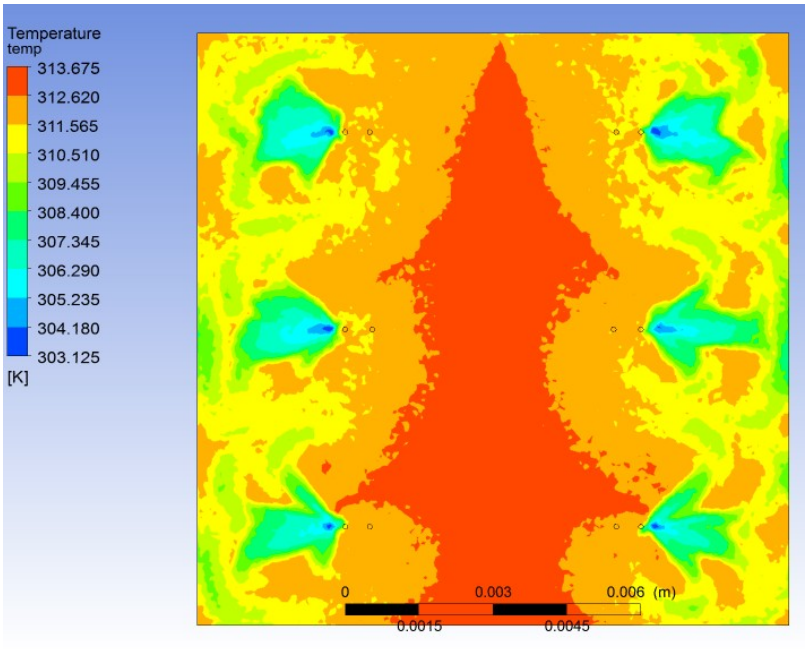


Figure 4.8: Temperature contour at solid-fluid interface across the channel for 6 jet 0.5% $TiO_2$ ¿ = 0.000182 kg/s)

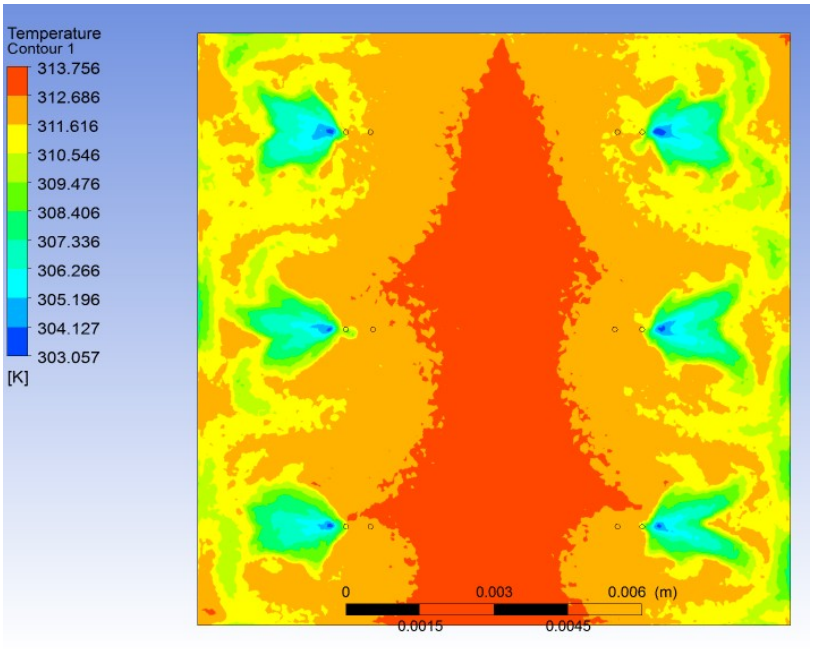


Figure 4.9: Temperature contour at solid-fluid interface across the channel for 6 jet 1% $TiO_2$ ¿ = 0.000182 kg/s)

## 4.4 Results for 6 micro jet impingement heat sink for 0.1%, 0.5%, 1% $Al_2O_3$ with $\dot{m}$ = 0.000062 kg/s

Figure 4.10, 4.11, 4.12 shows the interface temperature profile of the plate containing $Al_2O_3$ nanoparticles at varying concentration of 0.1%, 0.5%, 1% in water. After simulation, nanofluid (water + 0.1% $Al_2O_3$) obtained temperature difference of 27.51 K, nanofluid (water + 0.5% $Al_2O_3$) obtained temperature difference of 27.874 K, nanofluid (water + 1% $Al_2O_3$) obtained temperature difference of 28.331 K in micro-channel. The maximum temperature of 332.444 K, 332.737 K, 333.106 K was seen on the plate for concentration of 0.1%, 0.5%, 1% $Al_2O_3$ (nanoparticle) in water respectively. It was seen that both the average temperature of the plate and bulk mean temperature of nanofluid at the outlet increased with increase in concentration of the nanoparticles.

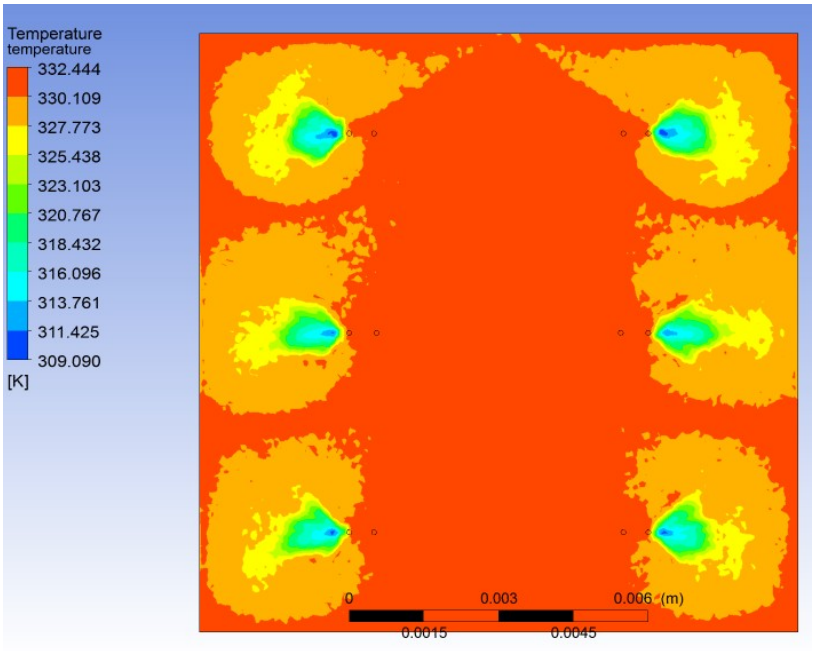


Figure 4.10: Temperature contour at solid-fluid interface across the channel for 6 jet 0.1% $Al_2O_3$ ¿ = 0.000062 kg/s)

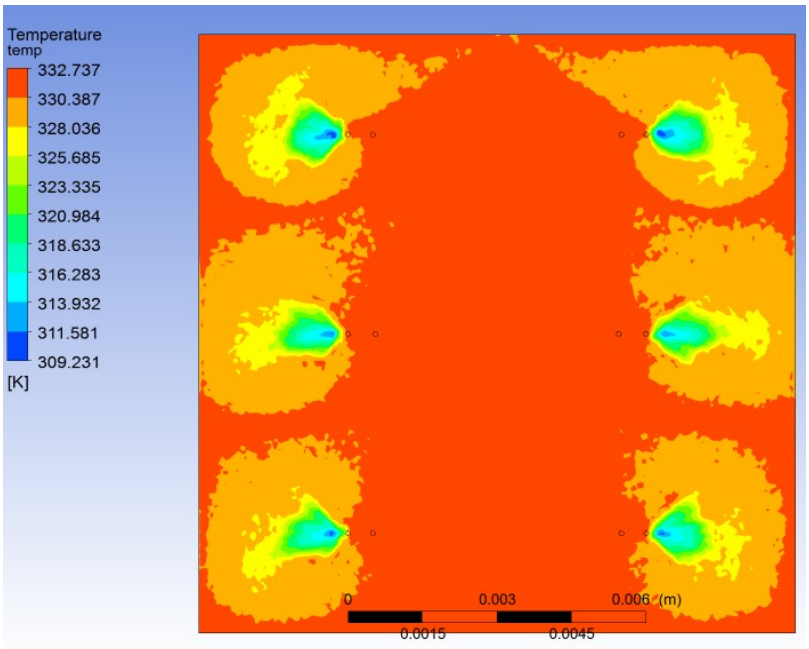


Figure 4.11: Temperature contour at solid-fluid interface across the channel for 6 jet 0.5% $Al_2O_3$ ¿ = 0.000062 kg/s)

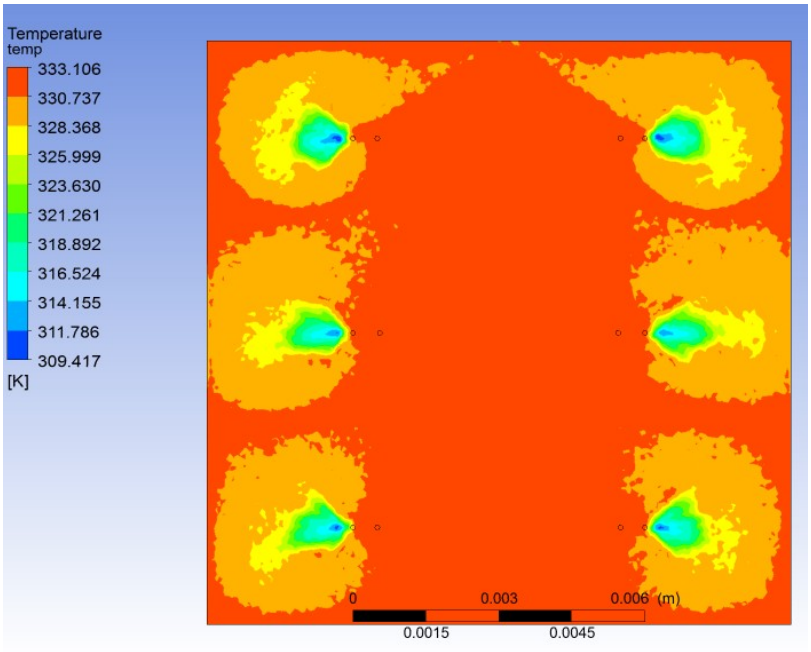


Figure 4.12: Temperature contour at solid-fluid interface across the channel for 6 jet 1% $Al_2O_3$ ¿ = 0.000062 kg/s)

## 4.5 Results for 6 micro jet impingement heat sink for 0.1%, 0.5%, 1% $Al_2O_3$ with $\dot{m}$ = 0.000122 kg/s

After simulation, nanofluid (water + 0.1% $Al_2O_3$) obtained temperature difference of 13.911 K, nanofluid (water + 0.5% $Al_2O_3$) obtained temperature difference of 14.095 K, nanofluid (water + 1% $Al_2O_3$) obtained temperature difference of 14.325 K in micro-channel. Figure 4.13, 4.14, 4.15 shows the maximum temperature of 318.653 K, 318.795 K, 318.974 K at the interface for concentration of 0.1%, 0.5%, 1% $Al_2O_3$ (nanoparticle) in water respectively. It was seen that both the average temperature of the plate and bulk mean temperature of nanofluid at the outlet increased with increase in concentration of the nanoparticles.

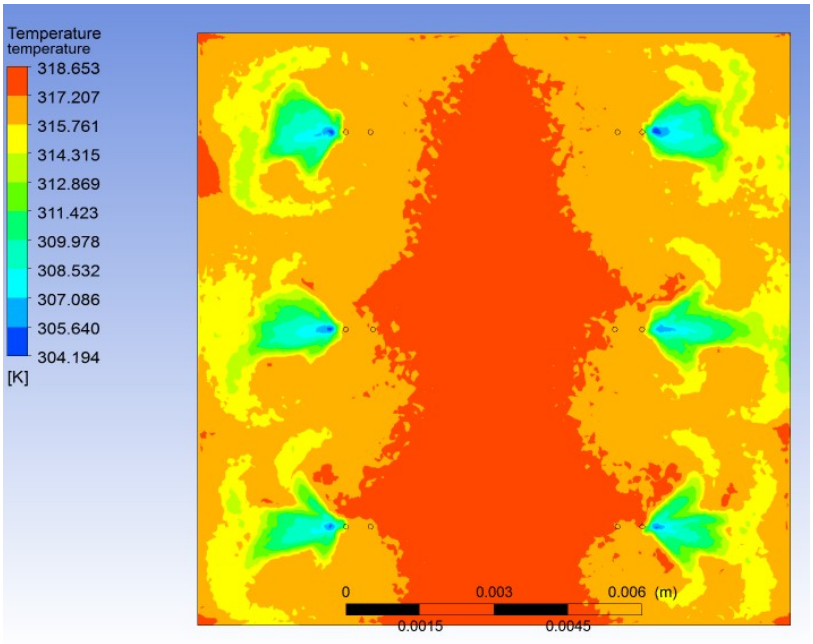


Figure 4.13: Temperature contour at solid-fluid interface across the channel for 6 jet 0.1% $Al_2O_3$ ( $\dot{m}$ = 0.000122 kg/s)

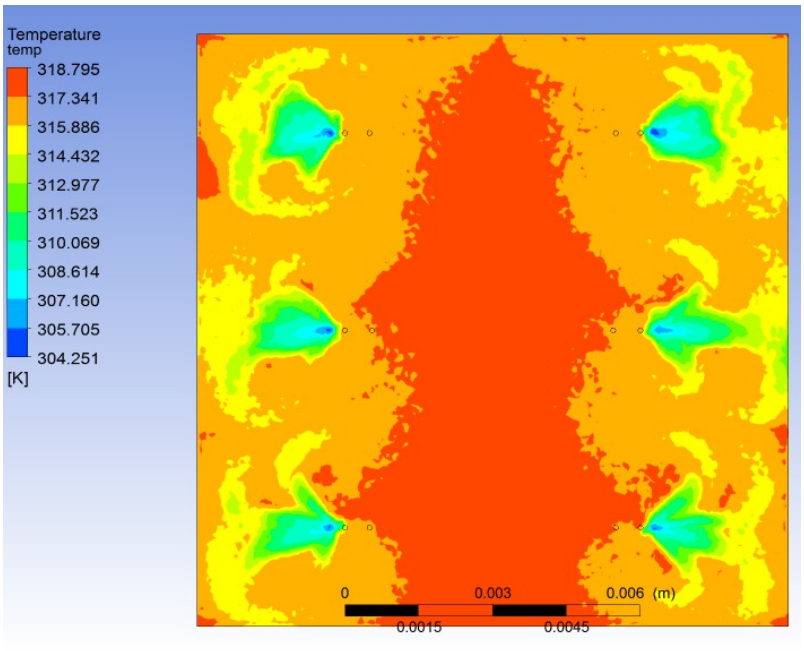


Figure 4.14: Temperature contour at solid-fluid interface across the channel for 6 jet 0.5% $Al_2O_3$ ( $\acute{m}$ = 0.000122 kg/s)

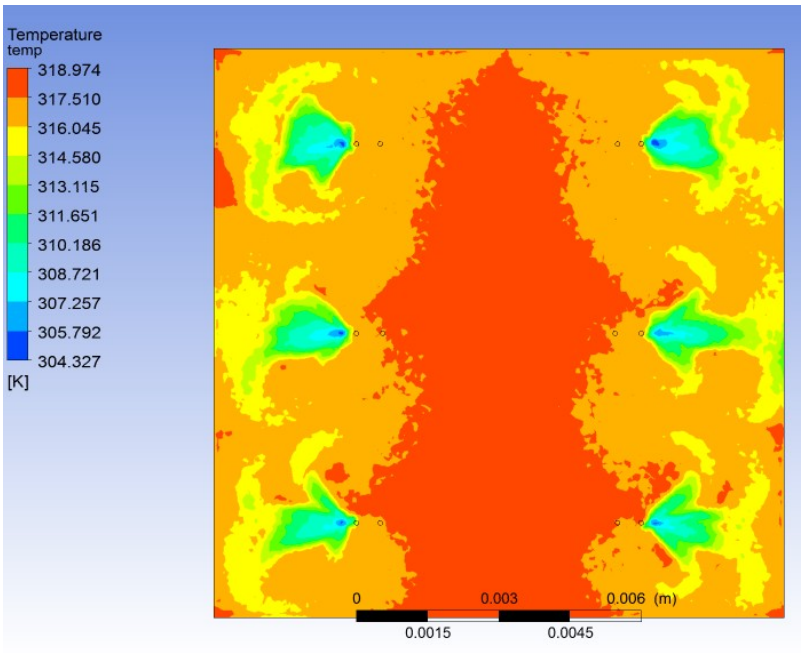


Figure 4.15: Temperature contour at solid-fluid interface across the channel for 6 jet 1% $Al_2O_3$ ( $\acute{m}$ = 0.000122 kg/s)

## 4.6 Results for 6 micro jet impingement heat sink for 0.1%, 0.5%, 1% $Al_2O_3$ with $\acute{m}$ = 0.000182 kg/s

Figure 4.16, 4.17, 4.18 shows the interface temperature profile of the plate containing $Al_2O_3$ nanoparticles at varying concentration of 0.1%, 0.5%, 1% in water. After simulation, nanofluid (water + 0.1% $Al_2O_3$) obtained temperature difference of 9.326 K, nanofluid (water + 0.5% $Al_2O_3$) obtained temperature difference of 9.447 K, nanofluid (water + 1% $Al_2O_3$) obtained temperature difference of 9.6 K, in micro-channel. The maximum temperature of 313.557 K (figure 4.16), 313.657 K (figure 4.17), 313.784 K (figure 4.18) was seen in nanofluid with concentration of 0.1%, 0.5%, 1%, $Al_2O_3$ nanoparticle ($\acute{m}$ = 0.000182 kg/s) in water respectively. It was observed that as the mass flow rate increased the average temperature and the maximum temperature of the plate decreased, the bulk mean temperature of the nanofluid at the outlet also decreased.

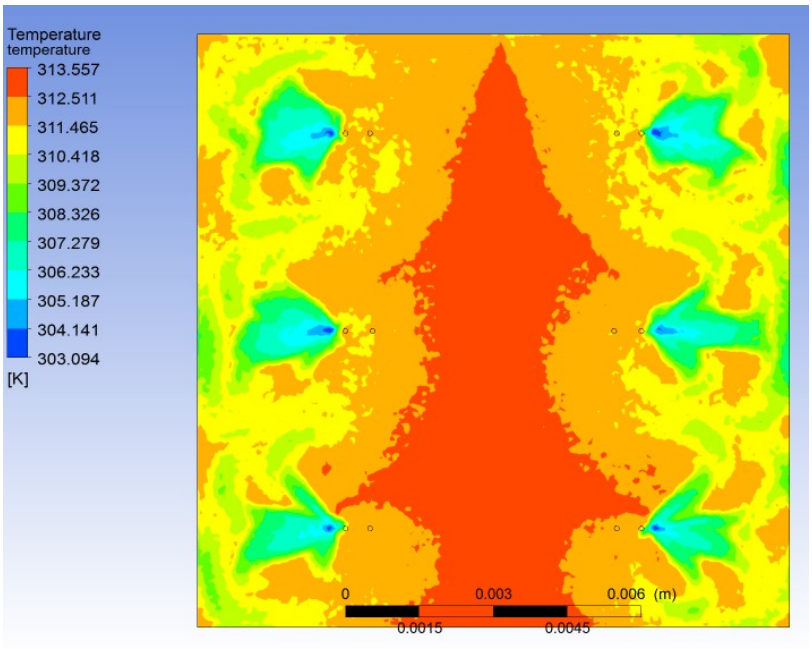


Figure 4.16: Temperature contour at solid-fluid interface across the channel for 6 jet 0.1% $Al_2O_3$ ( $\acute{m}$ = 0.000182 kg/s)

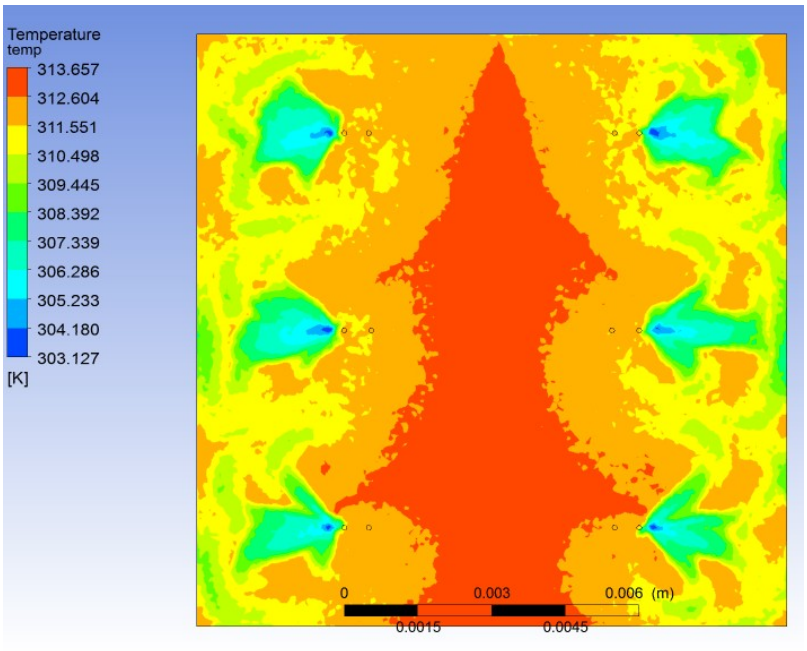


Figure 4.17: Temperature contour at solid-fluid interface across the channel for 6 jet 0.5% $Al_2O_3$ ( $\acute{m}$ = 0.000182 kg/s)

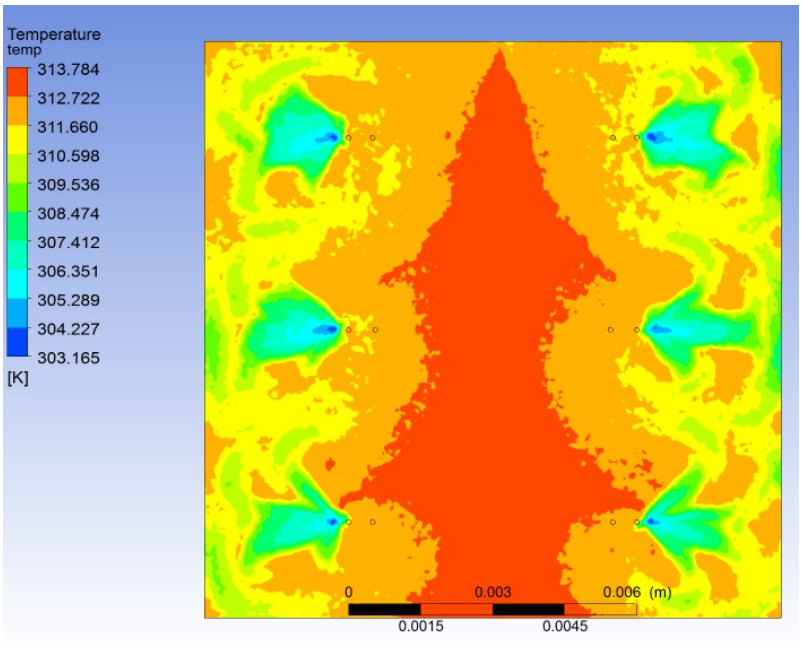


Figure 4.18: Temperature contour at solid-fluid interface across the channel for 6 jet 1% $Al_2O_3$ ( $\acute{m}$ = 0.000182 kg/s)

## 4.7 Results for 10 micro jet impingement heat sink for 0.1%, 0.5%, 1% $TiO_2$ with $\acute{m}$ = 0.000062 kg/s

After simulation, nanofluid (water + 0.1% $TiO_2$) obtained temperature difference of 27.662 K, nanofluid (water + 0.5% $TiO_2$) obtained temperature difference of 28.048 K, nanofluid (water + 1% $TiO_2$) obtained temperature difference of 28.531 K through micro-channel. The 10 jet arrangement used during simulation showed better results than 6 jet arrangement. At every concentration of the nanofluid used in this study, the 10 jet arrangement showed more temperature difference than 6 jet arrangement. This showed that for same mass flow rate heat transfer rate increased with increased in the number of jets.

The maximum temperature of 333.392 K (figure 4.19), 333.710 K (figure 4.20), 334.106 K (figure 4.21), was seen on the plate for arrangement with concentration of 0.1%, 0.5%, 1% $TiO_2$ (nanoparticle) in water. The bulk mean temperature at the outlet was found to be 327.662 K, 328.048 K, 328.531 K for concentration of 0.1%, 0.5%, 1% $TiO_2$ nanoparticle respectively.

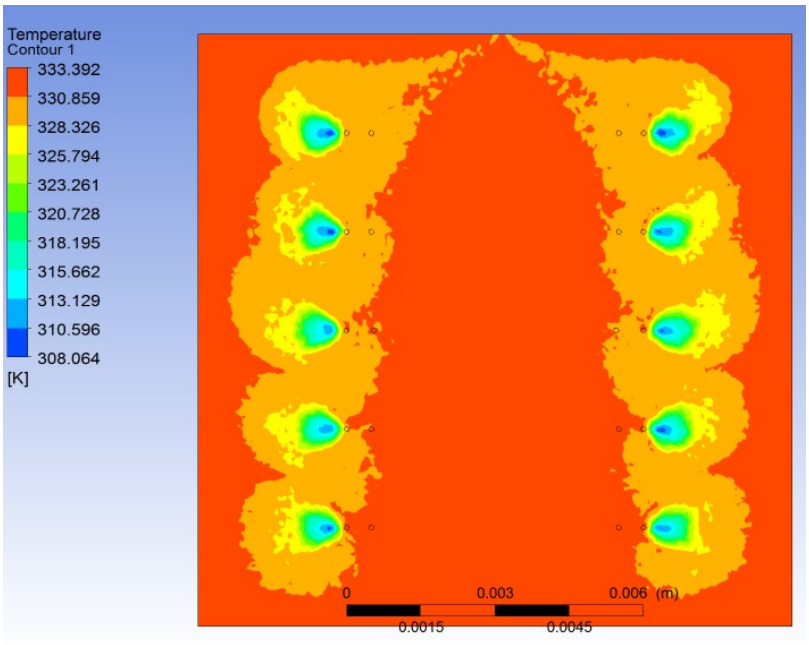


Figure 4.19: Temperature contour at solid-fluid interface across the channel for 10 jet 0.1% $TiO_2$ ¿´¿ = 0.000062 kg/s)

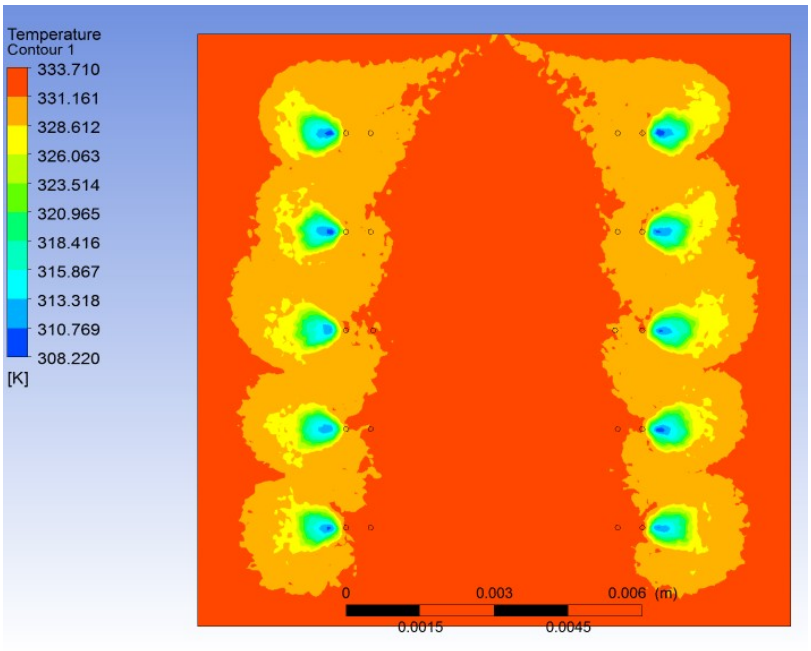


Figure 4.20: Temperature contour at solid-fluid interface across the channel for 10 jet 0.5% $TiO_2$ ¿´¿ = 0.000062 kg/s)

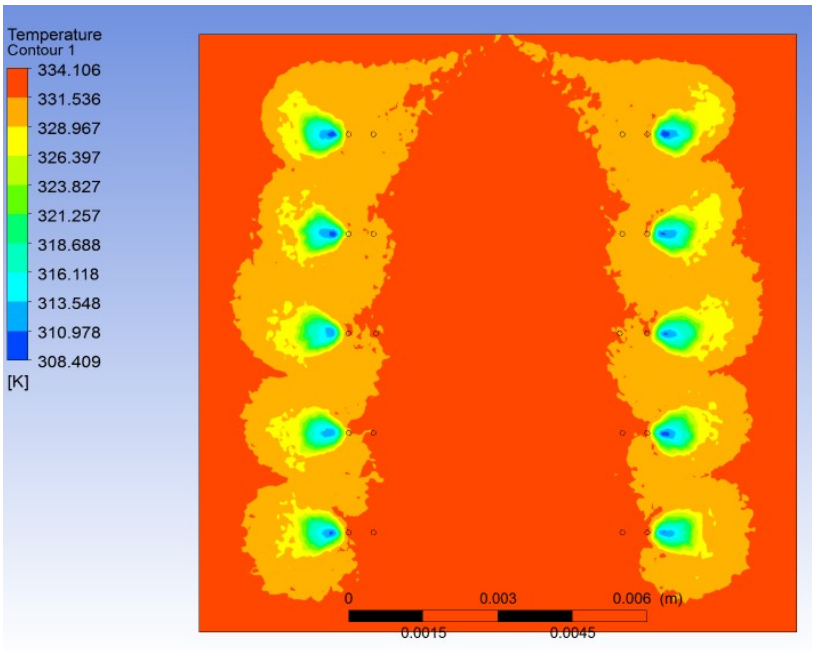


Figure 4.21: Temperature contour at solid-fluid interface across the channel for 10 jet 1% $TiO_2$ ¿´¿ = 0.000062 kg/s)

## 4.8 Results for 10 micro jet impingement heat sink for 0.1%, 0.5%, 1% $TiO_2$ with $\acute{m}$ = 0.000122 kg/s

Figure 4.22, 4.23, 4.24 shows the interface temperature profile of the plate containing $TiO_2$ nanoparticles ($\acute{m}$ = 0.000122 kg/s) at varying concentration of 0.1%, 0.5%, 1% in water. After simulation, nanofluid (water + 0.1% $TiO_2$) obtained temperature difference of 13.963 K, nanofluid (water + 0.5% $TiO_2$) obtained temperature difference of 14.22 K, nanofluid (water + 1% $TiO_2$) obtained temperature difference of 14.407 K through micro-channel.

The maximum temperature of 319.226 K, 319.388 K, 319.590 K was seen on the plate for arrangement with concentration of 0.1%, 0.5%, 1% $TiO_2$ (nanoparticle) in water. The bulk mean temperature at the outlet for concentration of 0.1%, 0.5%, 1%, $TiO_2$ nanoparticle was found to be 313.963 K, 314.22 K, 314.407 K, respectively.

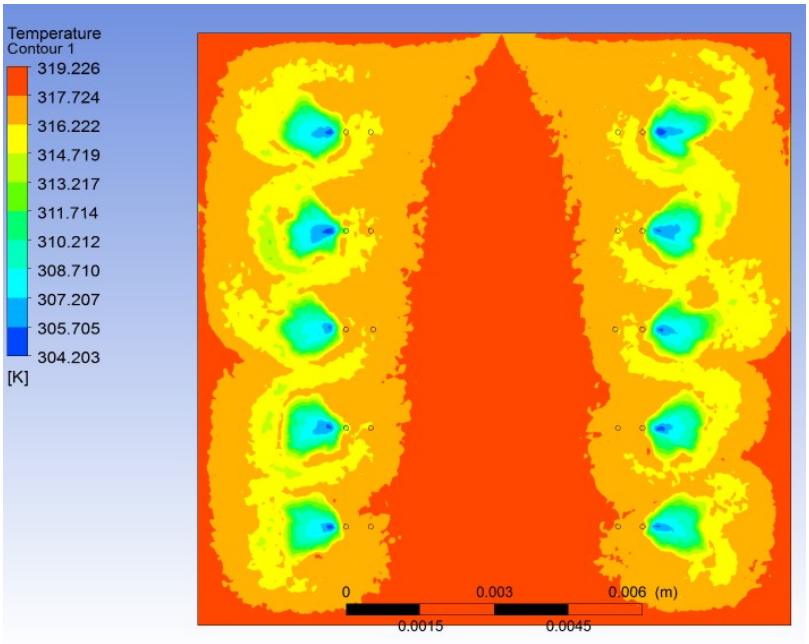


Figure 4.22: Temperature contour at solid-fluid interface across the channel for 10 jet 0.1% $TiO_2$ ¿´¿ = 0.000122 kg/s)

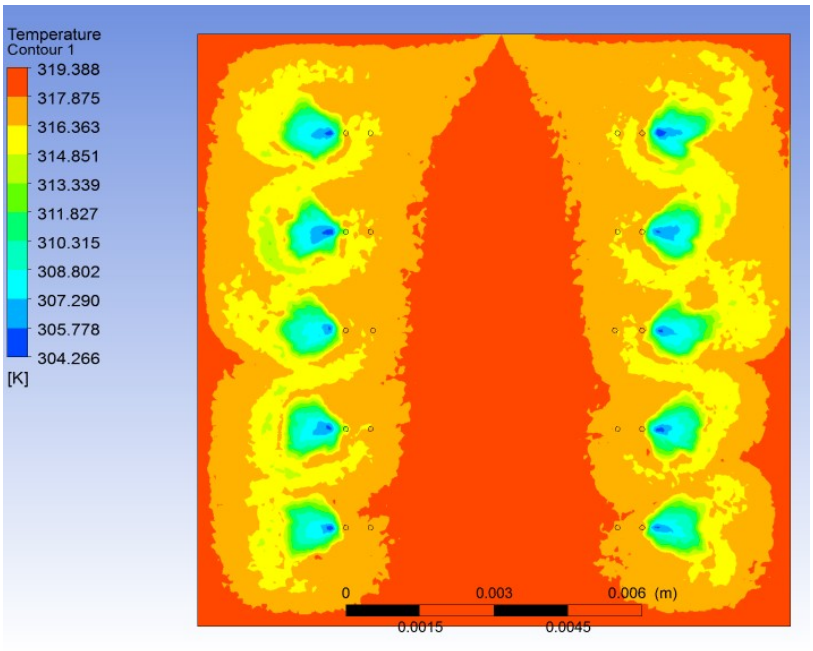


Figure 4.23: Temperature contour at solid-fluid interface across the channel for 10 jet 0.5% $TiO_2$ ¿´¿ = 0.000122 kg/s)

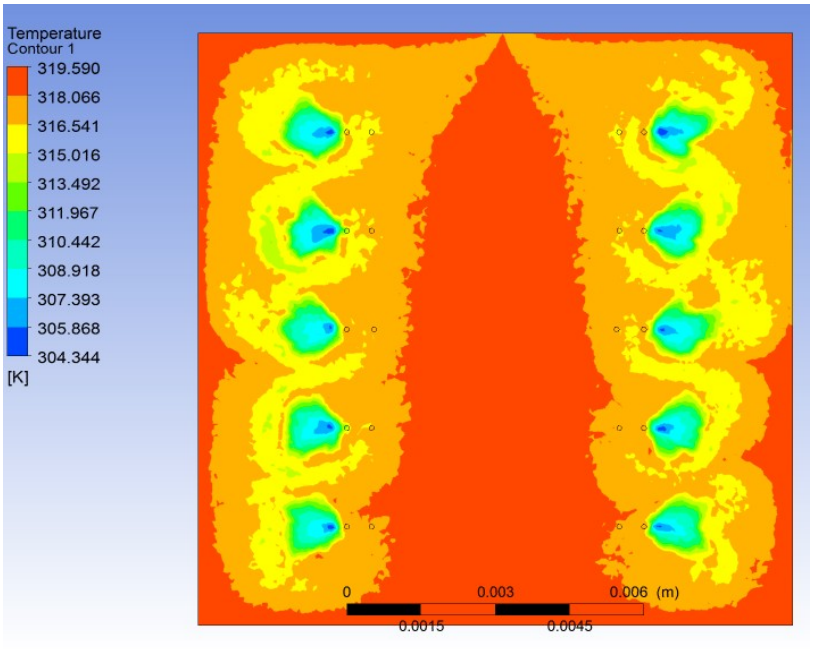


Figure 4.24: Temperature contour at solid-fluid interface across the channel for 10 jet 1% $TiO_2$ ¿´¿ = 0.000122 kg/s)

## 4.9 Results for 10 micro jet impingement heat sink for 0.1%, 0.5%, 1% $TiO_2$ with $\acute{m}$ = 0.000182 kg/s

After simulation, nanofluid (water + 0.1% $TiO_2$) obtained temperature difference of 9.375 K, nanofluid (water + 0.5% $TiO_2$) obtained temperature difference of 9.513 K, nanofluid (water + 1% $TiO_2$) obtained temperature difference of 9.678 K through micro-channel.

Figure 4.25, 4.26, 4.27 shows the maximum temperature of 313.871 K, 313.985 K, 314.127 K on the plate for concentration of 0.1%, 0.5%, 1% $TiO_2$ nanoparticle ($\acute{m}$ = 0.000182 kg/s) in water. The bulk mean temperature of the nanofluid was found to be 309.375 K, 309.513 K, 309.678 K at the outlet for concentration of 0.1%, 0.5%, 1% $TiO_2$ respectively. It was observed that as the mass flow rate increased the average temperature and the maximum temperature of the plate decreased, the bulk mean temperature of the nanofluid at the outlet also decreased.

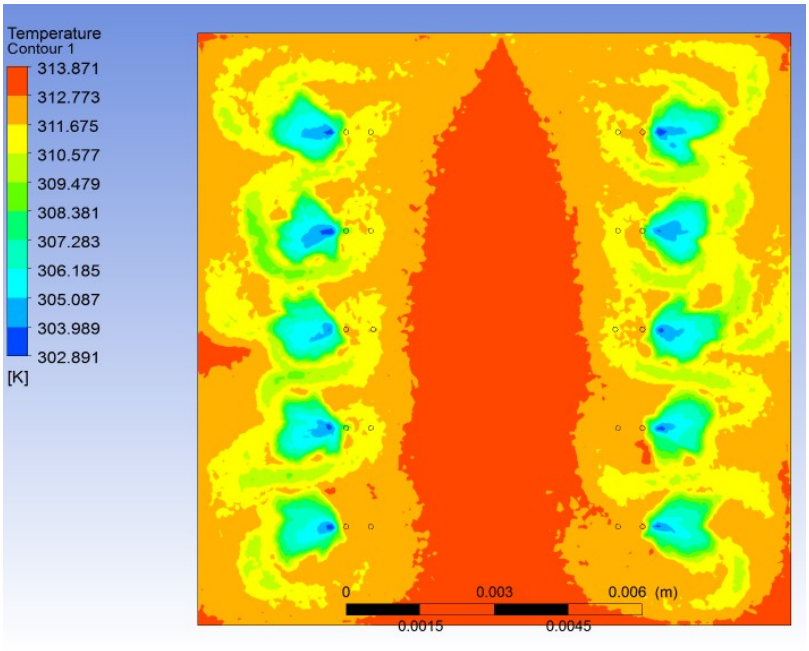


Figure 4.25: Temperature contour at solid-fluid interface across the channel for 10 jet 0.1% $TiO_2$ ¿´¿ = 0.000182 kg/s)

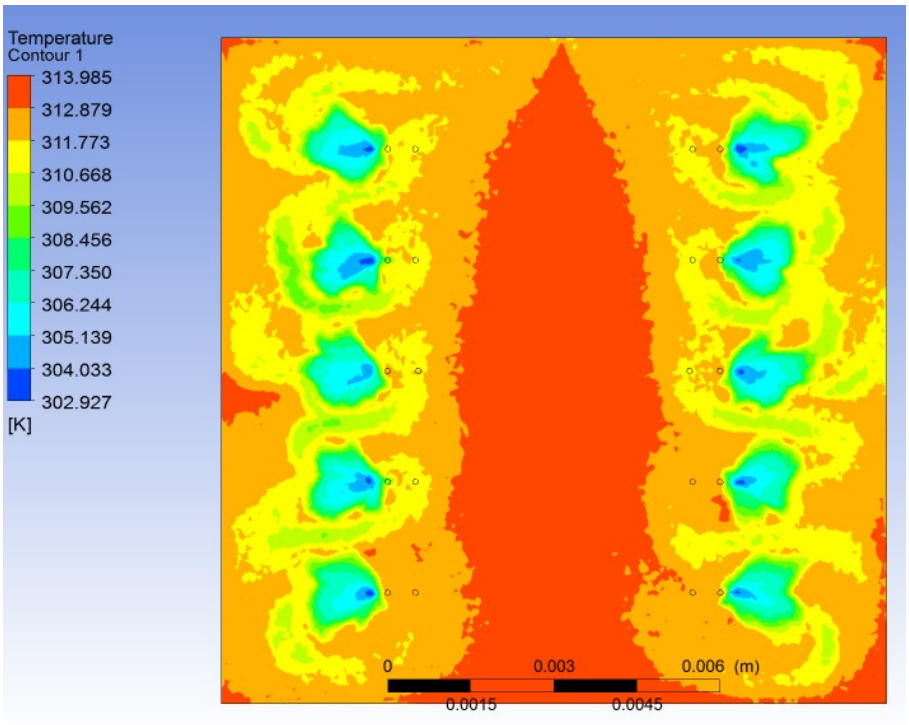


Figure 4.26: Temperature contour at solid-fluid interface across the channel for 10 jet 0.5% $TiO_2$ ¿´¿ = 0.000182 kg/s)

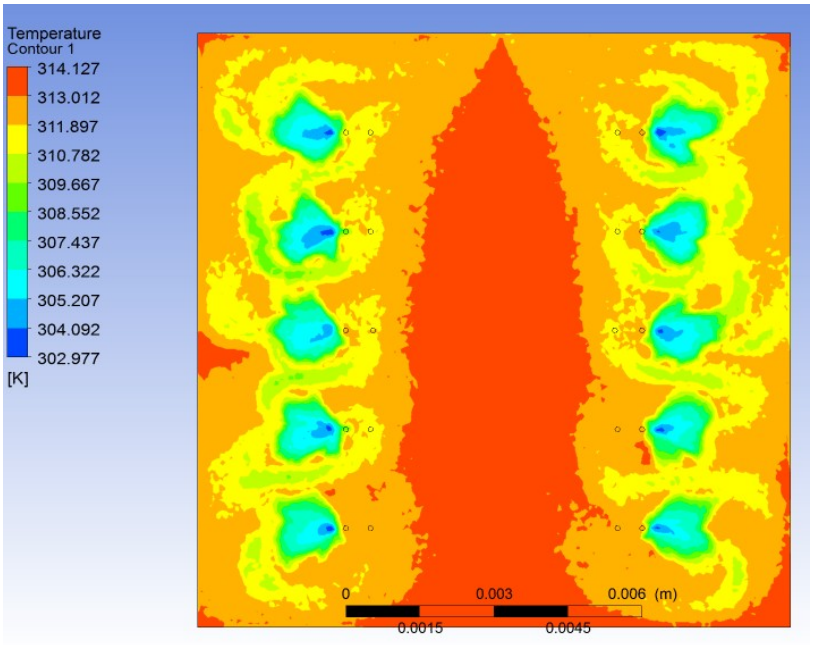


Figure 4.27: Temperature contour at solid-fluid interface across the channel for 10 jet 1% $TiO_2$ ¿´¿ = 0.000182 kg/s)

## 4.10 Results for 10 micro jet impingement heat sink for 0.1%, 0.5%, 1% $Al_2O_3$ with $\acute{m}$ = 0.000062 kg/s

Figure 4.28, 4.29, 4.30 shows the interface temperature profile of the plate containing $Al_2O_3$ nanoparticles ($\acute{m}$ = 0.000062 kg/s) at varying concentration of 0.1%, 0.5%, 1% in water. After simulation, nanofluid (water + 0.1% $Al_2O_3$) obtained temperature difference of 27.656 K, nanofluid (water + 0.5% $Al_2O_3$) obtained temperature difference of 28.019 K, nanofluid (water + 1% $Al_2O_3$) obtained temperature difference of 28.474 K through micro-channel. The maximum temperature of 333.385 K, 333.669 K, 334.026 K was seen on the plate for arrangement with concentration of 0.1%, 0.5%, 1% $Al_2O_3$ (nanoparticle) in water respectively. It was seen that both the average temperature of the plate and bulk mean temperature of nanofluid at the outlet increased with increase in concentration of the nanoparticles. The bulk mean temperature of the nanofluid at the outlet for concentration of 0.1%, 0.5%, 1% $Al_2O_3$ was found to be 327.656 K, 328.019 K, 328.474 K respectively.

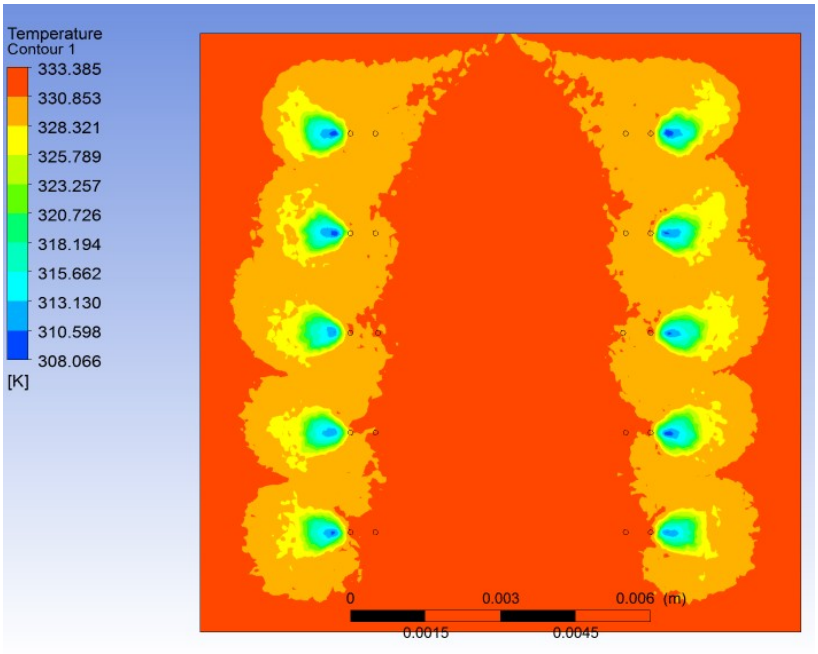


Figure 4.28: Temperature contour at solid-fluid interface across the channel for 10 jet 0.1% $Al_2O_3$ ¿´¿ = 0.000062 kg/s)

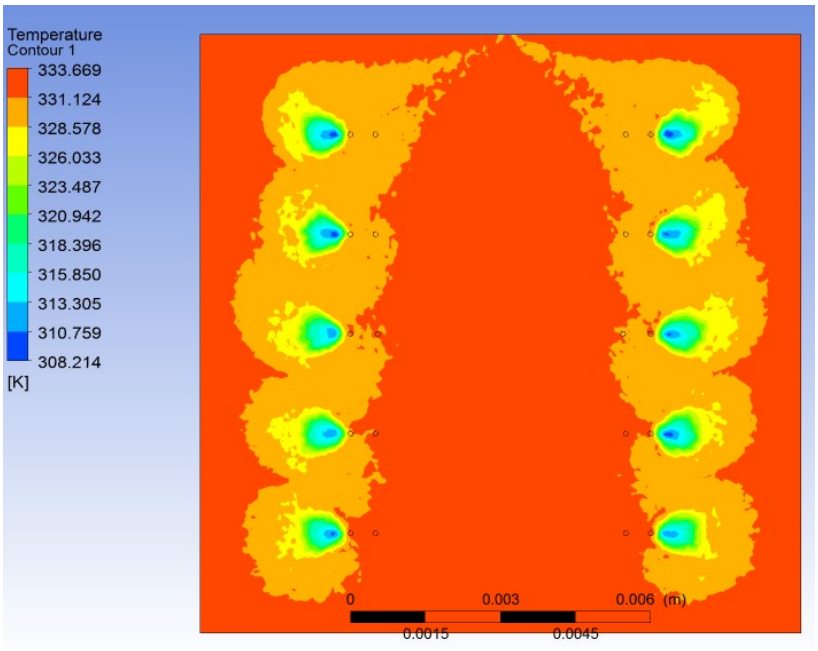


Figure 4.29: Temperature contour at solid-fluid interface across the channel for 10 jet 0.5% $Al_2O_3$ ¿´¿ = 0.000062 kg/s)

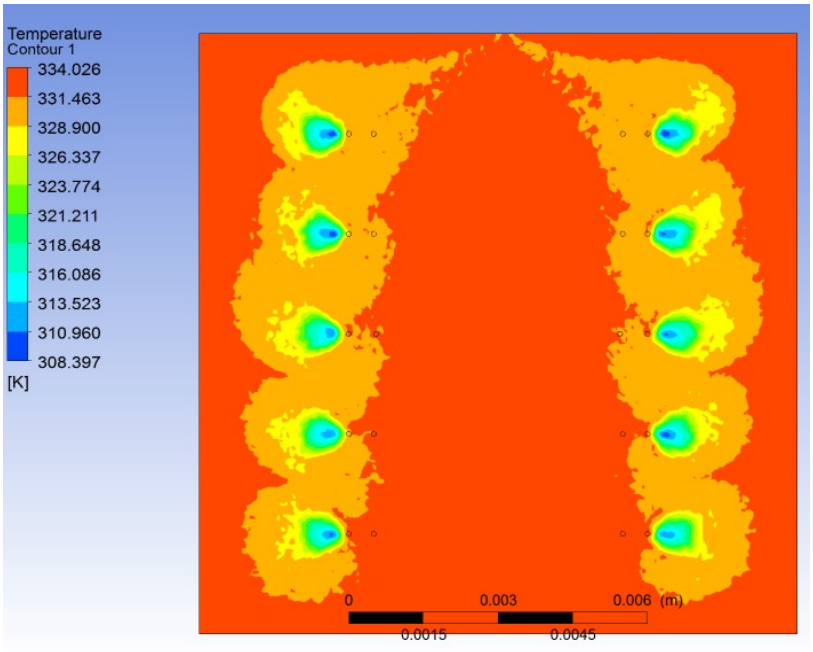


Figure 4.30: Temperature contour at solid-fluid interface across the channel for 10 jet 1% $Al_2O_3$ ¿´¿ = 0.000062 kg/s)

## 4.11 Results for 10 micro jet impingement heat sink for 0.1%, 0.5%, 1%

### $Al_2O_3$ with $\acute{m}$ = 0.000122 kg/s

Figure 4.31, 4.32, 4.33 shows the interface temperature profile of the plate containing $Al_2O_3$ nanoparticles ($\acute{m}$ = 0.000122 kg/s) at varying concentration of 0.1%, 0.5%, 1% in water. After simulation, nanofluid (water + 0.1% $Al_2O_3$) obtained temperature difference of 13.96 K, nanofluid (water + 0.5% $Al_2O_3$) obtained temperature difference of 14.145 K, nanofluid (water + 1% $Al_2O_3$) obtained temperature difference of 14.378 K through micro-channel. The maximum temperature of 319.222 K, 319.364 K, 319.543 K was seen on the plate for arrangement with concentration of 0.1%, 0.5%, 1% $Al_2O_3$ (nanoparticle) in water respectively. It was seen that both the average temperature of the plate and bulk mean temperature of nanofluid at the outlet increased with increase in concentration of the nanoparticles.

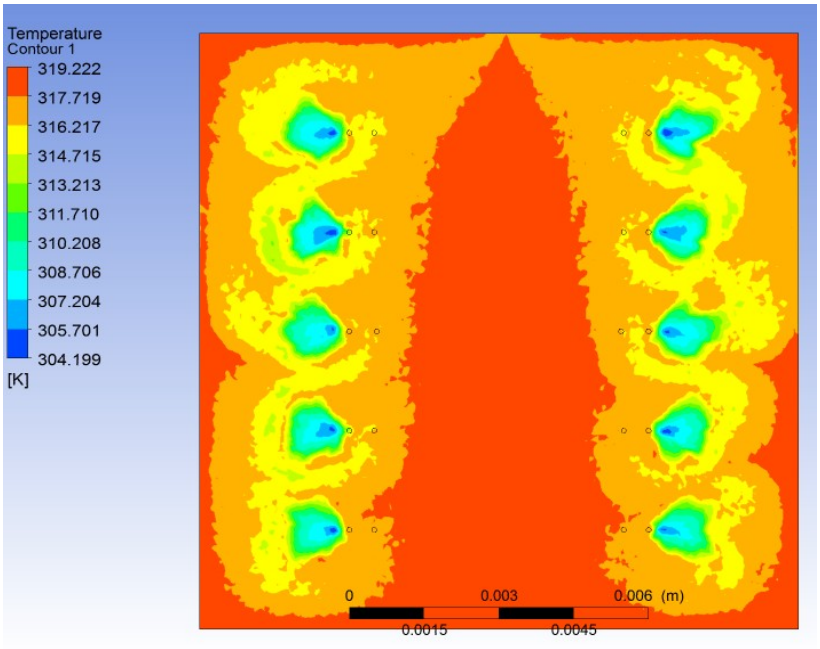


Figure 4.31: Temperature contour at solid-fluid interface across the channel for 10 jet 0.1% $Al_2O_3$ ¿ = 0.000122 kg/s)

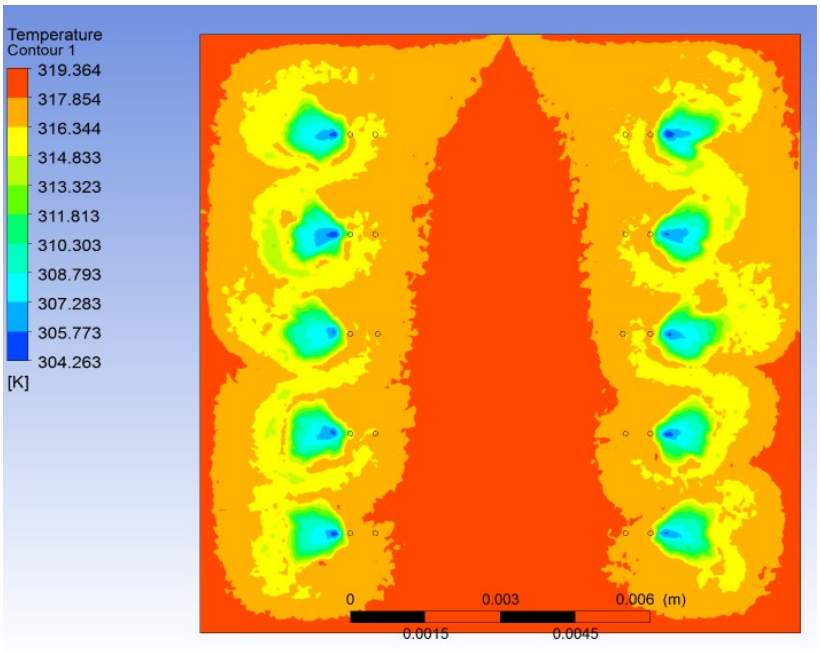


Figure 4.32: Temperature contour at solid-fluid interface across the channel for 10 jet 0.5% $Al_2O_3$ ¿ = 0.000122 kg/s)

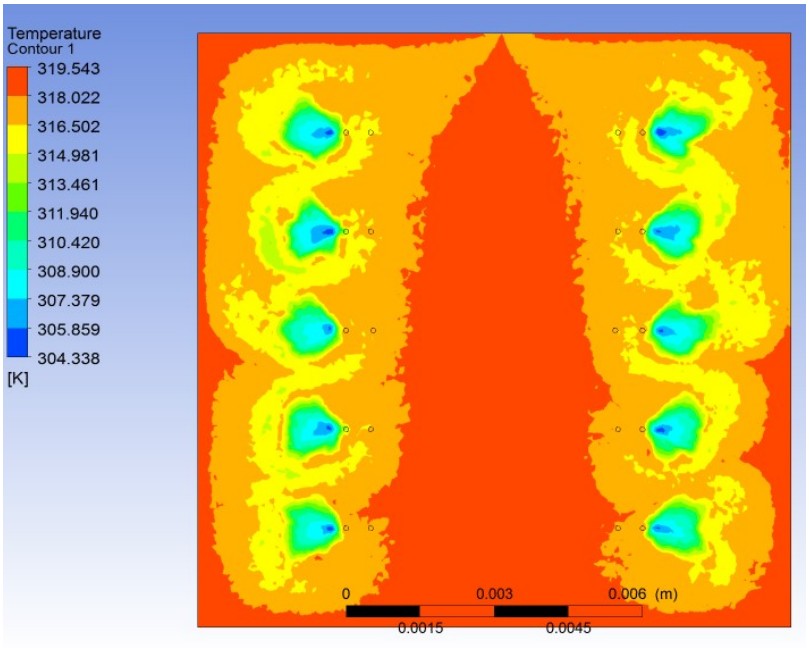


Figure 4.33: Temperature contour at solid-fluid interface across the channel for 10 jet 1% $Al_2O_3$ ¿ = 0.000122 kg/s)

## 4.12 Results for 10 micro jet impingement heat sink for 0.1%, 0.5%, 1% $Al_2O_3$ with $\acute{m}$ = 0.000182 kg/s

After simulation, nanofluid (water + 0.1% $Al_2O_3$) obtained temperature difference of 9.36 K, nanofluid (water + 0.5% $Al_2O_3$) obtained temperature difference of 9.471 K, nanofluid (water + 1% $Al_2O_3$) obtained temperature difference of 9.626 K through micro-channel. The maximum temperature of 313.868 K (figure 4.34), 313.967 K (figure 4.35), 314.092 K(figure 4.36), was seen on the plate for arrangement with concentration of 0.1%, 0.5%, 1% $Al_2O_3$ nanoparticle ($\acute{m}$ = 0.000182 kg/s) in water respectively. It was found that maximum temperature of the plate increased with increase in the concentration of $Al_2O_3$ nanoparticle.

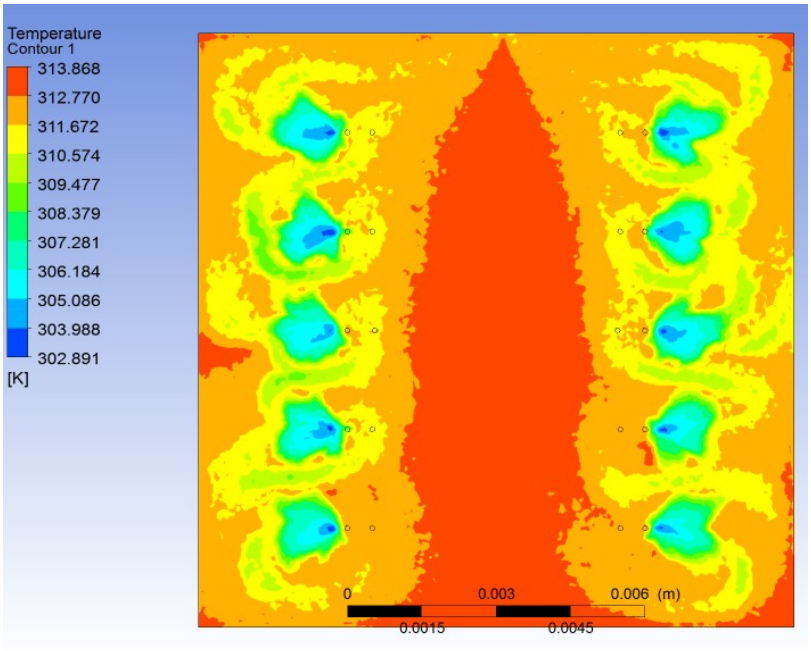


Figure 4.34: Temperature contour at solid-fluid interface across the channel for 10 jet 0.1% $Al_2O_3$ ¿¿ = 0.000182 kg/s)

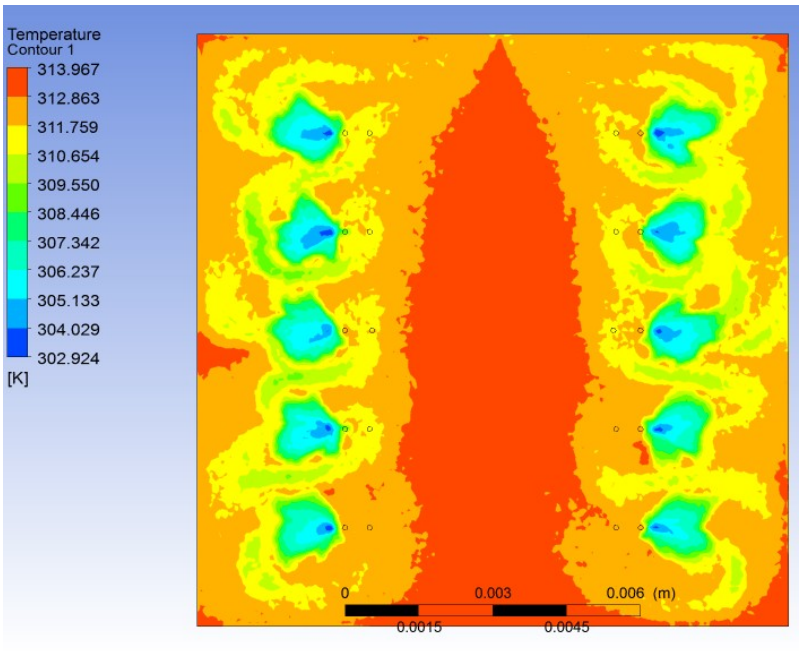


Figure 4.35: Temperature contour at solid-fluid interface across the channel for 10 jet 0.5% $Al_2O_3$ ($\dot{m}$ = 0.000182 kg/s)

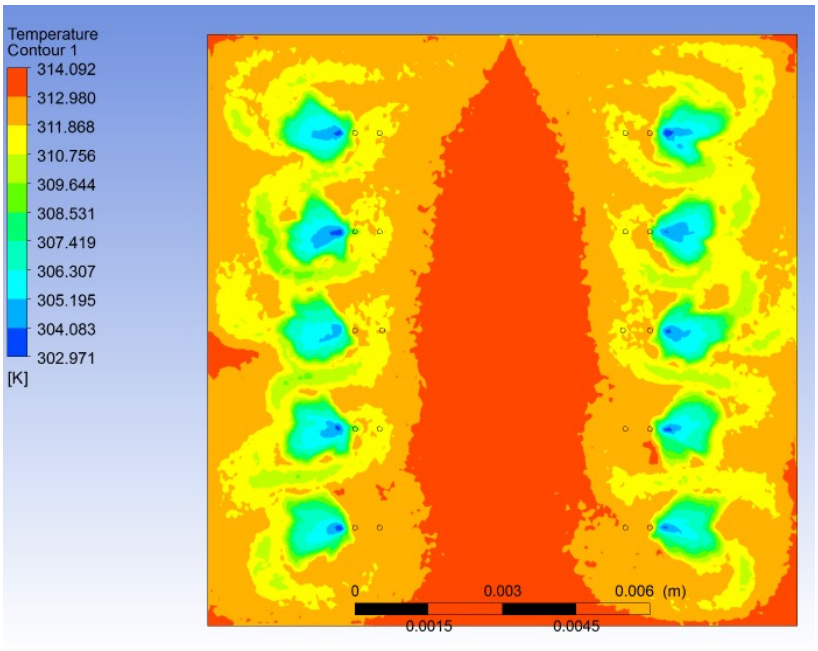


Figure 4.36: Temperature contour at solid-fluid interface across the channel for 10 jet 1% $Al_2O_3$ ($\dot{m}$ = 0.000182 kg/s)

## 4.13 Results for 14 micro jet impingement heat sink for 0.1%, 0.5%, 1% $TiO_2$ with $\dot{m}$ = 0.000062 kg/s

Figure 4.28, 4.29, 4.30 shows the interface temperature profile of the plate containing $TiO_2$ nanoparticles ($\acute{m}$ = 0.000062 kg/s) at varying concentration of 0.1%, 0.5%, 1% in water. After simulation, nanofluid (water + 0.1% $TiO_2$) obtained temperature difference of 27.779 K, nanofluid (water + 0.5% $TiO_2$) obtained temperature difference of 28.163 K, nanofluid (water + 1% $TiO_2$) obtained temperature difference of 28.643 K through micro-channel. The 14 jet arrangement used during simulation showed better results than 10 and 6 jet arrangement. This showed that for same mass flow rate heat transfer rate increased with increased in the number of jets.

The maximum temperature of 332.499 K, 332.811 K, 333.203 K was seen on the plate for arrangement with concentration of 0.1%, 0.5%, 1% $TiO_2$ (nanoparticle) in water. The maximum temperature of the plate increases with increase in the nanoparticle concentration.

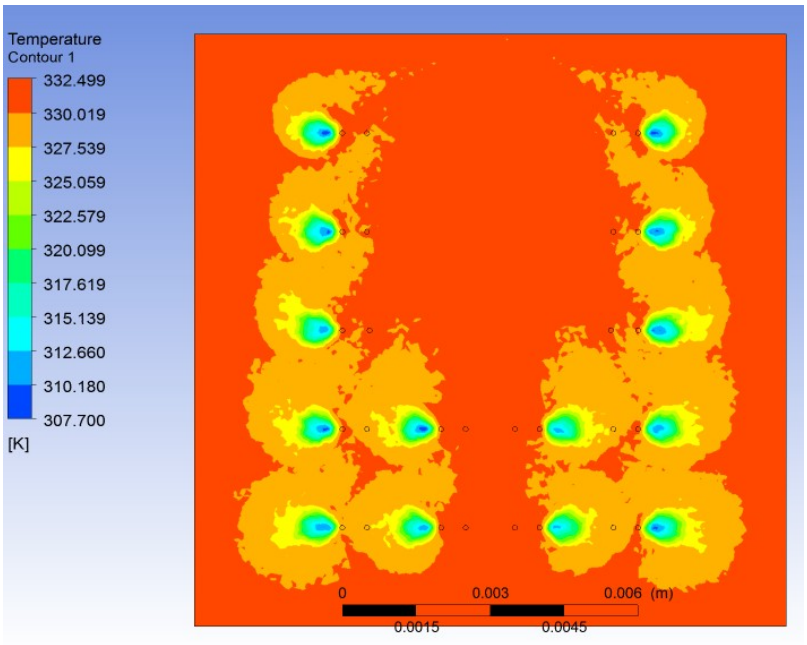


Figure 4.37: Temperature contour at solid-fluid interface across the channel for 14 jet 0.1% $TiO_2$ ¿´¿ = 0.000062 kg/s)

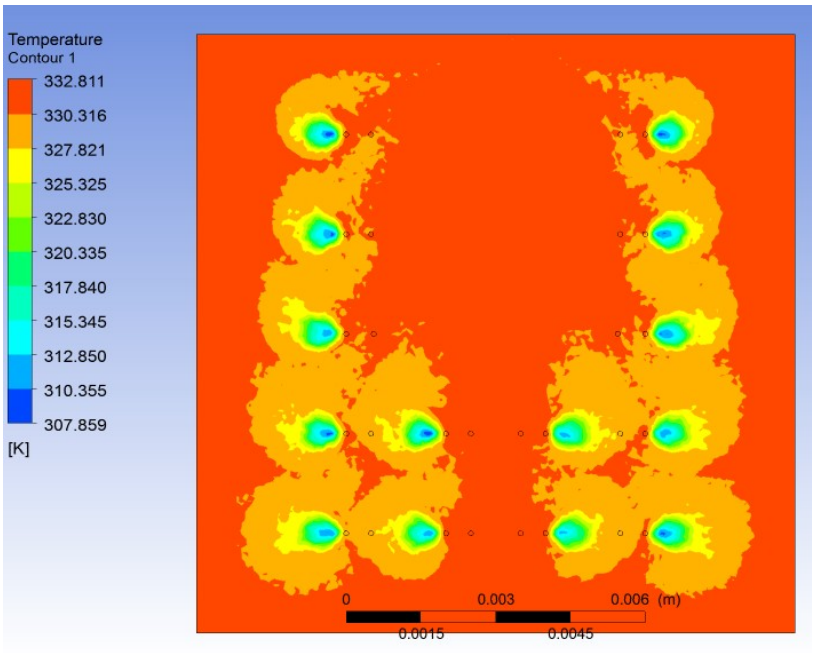


Figure 4.38: Temperature contour at solid-fluid interface across the channel for 14 jet 0.5% $TiO_2$ ¿´¿ = 0.000062 kg/s)

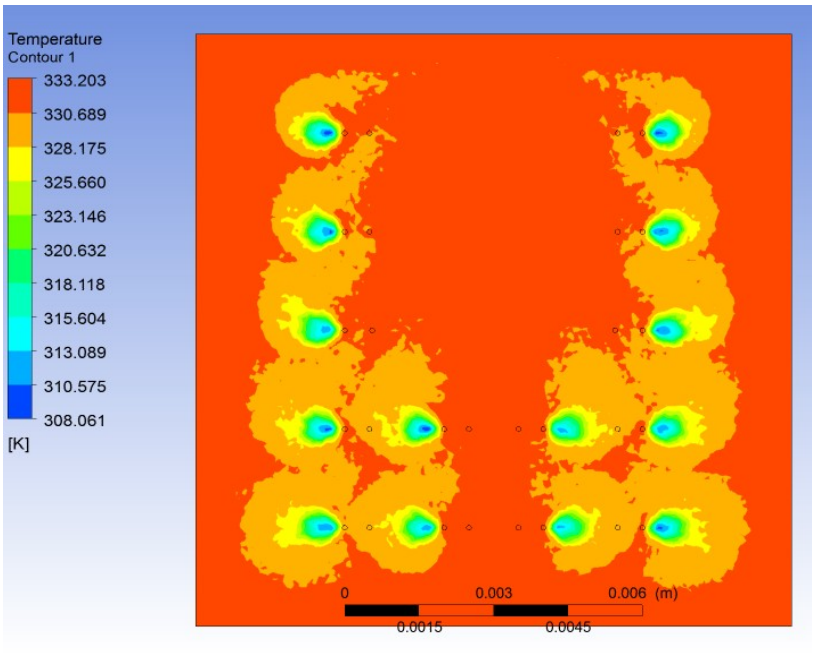


Figure 4.39: Temperature contour at solid-fluid interface across the channel for 14 jet 1% $TiO_2$ ¿´¿ = 0.000062 kg/s)

## 4.14 Results for 14 micro jet impingement heat sink for 0.1%, 0.5%, 1% $TiO_2$ with $\dot{m}$ = 0.000122 kg/s

After simulation, nanofluid (water + 0.1% $TiO_2$) obtained temperature difference of 14.119 K, nanofluid (water + 0.5% $TiO_2$) obtained temperature difference of 14.315 K, nanofluid (water + 1% $TiO_2$) obtained temperature difference of 14.559 K through micro-channel. Figure 4.40, 4.41, 4.42 shows the maximum temperature of 318.786 K, 318.940 K, 319.131 K on the plate for concentration of 0.1%, 0.5%, 1% $TiO_2$ nanoparticle ($\dot{m}$ = 0.000122 kg/s) in water. The maximum temperature of the plate increases with increase in the nanoparticle concentration.

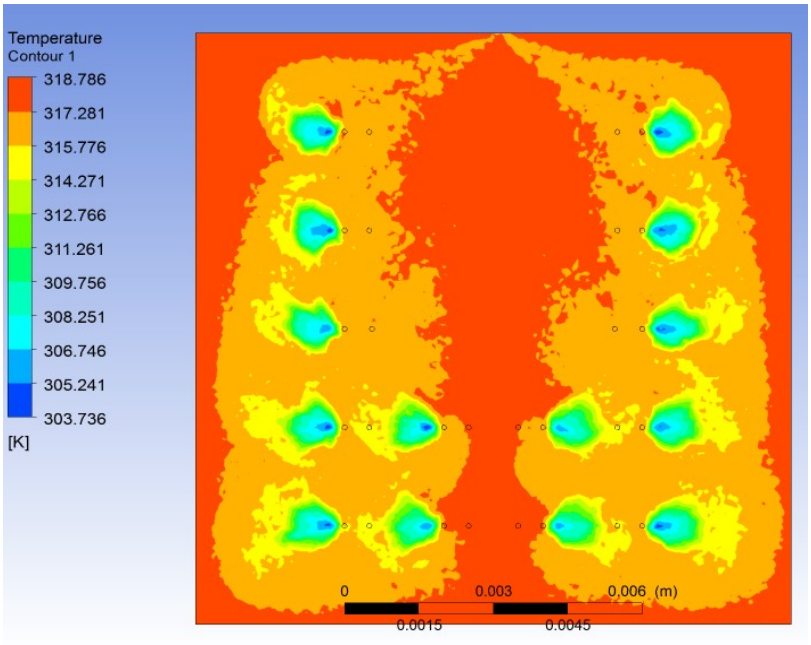


Figure 4.40: Temperature contour at solid-fluid interface across the channel for 14 jet 0.1% $TiO_2$ ¿´¿ = 0.000122 kg/s)

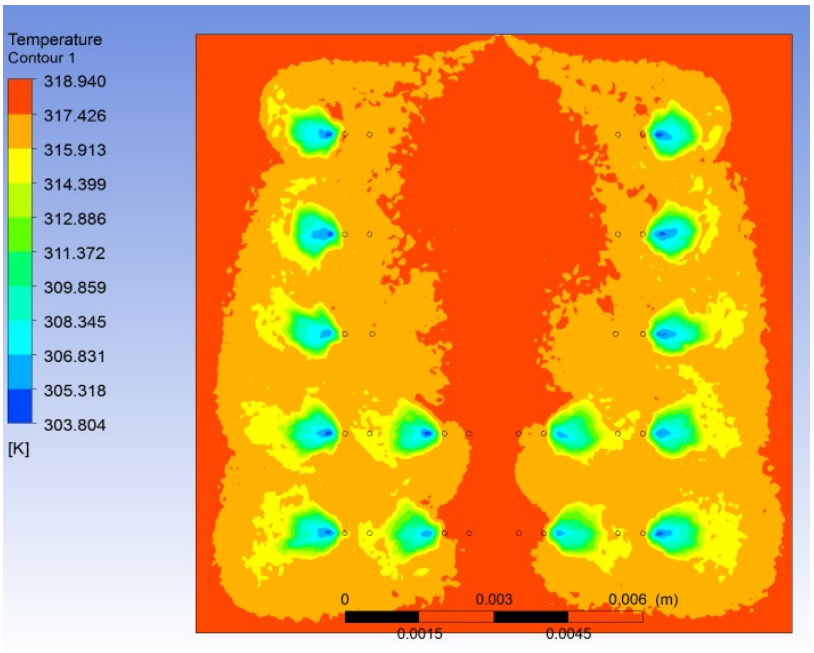


Figure 4.41: Temperature contour at solid-fluid interface across the channel for 14 jet 0.5% $TiO_2$ ¿´¿ = 0.000122 kg/s)

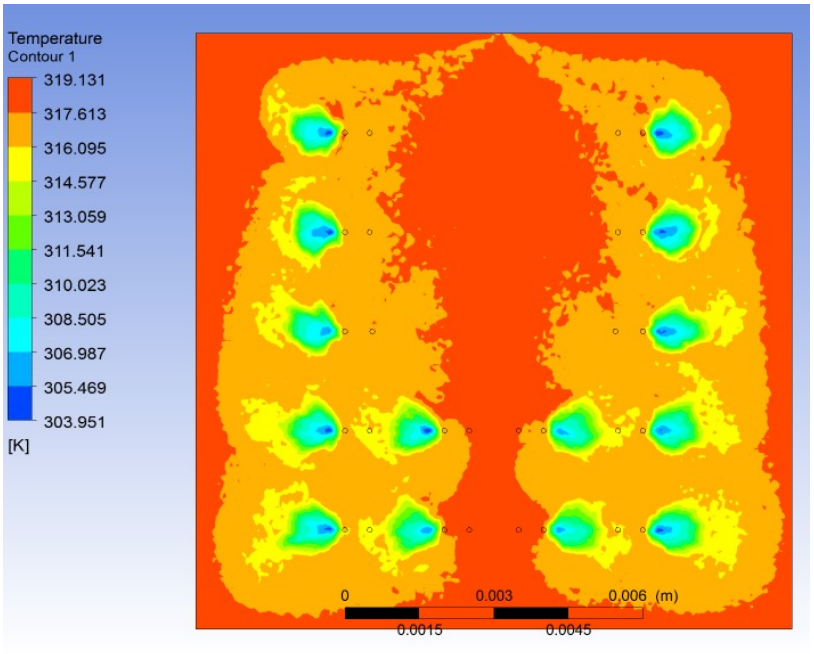


Figure 4.42: Temperature contour at solid-fluid interface across the channel for 14 jet 1% $TiO_2$ ¿´¿ = 0.000122 kg/s)

## 4.15 Results for 14 micro jet impingement heat sink for 0.1%, 0.5%, 1% $TiO_2$ with $\acute{m}$ = 0.000182 kg/s

After simulation, nanofluid (water + 0.1% $TiO_2$) obtained temperature difference of 14.119 K, nanofluid (water + 0.5% $TiO_2$) obtained temperature difference of 14.315 K, nanofluid (water + 1% $TiO_2$) obtained temperature difference of 14.559 K through micro-channel. The maximum temperature of 318.786 K (figure 4.43), 318.940 K (figure 4.44), 319.131 K (figure 4.45) was seen on the plate for concentration of 0.1%, 0.5%, 1% $TiO_2$ nanoparticle ( $\acute{m}$ = 0.000182 kg/s) in water. The maximum temperature of the plate increases with increase in the nanoparticle concentration.

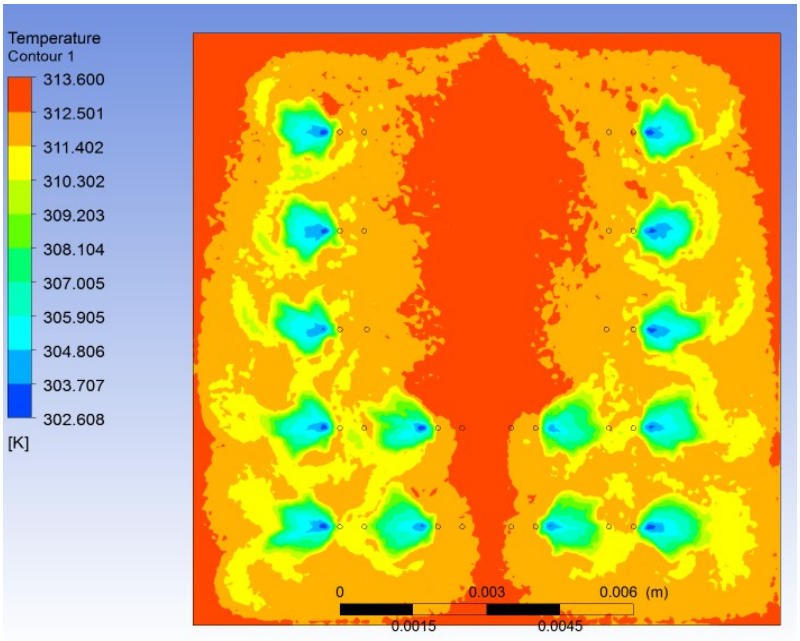


Figure 4.43: Temperature contour at solid-fluid interface across the channel for 14 jet 0.1% $TiO_2$ ¿´¿ = 0.000182 kg/s)

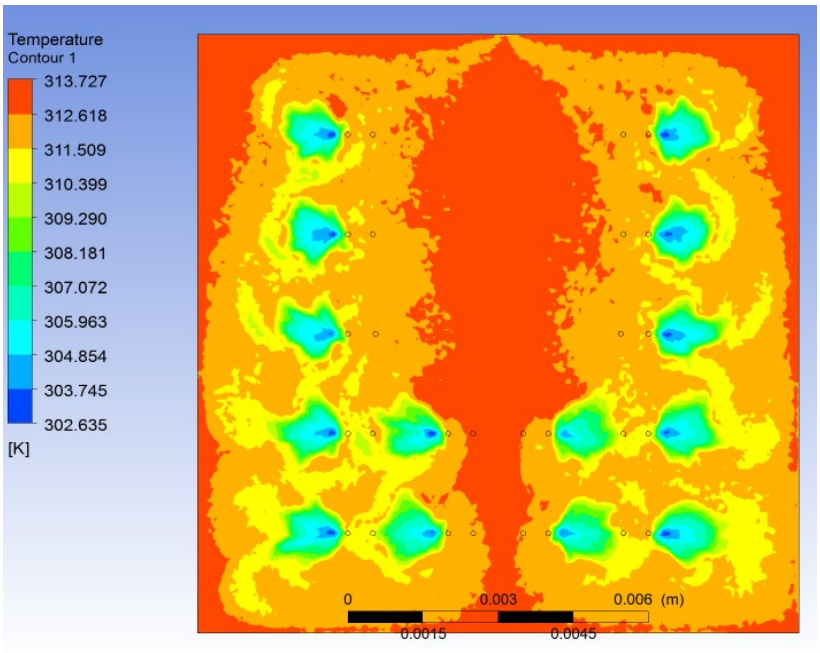


Figure 4.44: Temperature contour at solid-fluid interface across the channel for 14 jet 0.5% $TiO_2$ ¿´¿ = 0.000182 kg/s)

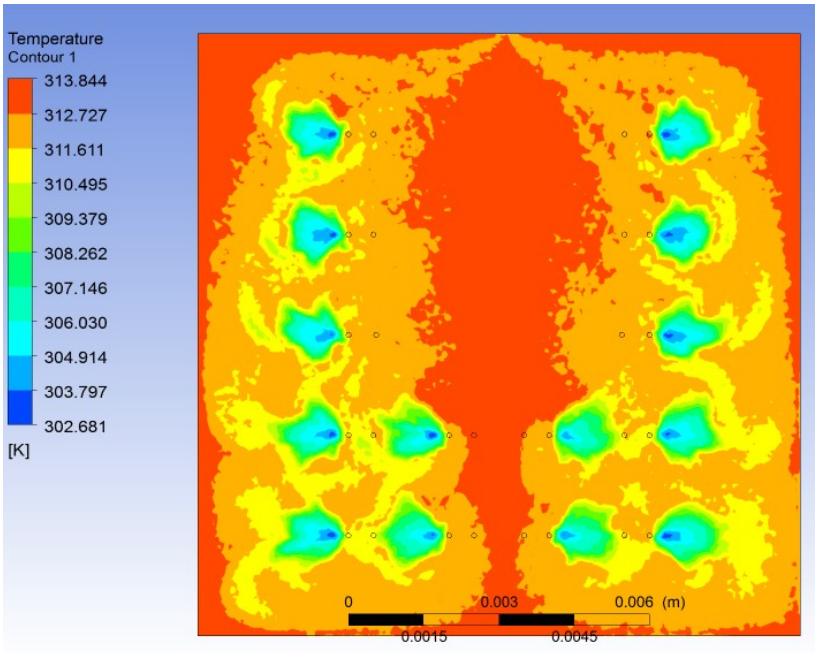


Figure 4.45: Temperature contour at solid-fluid interface across the channel for 14 jet 1% $TiO_2$ ¿´¿ = 0.000182 kg/s)

## 4.16 Results for 14 micro jet impingement heat sink for 0.1%, 0.5%, 1% $Al_2O_3$ with $\acute{m}$ = 0.000062 kg/s

After simulation, nanofluid (water + 0.1% $Al_2O_3$) obtained temperature difference of 27.774 K, nanofluid (water + 0.5% $Al_2O_3$) obtained temperature difference of 28.134 K, nanofluid (water + 1% $Al_2O_3$) obtained temperature difference of 28.585 K through micro-channel. The maximum temperature of 332.491 K (figure 4.46), 332.771 K (figure 4.47), 333.124 K (figure 4.48) was seen on the plate for concentration of 0.1%, 0.5%, 1% $Al_2O_3$ nanoparticle ($\acute{m}$ = 0.000062 kg/s) in water respectively. It was seen that both the average temperature of the plate and bulk mean temperature of nanofluid at the outlet increased with increase in concentration of the nanoparticles.

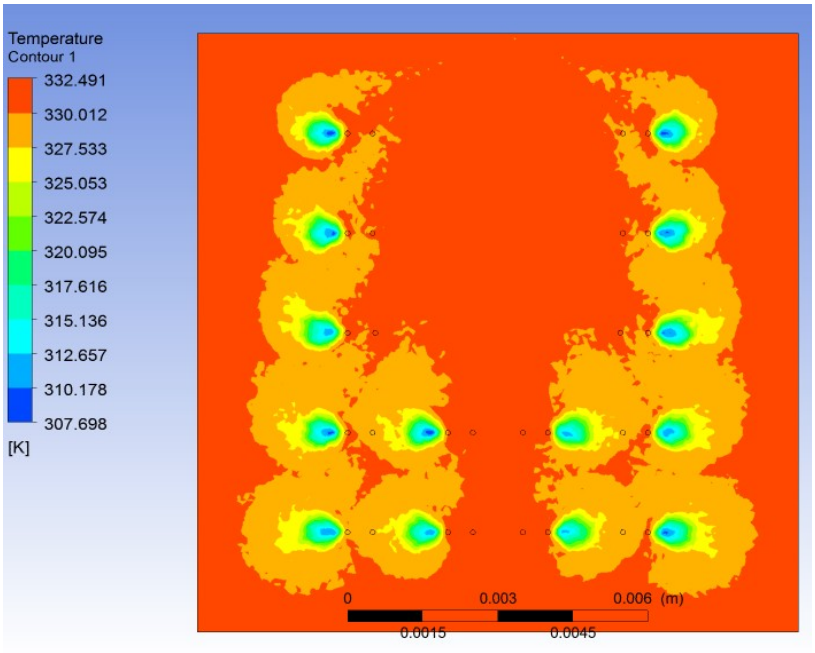


Figure 4.46: Temperature contour at solid-fluid interface across the channel for 14 jet 0.1% $Al_2O_3$ ¿´¿ = 0.000062 kg/s)

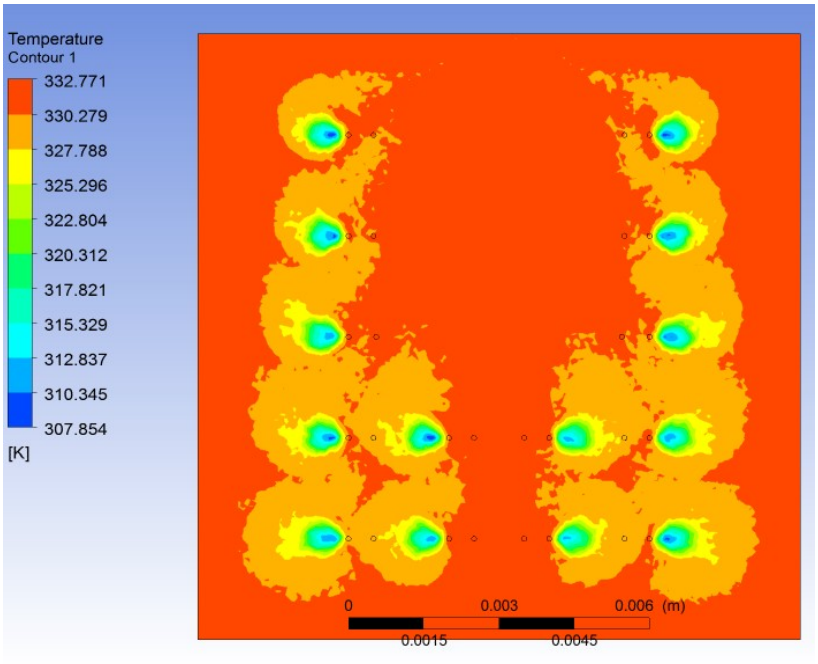


Figure 4.47: Temperature contour at solid-fluid interface across the channel for 14 jet 0.5% $Al_2O_3$ ¿´¿ = 0.000062 kg/s)

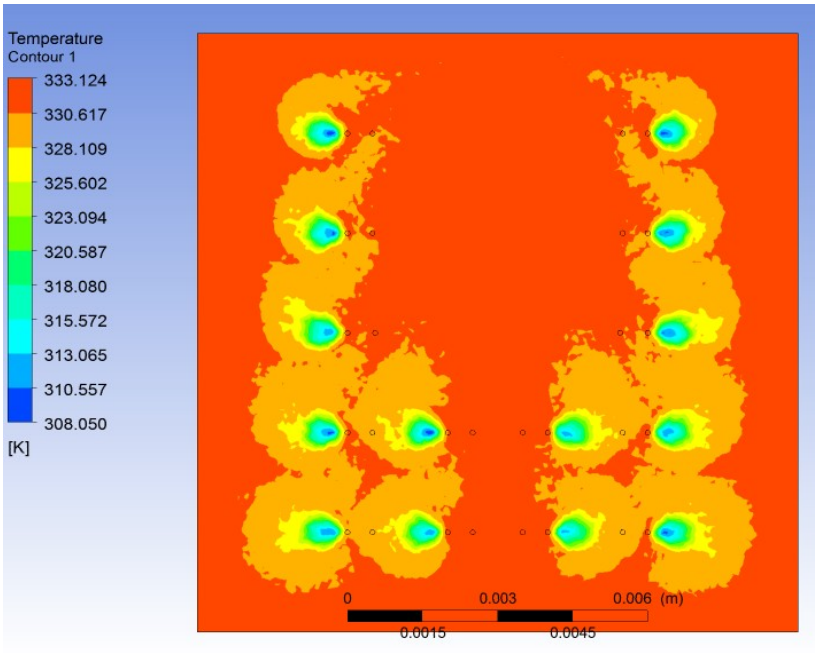


Figure 4.48: Temperature contour at solid-fluid interface across the channel for 14 jet 1% $Al_2O_3$ ¿´¿ = 0.000062 kg/s)

## 4.17 Results for 14 micro jet impingement heat sink for 0.1%, 0.5%, 1% $Al_2O_3$ with $\acute{m}$ = 0.000122 kg/s

Figure 4.49, 4.50, 4.51 shows the interface temperature profile of the plate containing $Al_2O_3$ nanoparticles ($\acute{m}$ = 0.000122 kg/s) at varying concentration of 0.1%, 0.5%, 1% in water. After simulation, nanofluid (water + 0.1% $Al_2O_3$) obtained temperature difference of 14.116 K, nanofluid (water + 0.5% $Al_2O_3$) obtained temperature difference of 14.3 K, nanofluid (water + 1% $Al_2O_3$) obtained temperature difference of 14.53 K through micro-channel. The maximum temperature of 332.491 K, 332.771 K, 333.124 K was obtained at the interface of the plate for concentration of 0.1%, 0.5%, 1% $Al_2O_3$ (nanoparticle) in water respectively. It was seen that both the average temperature of the plate and bulk mean temperature of nanofluid at the outlet increased with increase in concentration of the nanoparticles.

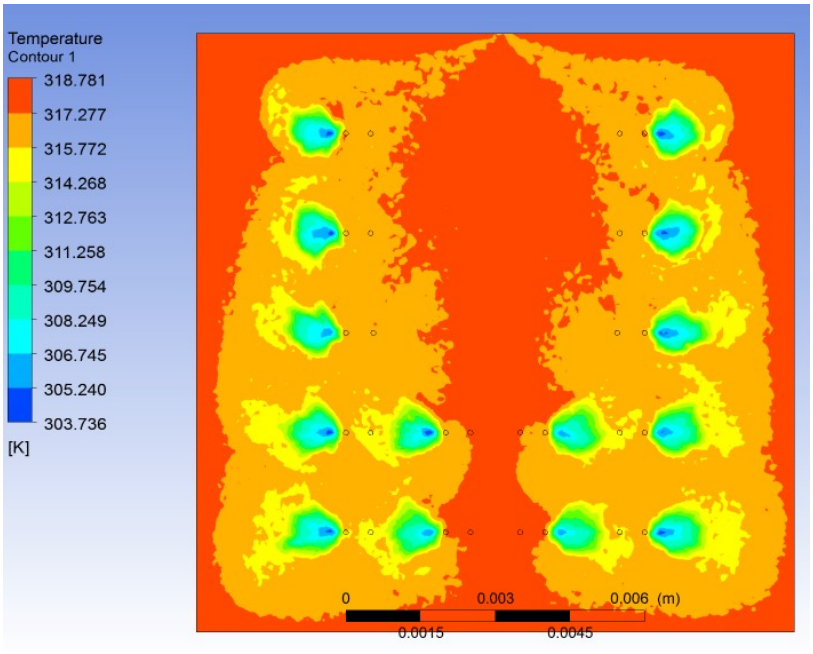


Figure 4.49: Temperature contour at solid-fluid interface across the channel for 14 jet 0.1% $Al_2O_3$ ¿´¿ = 0.000122 kg/s)

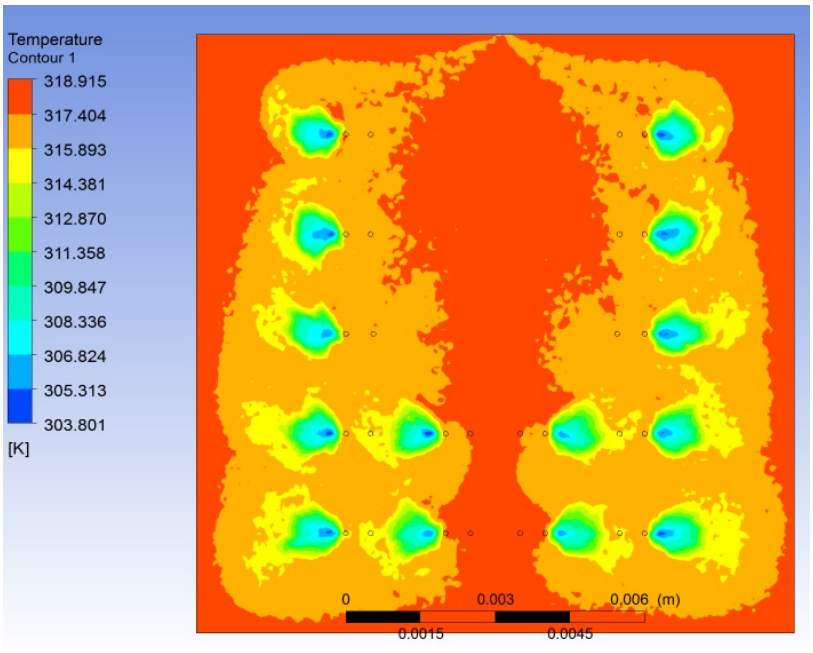


Figure 4.50: Temperature contour at solid-fluid interface across the channel for 14 jet 0.5% $Al_2O_3$ ¿´¿ = 0.000122 kg/s)

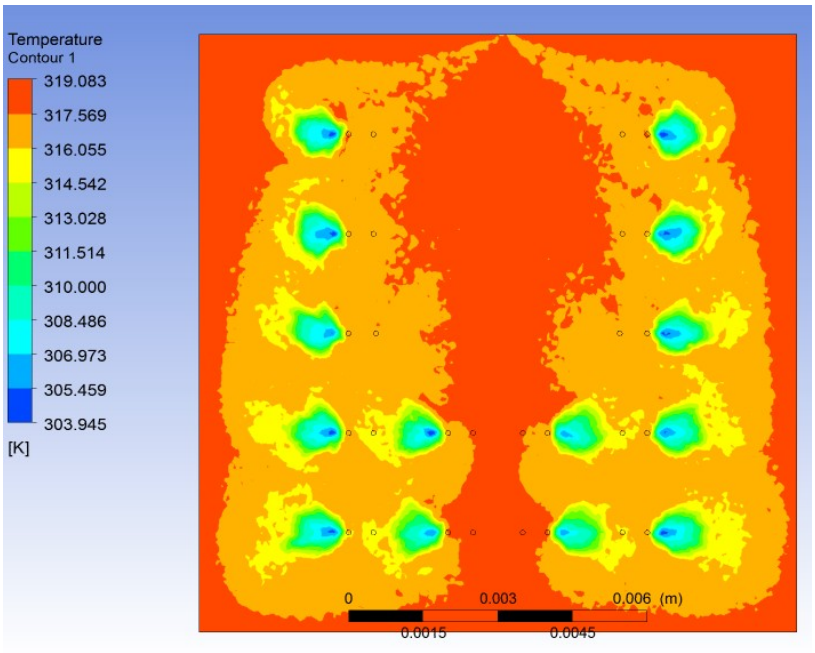


Figure 4.51: Temperature contour at solid-fluid interface across the channel for 14 jet 1% $Al_2O_3$ ¿´¿ = 0.000122 kg/s)

## 4.18 Results for 14 micro jet impingement heat sink for 0.1%, 0.5%, 1%

### $Al_2O_3$ with $\acute{m}$ = 0.000182 kg/s

Figure 4.52, 4.53, 4.54 shows the interface temperature profile of the plate containing $Al_2O_3$ nanoparticles ($\acute{m}$ = 0.000182 kg/s) at varying concentration of 0.1%, 0.5%, 1% in water. After simulation, nanofluid (water + 0.1% $Al_2O_3$) obtained temperature difference of 9.446 K, nanofluid (water + 0.5% $Al_2O_3$) obtained temperature difference of 9.57 K, nanofluid (water + 1% $Al_2O_3$) obtained temperature difference of 9.725 K through micro-channel. The maximum temperature of 313.597 K, 313.690 K, 313.808 K was observed at the interface of the plate for concentration of 0.1%, 0.5%, 1% $Al_2O_3$ (nanoparticle) in water respectively. It was seen that both the average temperature of the plate and bulk mean temperature of nanofluid at the outlet increased with increase in concentration of the nanoparticles.

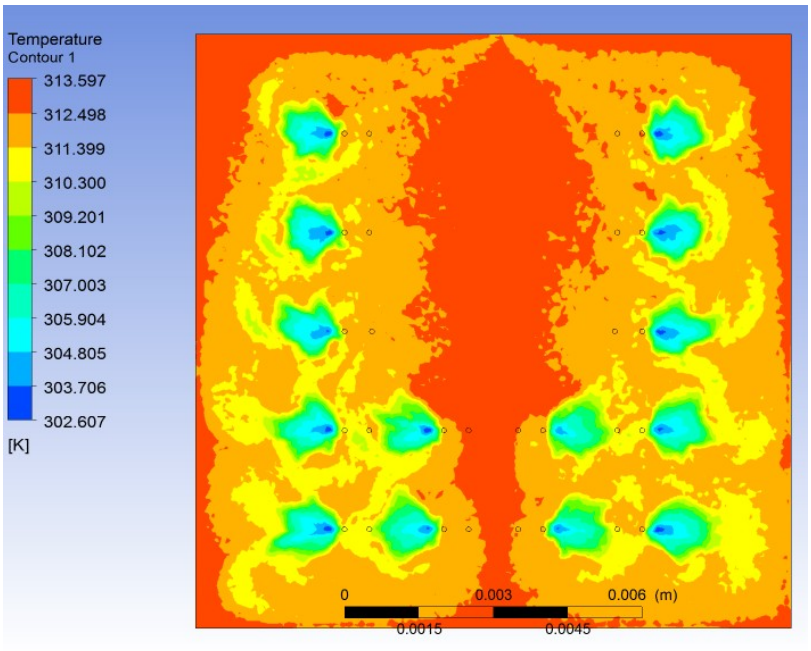


Figure 4.52: Temperature contour at solid-fluid interface across the channel for 14 jet 0.1% $Al_2O_3$ ¿´¿ = 0.000122 kg/s)

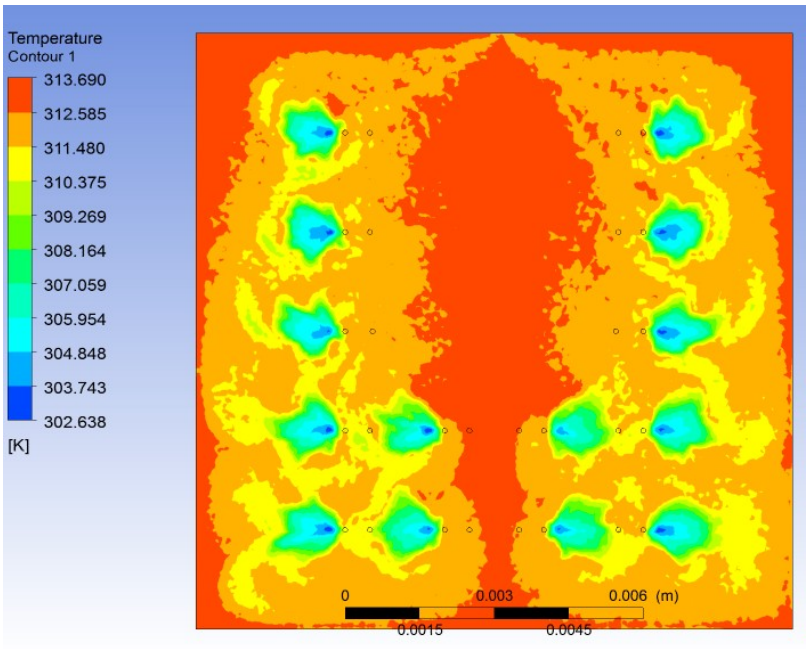


Figure 4.53: Temperature contour at solid-fluid interface across the channel for 14 jet 0.5% $Al_2O_3$ ¿´¿ = 0.000122 kg/s)

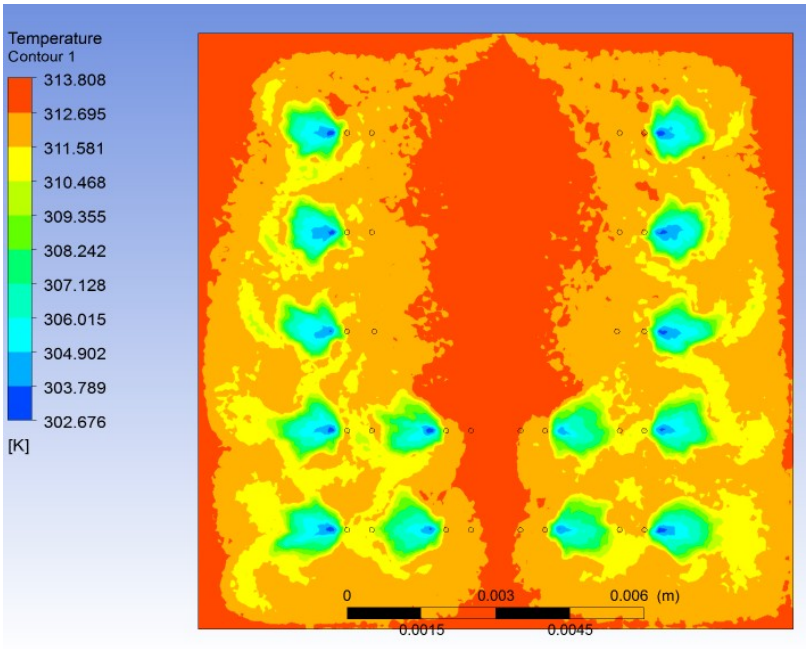


Figure 4.54: Temperature contour at solid-fluid interface across the channel for 14 jet 1% $Al_2O_3$ ¿´¿ = 0.000122 kg/s)

## 4.19 Results for 18 micro jet impingement heat sink for 0.1%, 0.5%, 1% $TiO_2$ with $\acute{m}$ = 0.000062 kg/s

After simulation, nanofluid (water + 0.1% $TiO_2$) obtained temperature difference of 28.017 K, nanofluid (water + 0.5% $TiO_2$) obtained temperature difference of 28.401 K, nanofluid (water + 1% $TiO_2$) obtained temperature difference of 28.881 K through micro-channel. The 18 jet arrangement used during simulation showed better results than 14 jet arrangement. This showed that for same mass flow rate heat transfer rate increased with increased in the number of jets. The maximum temperature of 333.721 K (figure 4.55), 334.041 K (figure 4.56), 334.444 K (figure 4.57) was observed at the interface of the plate for concentration of 0.1%, 0.5%, 1% $TiO_2$ nanoparticle ($\acute{m}$ = 0.000062 kg/s) in water.

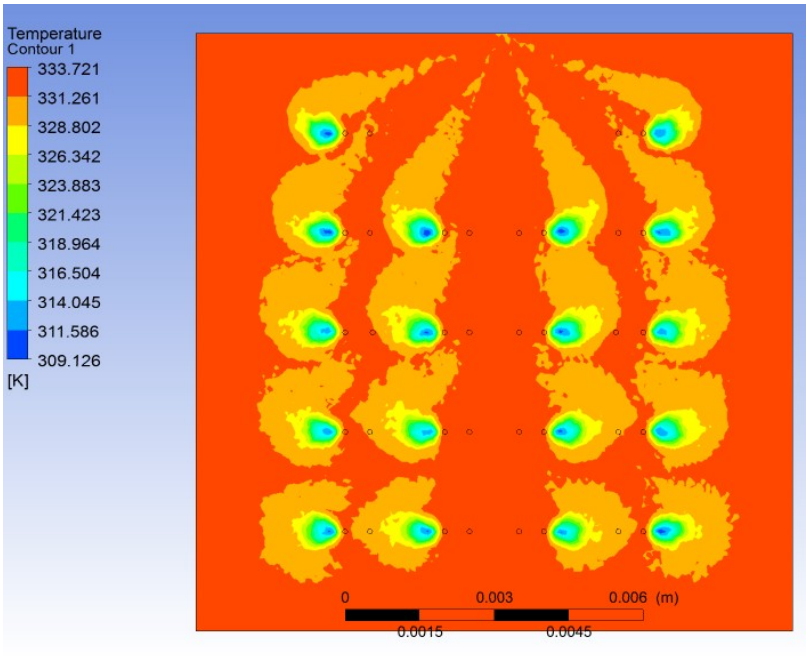


Figure 4.55: Temperature contour at solid-fluid interface across the channel for 18 jet 0.1% $TiO_2$ ¿´¿ = 0.000062 kg/s)

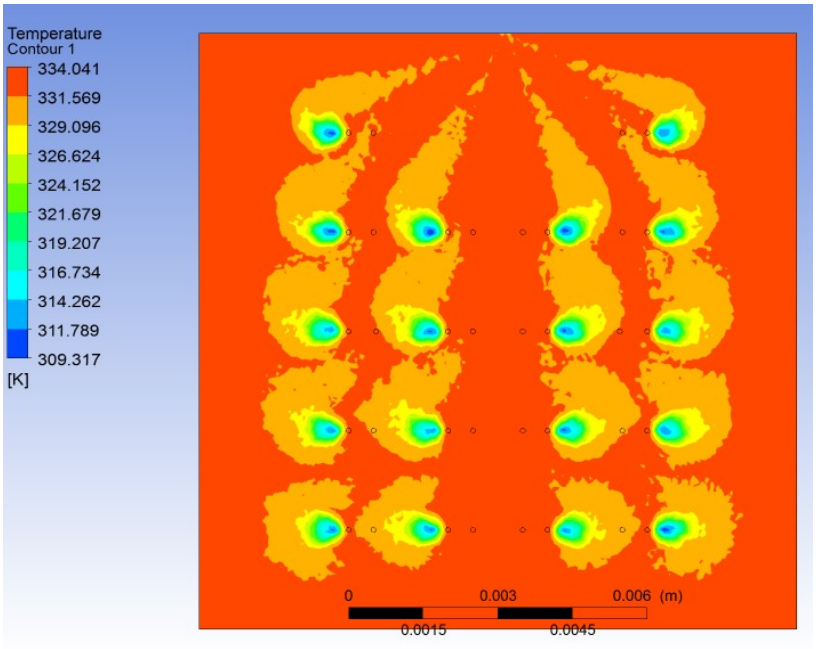


Figure 4.56: Temperature contour at solid-fluid interface across the channel for 18 jet 0.5% $TiO_2$ ¿´¿ = 0.000062 kg/s)

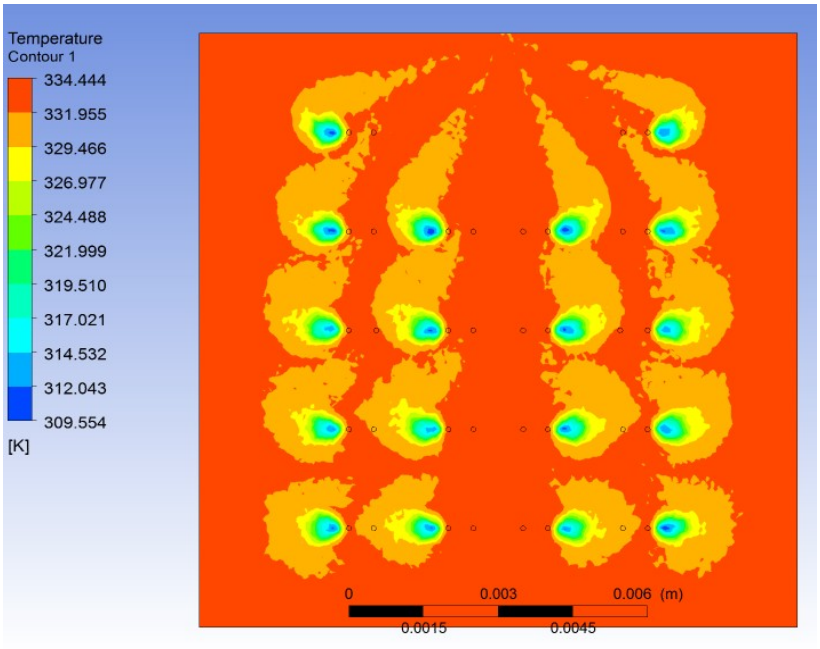


Figure 4.57: Temperature contour at solid-fluid interface across the channel for 18 jet 1% $TiO_2$ ¿´¿ = 0.000062 kg/s)

## 4.20 Results for 18 micro jet impingement heat sink for 0.1%, 0.5%, 1% $TiO_2$ with $\acute{m}$ = 0.000122 kg/s

After simulation, nanofluid (water + 0.1% $TiO_2$) obtained temperature difference of 14.288 K, nanofluid (water + 0.5% $TiO_2$) obtained temperature difference of 14.484 K, nanofluid (water + 1% $TiO_2$) obtained temperature difference of 14.73 K through micro-channel. Figure 4.58, 4.59, 4.60 shows maximum temperature of 319.505 K, 319.662 K, 319.858 K for concentration of 0.1%, 0.5%, 1% $TiO_2$ nanoparticle ($\acute{m}$ = 0.000122 kg/s) in water. The maximum temperature of the plate increases with increase in the nanoparticle concentration.

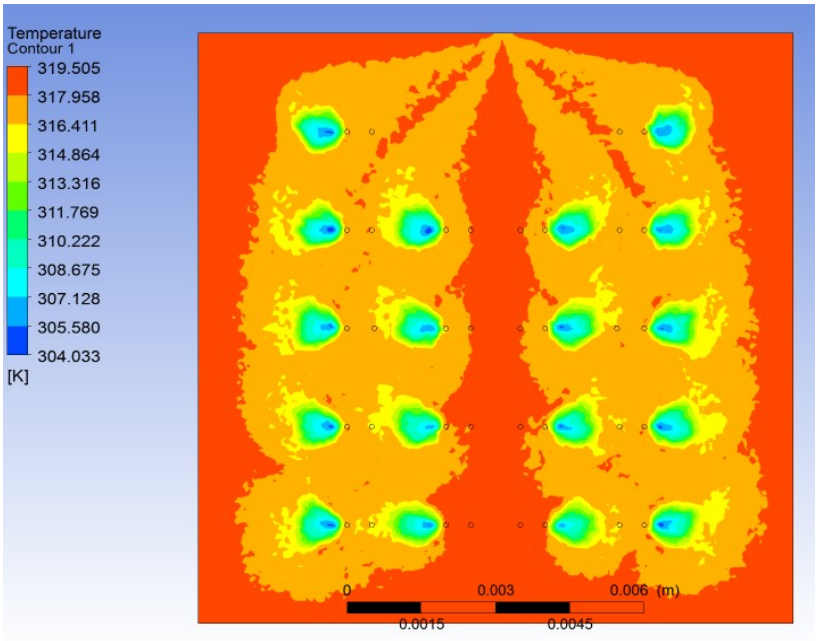


Figure 4.58: Temperature contour at solid-fluid interface across the channel for 18 jet 0.1% $TiO_2$ ¿´¿ = 0.000122 kg/s)

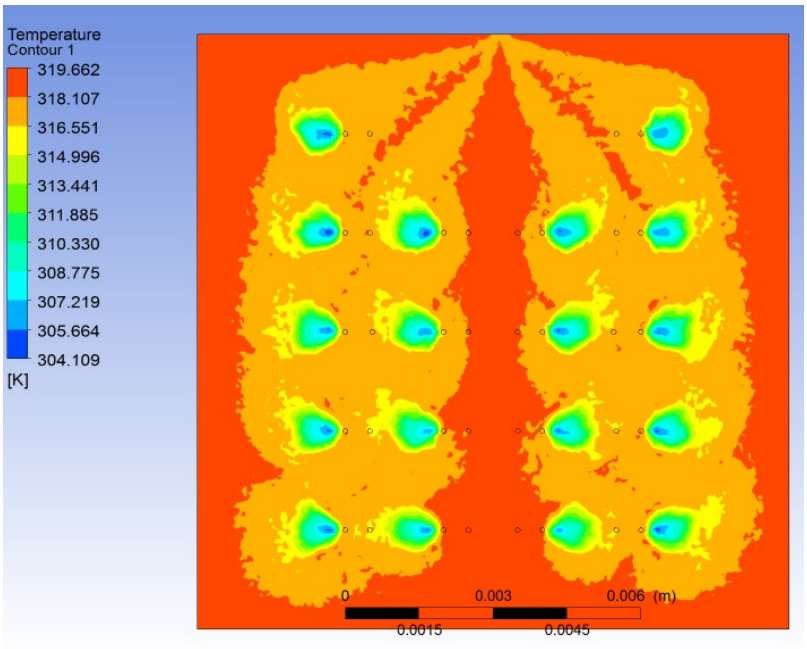


Figure 4.59: Temperature contour at solid-fluid interface across the channel for 18 jet 0.5% $TiO_2$ ¿´¿ = 0.000122 kg/s)

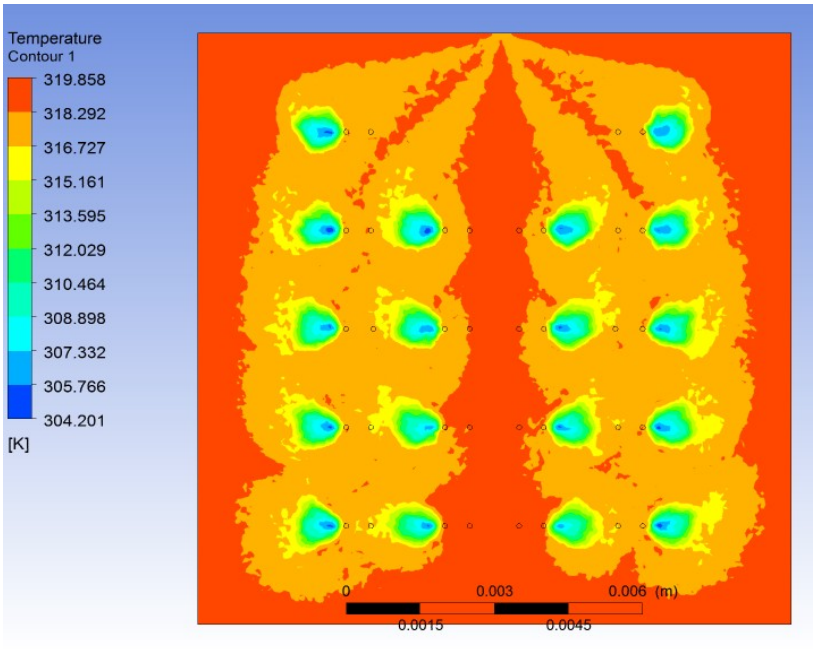


Figure 4.60: Temperature contour at solid-fluid interface across the channel for 18 jet 1% $TiO_2$ ¿´¿ = 0.000122 kg/s)

## 4.21 Results for 18 micro jet impingement heat sink for 0.1%, 0.5%, 1% $TiO_2$ with $\acute{m}$ = 0.000182 kg/s

Figure 4.61, 4.62, 4.63 shows the interface temperature profile of the plate containing $TiO_2$ nanoparticles ($\acute{m}$ = 0.000182 kg/s) at varying concentration of 0.1%, 0.5%, 1% in water. After simulation, nanofluid (water + 0.1% $TiO_2$) obtained temperature difference of 9.568 K, nanofluid (water + 0.5% $TiO_2$) obtained temperature difference of 9.701 K, nanofluid (water + 1% $TiO_2$) obtained temperature difference of 9.867 K through micro-channel. The maximum temperature of 314.180 K, 314.290 K, 314.427 K was obtained at the interface of plate for concentration of 0.1%, 0.5%, 1% $TiO_2$ (nanoparticle). The maximum temperature of the plate increases with increase in the nanoparticle concentration.

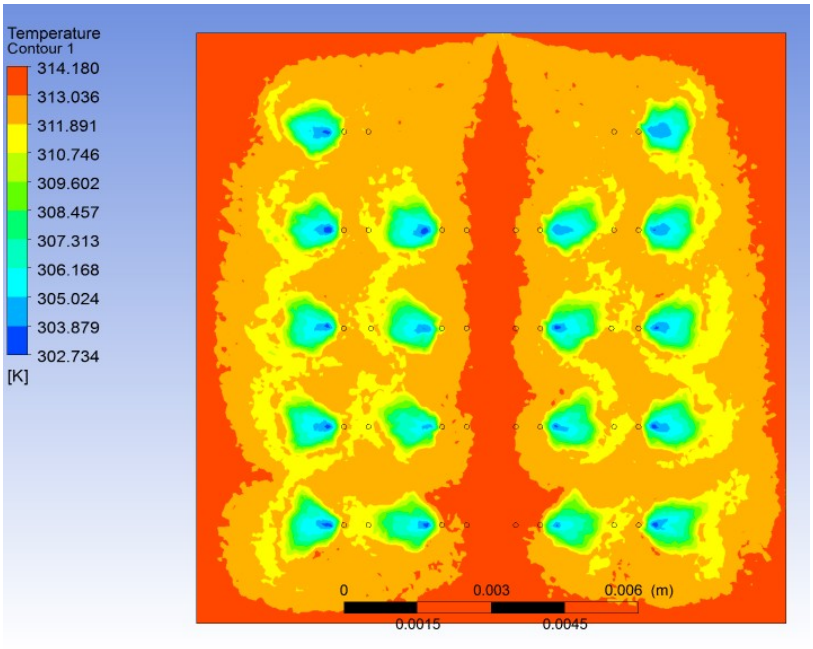


Figure 4.61: Temperature contour at solid-fluid interface across the channel for 18 jet 0.1% $TiO_2$ ¿´¿ = 0.000182 kg/s)

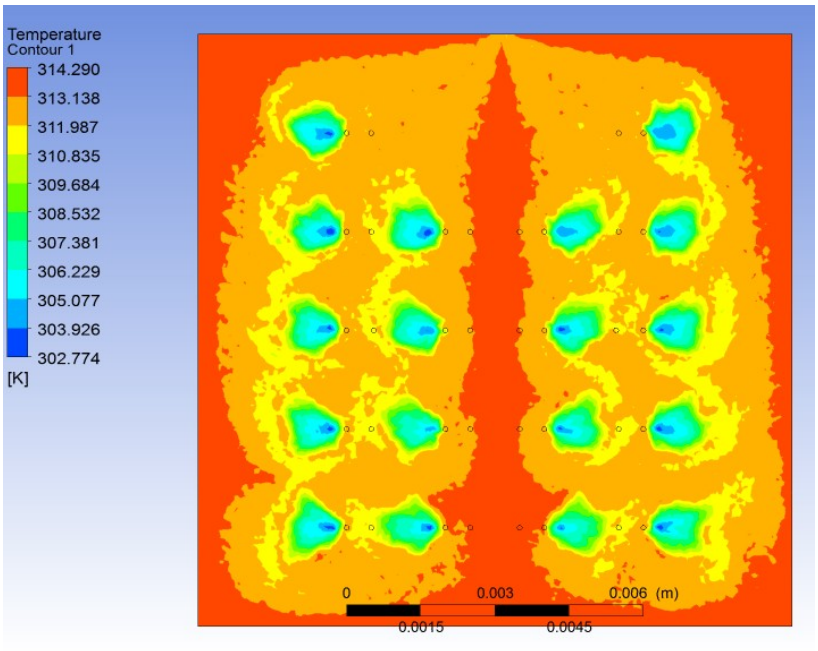


Figure 4.62: Temperature contour at solid-fluid interface across the channel for 18 jet 0.5% $TiO_2$ ¿´¿ = 0.000182 kg/s)

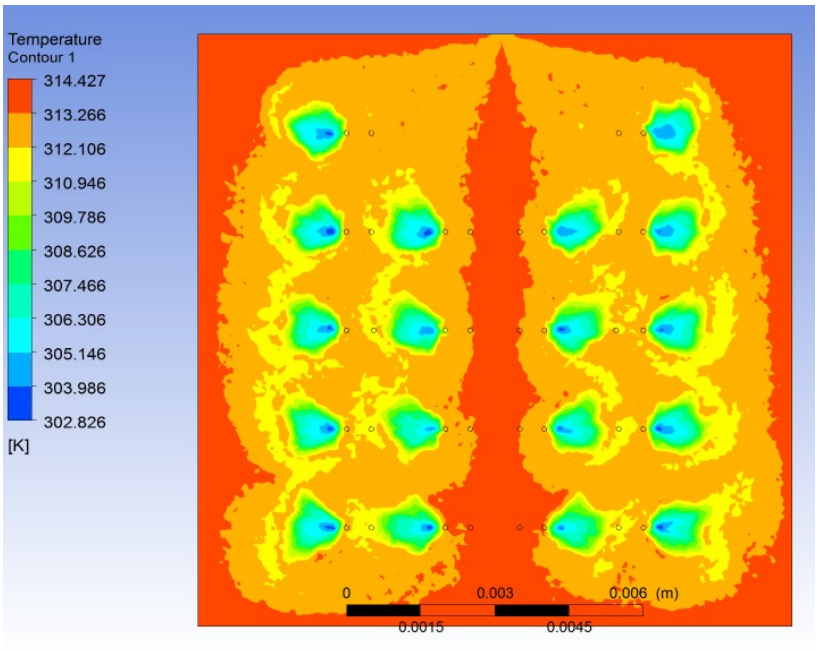


Figure 4.63: Temperature contour at solid-fluid interface across the channel for 18 jet 1% $TiO_2$ ¿´¿ = 0.000182 kg/s)

## 4.22 Results for 18 micro jet impingement heat sink for 0.1%, 0.5%, 1% $Al_2O_3$ with $\acute{m}$ = 0.000062 kg/s

After simulation, nanofluid (water + 0.1% $Al_2O_3$) obtained temperature difference of 28.011 K, nanofluid (water + 0.5% $Al_2O_3$) obtained temperature difference of 28.371 K, nanofluid (water + 1% $Al_2O_3$) obtained temperature difference of 28.822 K through micro-channel. The maximum temperature of 333.713 K (Figure 4.64), 334 K (Figure 4.65), 334.361 K (Figure 4.66) was observed on the plate for concentration of 0.1%, 0.5%, 1% $Al_2O_3$ nanoparticle ($\acute{m}$ = 0.000062 kg/s) in water respectively. It was seen that both the average temperature of the plate and bulk mean temperature of nanofluid at the outlet increased with increase in concentration of the nanoparticles.

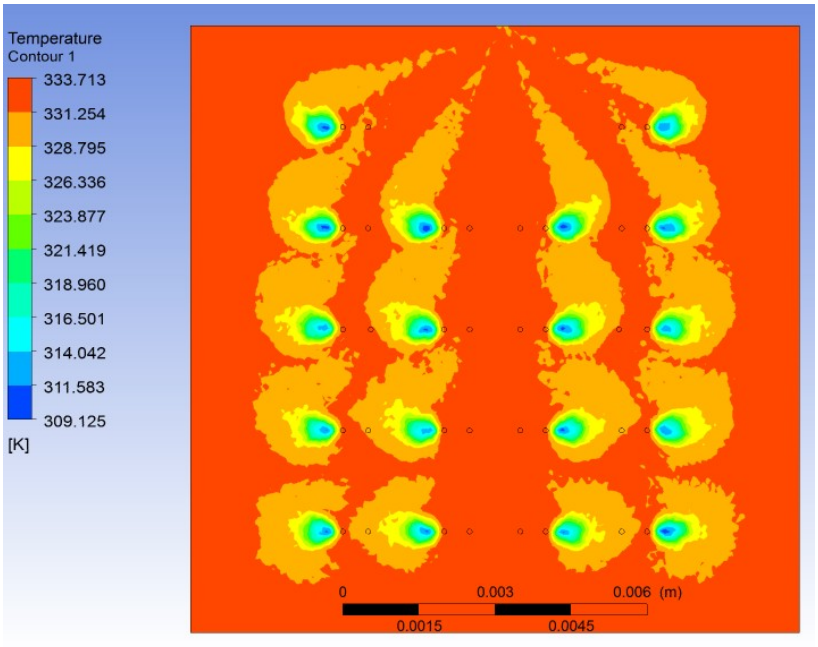


Figure 4.64: Temperature contour at solid-fluid interface across the channel for 18 jet 0.1% $Al_2O_3$ ¿´¿ = 0.000062 kg/s)

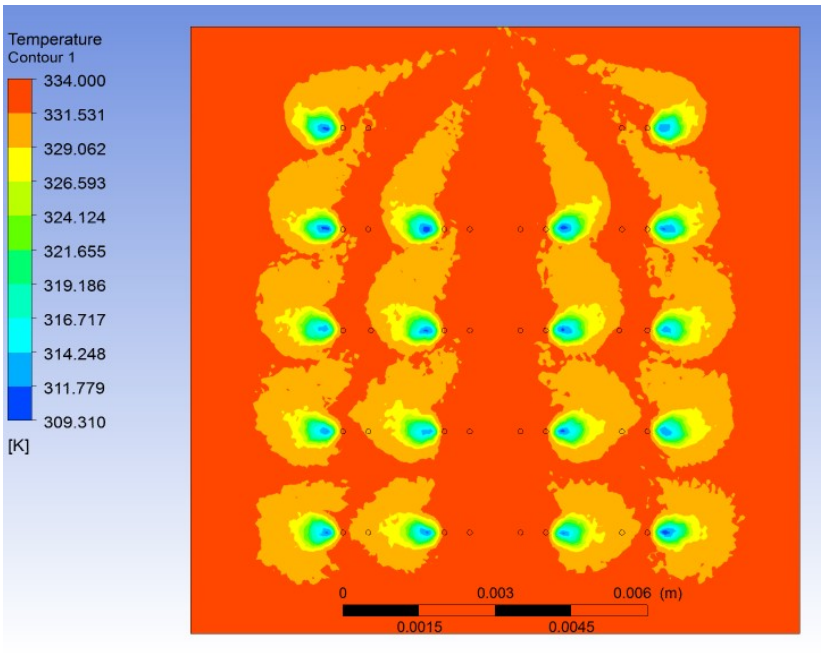


Figure 4.65: Temperature contour at solid-fluid interface across the channel for 18 jet 0.5% $Al_2O_3$ ¿´¿ = 0.000062 kg/s)

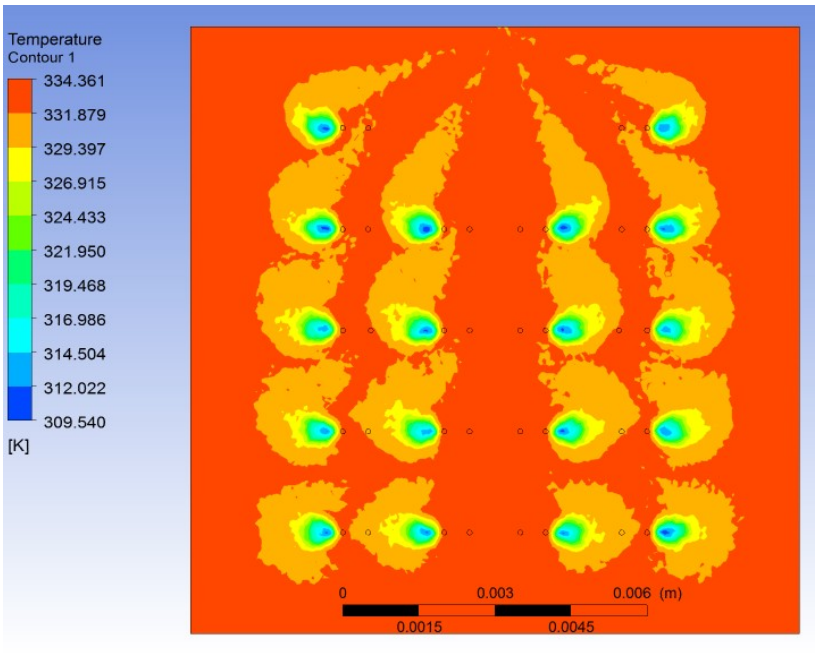


Figure 4.66: Temperature contour at solid-fluid interface across the channel for 18 jet 1% $Al_2O_3$ ¿´¿ = 0.000062 kg/s)

## 4.23 Results for 18 micro jet impingement heat sink for 0.1%, 0.5%, 1%

### $Al_2O_3$ with $\acute{m}$ = 0.000122 kg/s

After simulation, nanofluid (water + 0.1% $Al_2O_3$) obtained temperature difference of 14.285 K, nanofluid (water + 0.5% $Al_2O_3$) obtained temperature difference of 14.468 K, nanofluid (water + 1% $Al_2O_3$) obtained temperature difference of 14.699 K through micro-channel. The maximum temperature of 319.5 K (Figure 4.67), 319.637 K (Figure 4.68), 319.808 K (Figure 4.69) was observed at the interface of the plate for concentration of 0.1%, 0.5%, 1% $Al_2O_3$ nanoparticle. It was seen that both the average temperature of the plate and bulk mean temperature of nanofluid at the outlet increased with increase in concentration of the nanoparticles.

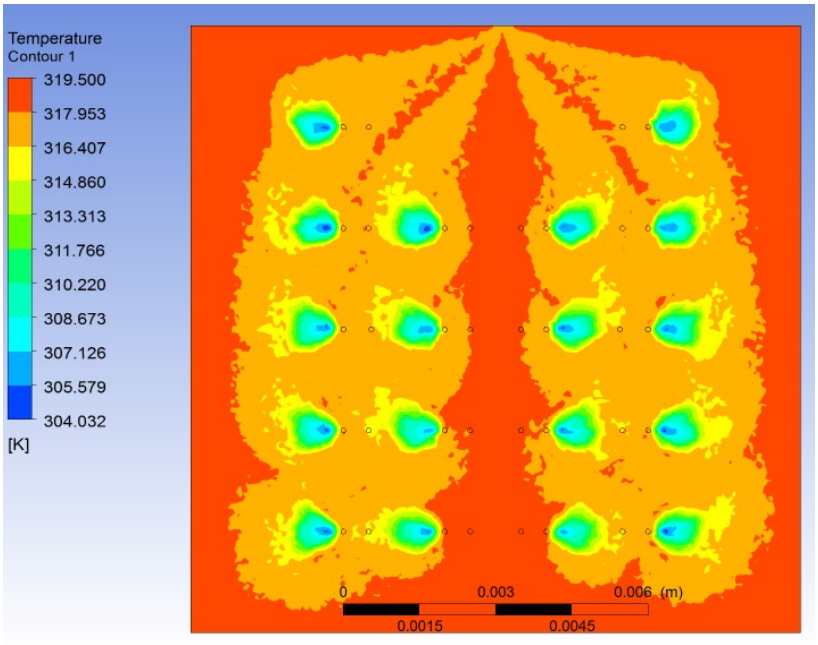


Figure 4.67: Temperature contour at solid-fluid interface across the channel for 18 jet 0.1% $Al_2O_3$ ¿´¿ = 0.000122 kg/s)

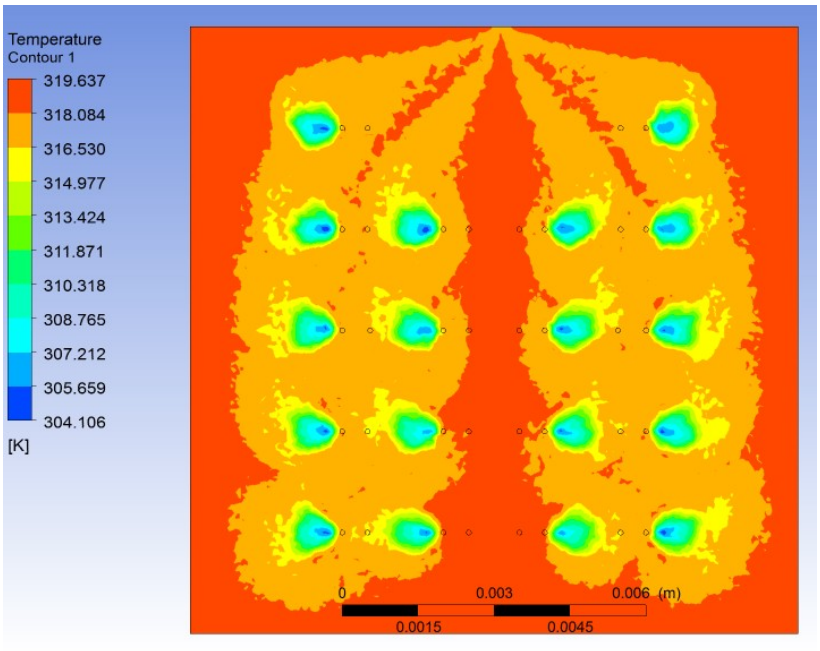


Figure 4.68: Temperature contour at solid-fluid interface across the channel for 18 jet 0.5% $Al_2O_3$ $Al_2O_3$ ¿´¿ = 0.000122 kg/s)

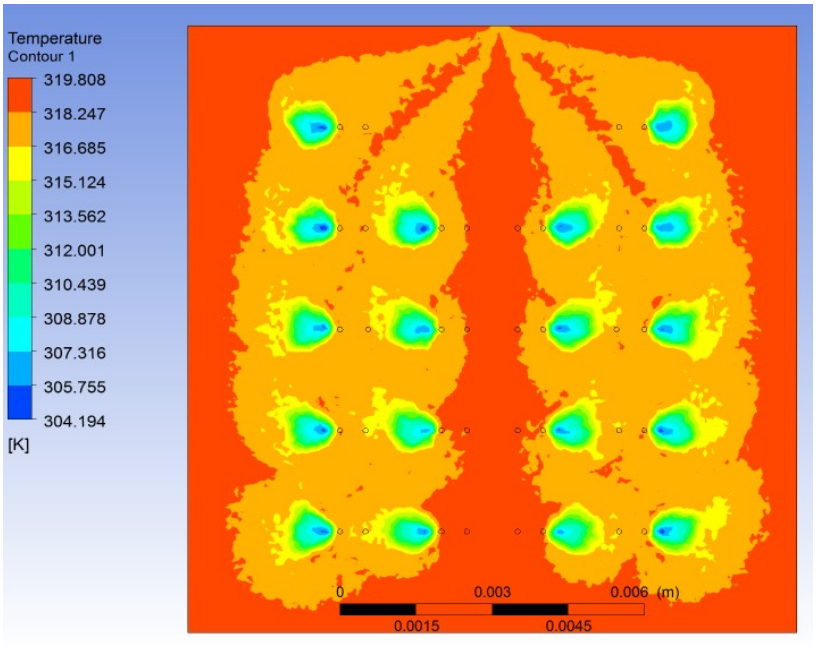


Figure 4.69: Temperature contour at solid-fluid interface across the channel for 18 jet 1% $Al_2O_3$ ¿´¿ = 0.000122 kg/s)

## 4.24 Results for 18 micro jet impingement heat sink for 0.1%, 0.5%, 1%

### $Al_2O_3$ with $\acute{m}$ = 0.000182 kg/s

Figure 4.61, 4.62, 4.63 shows the interface temperature profile of the plate containing $Al_2O_3$ nanoparticles ($\acute{m}$ = 0.000182 kg/s) at varying concentration of 0.1%, 0.5%, 1% in water. After simulation, nanofluid (water + 0.1% $Al_2O_3$) obtained temperature difference of 9.566 K, nanofluid (water + 0.5% $Al_2O_3$) obtained temperature difference of 9.691 K, nanofluid (water + 1% $Al_2O_3$) obtained temperature difference of 9.848 K through micro-channel. The maximum temperature of 314.178 K, 314.271 K, 314.389 K was seen on the plate for arrangement with concentration of 0.1%, 0.5%, 1% $Al_2O_3$ (nanoparticle) in water respectively. It was seen that both the average temperature of the plate and bulk mean temperature of nanofluid at the outlet increased with increase in concentration of the nanoparticles.

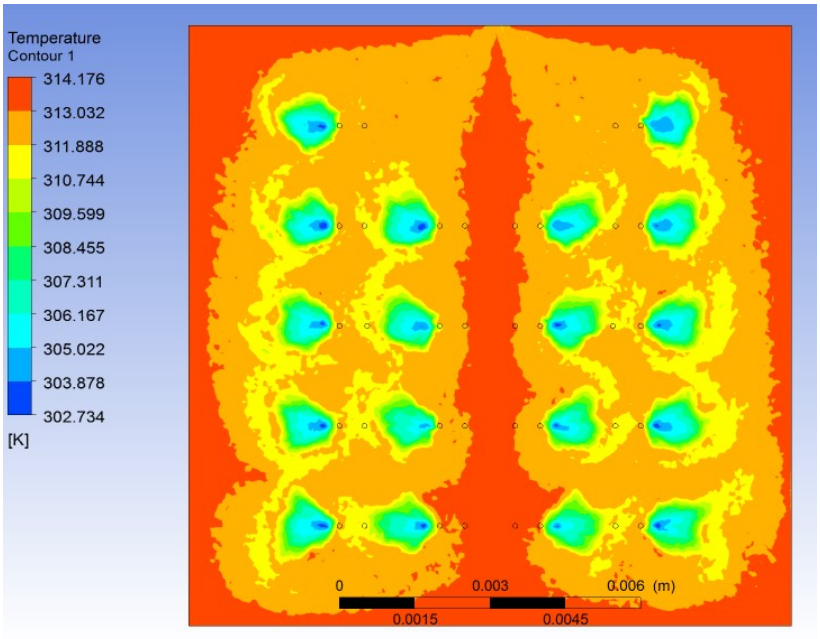


Figure 4.70: Temperature contour at solid-fluid interface across the channel for 18 jet 0.1% $Al_2O_3$ ¿´¿ = 0.000182 kg/s)

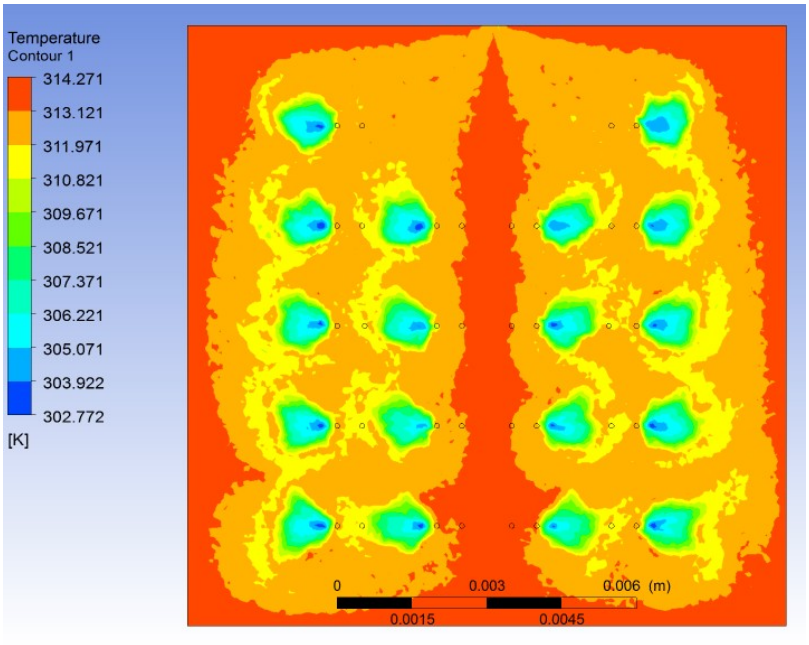


Figure 4.71: Temperature contour at solid-fluid interface across the channel for 18 jet 0.5% $Al_2O_3$ ¿´¿ = 0.000182 kg/s)

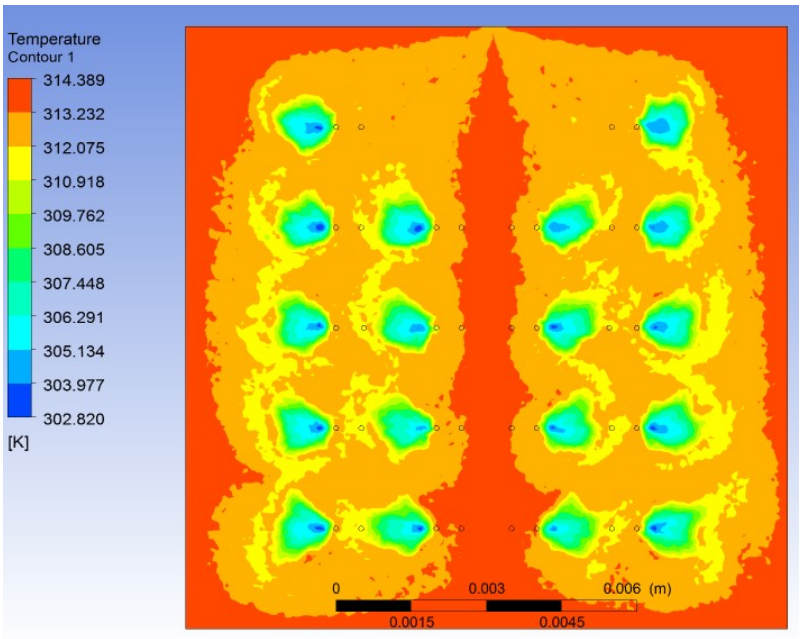


Figure 4.72: Temperature contour at solid-fluid interface across the channel for 18 jet 1% $Al_2O_3$ ¿´¿ = 0.000182 kg/s)

## 4.25 Variation of bulk mean temperature at outlet with no. of jets

In figure 4.73 – 4.78, it was observed that bulk mean temperature of nanofluid at the outlet increased with increase in concentration of the nanoparticles and the number of jets. The 18 jet arrangement used during the simulation showed maximum bulk mean temperature at the outlet for all the arrangements of mass flow rate. When mass flow rate was varied keeping number of jets constant than bulk mean temperature at outlet decreased thus decreasing the heat transfer rate. This showed that for same mass flow rate heat transfer rate increased with increased number of jets.

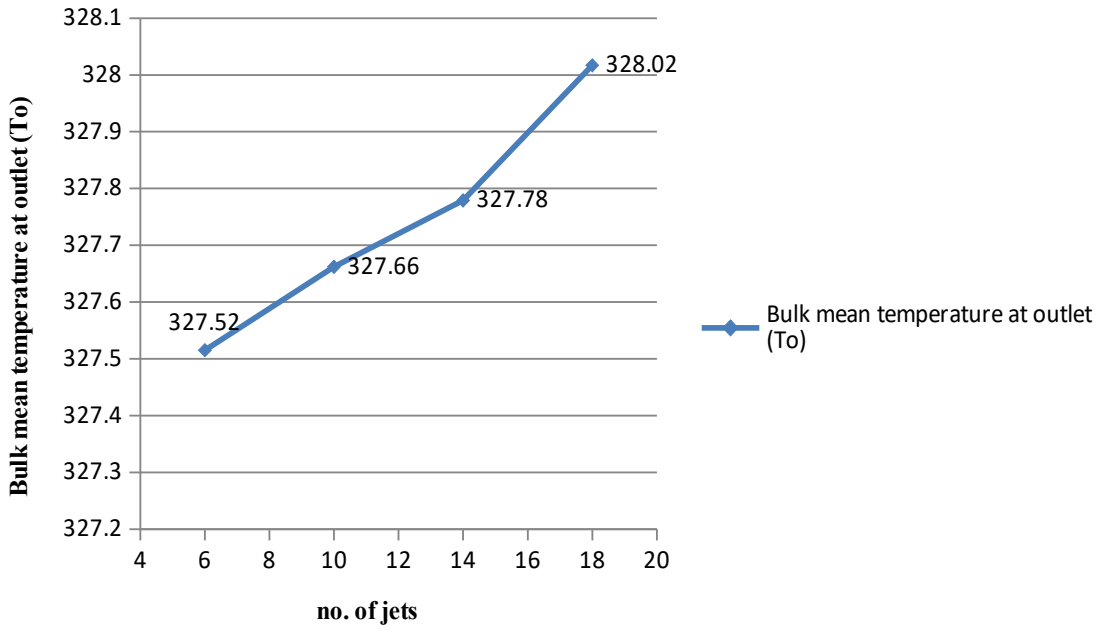


Figure 4.73: Variation of bulk mean temperature at outlet ($T_o$) with no. of jets for $\dot{m}$ = 0.000062 kg/s (water + 0.1 % $TiO_2$)

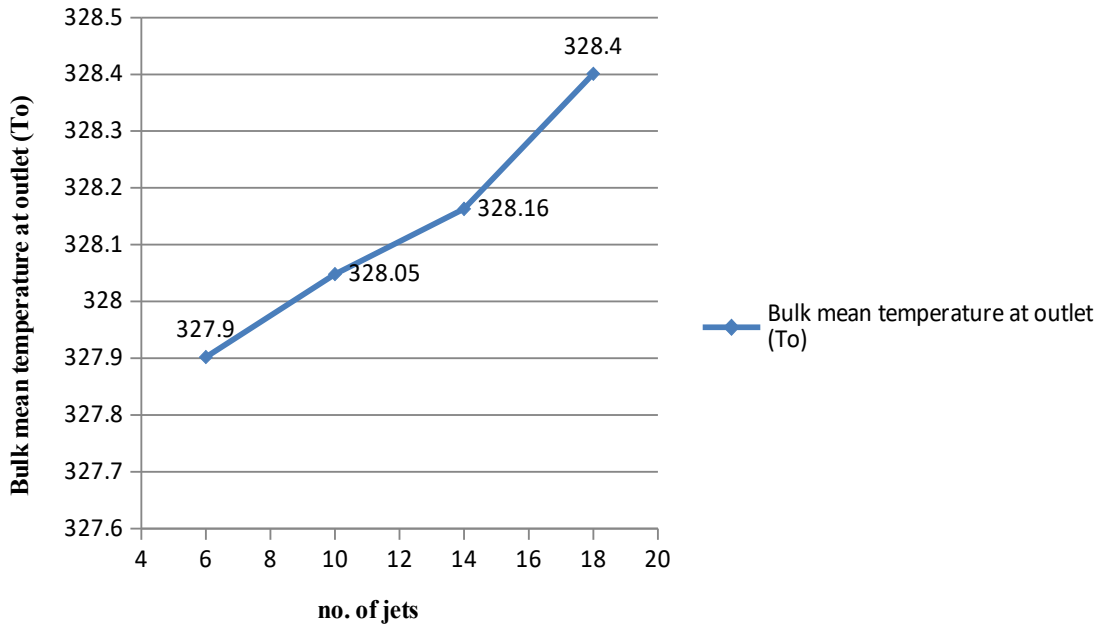


Figure 4.74: Variation of bulk mean temperature at outlet ($T_o$) with no. of jets for $\dot{m}$ = 0.000062 kg/s (water + 0.5 % $TiO_2$)

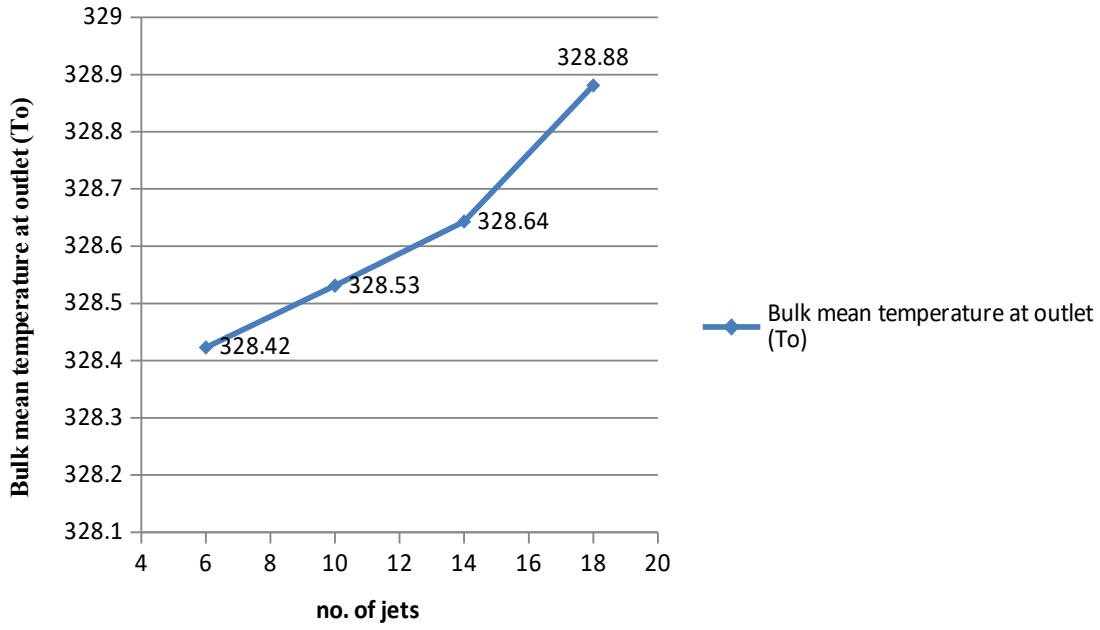


Figure 4.75: Variation of bulk mean temperature at outlet ($T_o$) with no. of jets for $\dot{m}$ = 0.000062 kg/s (water + 1 % $TiO_2$)

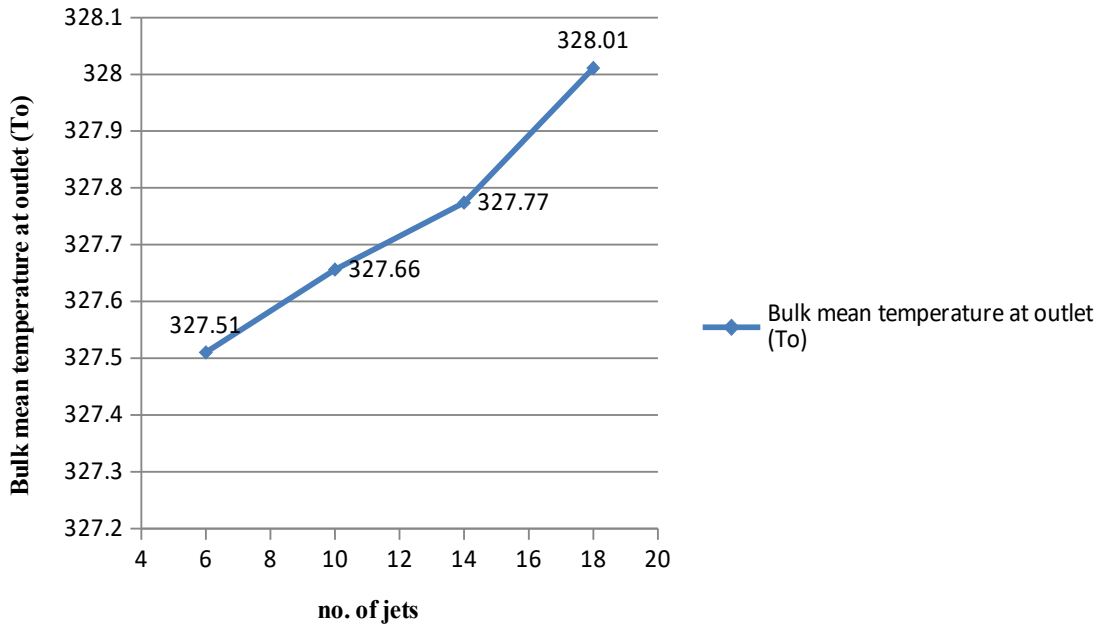


Figure 4.76: Variation of bulk mean temperature at outlet ($T_o$) with no. of jets for $\dot{m}$ = 0.000062 kg/s (water + 0.1 % $Al_2O_3$)

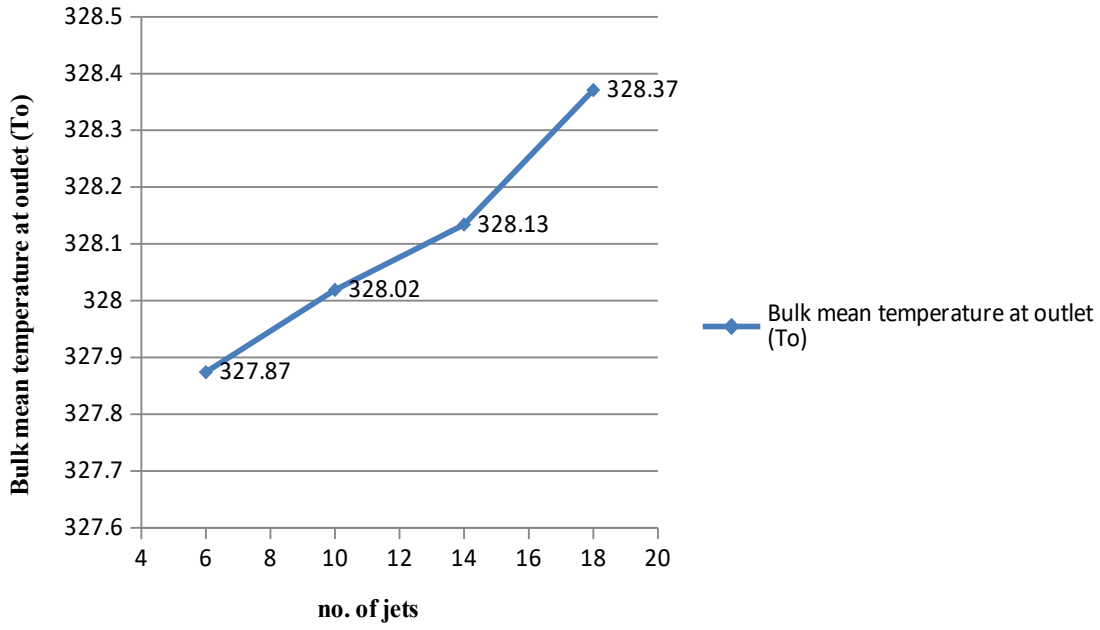


Figure 4.77: Variation of bulk mean temperature at outlet ($T_o$) with no. of jets for $\dot{m}$ = 0.000062 kg/s (water + 0.5 % $Al_2O_3$)

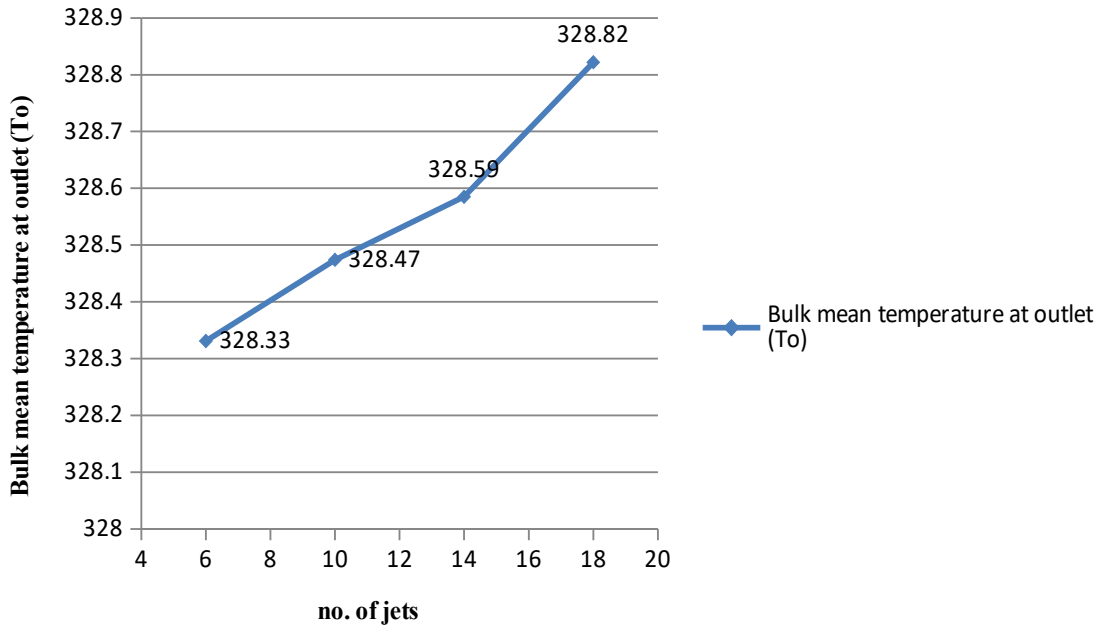


Figure 4.78: Variation of bulk mean temperature at outlet ($T_o$) with no. of jets for $\dot{m}$ = 0.000062 kg/s (water + 1 % $Al_2O_3$)

## 4.26 Variation of average interface temperature with % concentration

In figure 4.79 – 4.84, it was observed that average interface temperature increased with increase in concentration of the nanoparticles. Results also showed that as mass flow rate of nanofluid was increased, the average surface temperature decreased.

When mass flow rate was varied keeping number of jets constant than the average interface temperature and the maximum temperature of the plate decreased. It was seen in Figure 4.79 – 4.84 that both the average temperature of the plate and bulk mean temperature of nanofluid at the outlet increased with increase in concentration of the nanoparticles.

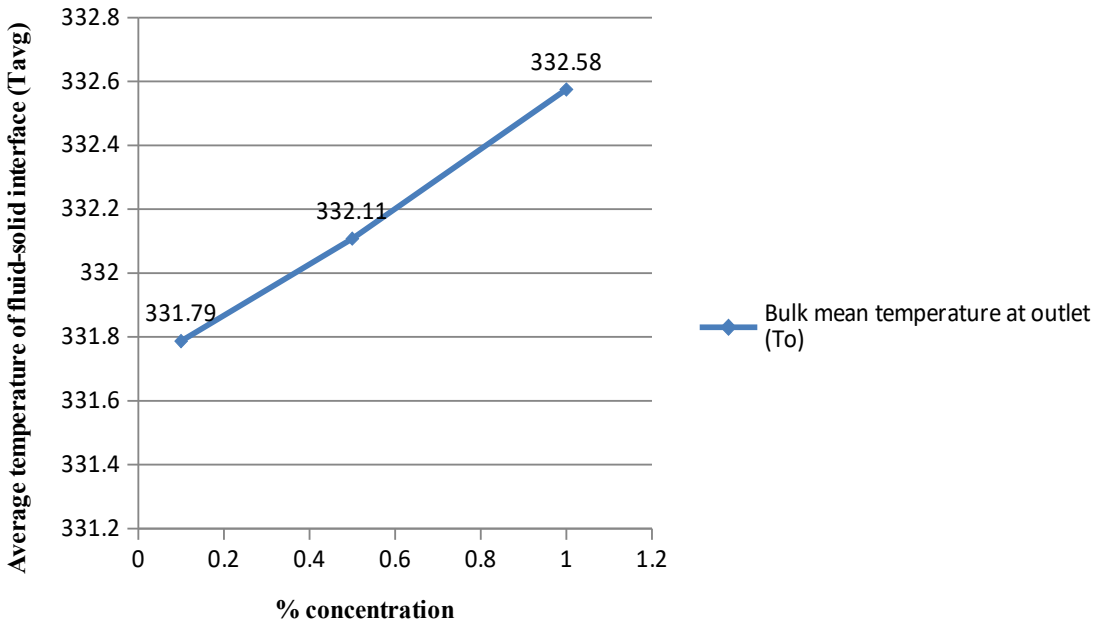


Figure 4.79: Variation of average temperature of fluid-solid interface ($T_{avg}$) with % concentration for $\dot{m}$ = 0.000062 kg/s for 6 jet (water + $TiO_2$)

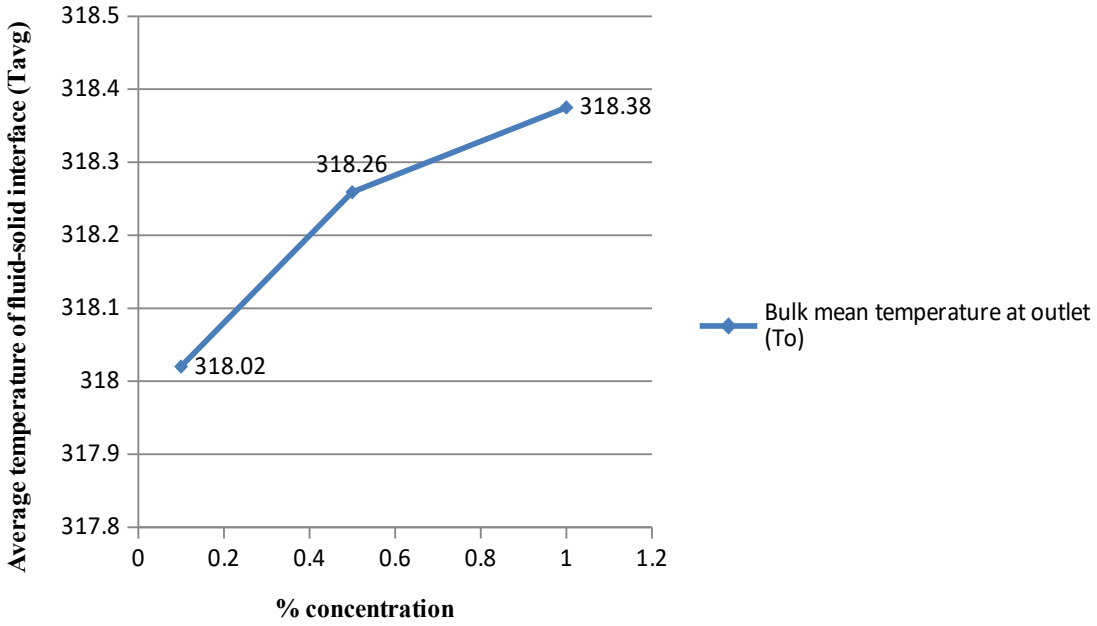


Figure 4.80: Variation of average temperature of fluid-solid interface ($T_{avg}$) with % concentration for $\dot{m}$ = 0.000122 kg/s for 6 jet (water + $TiO_2$)

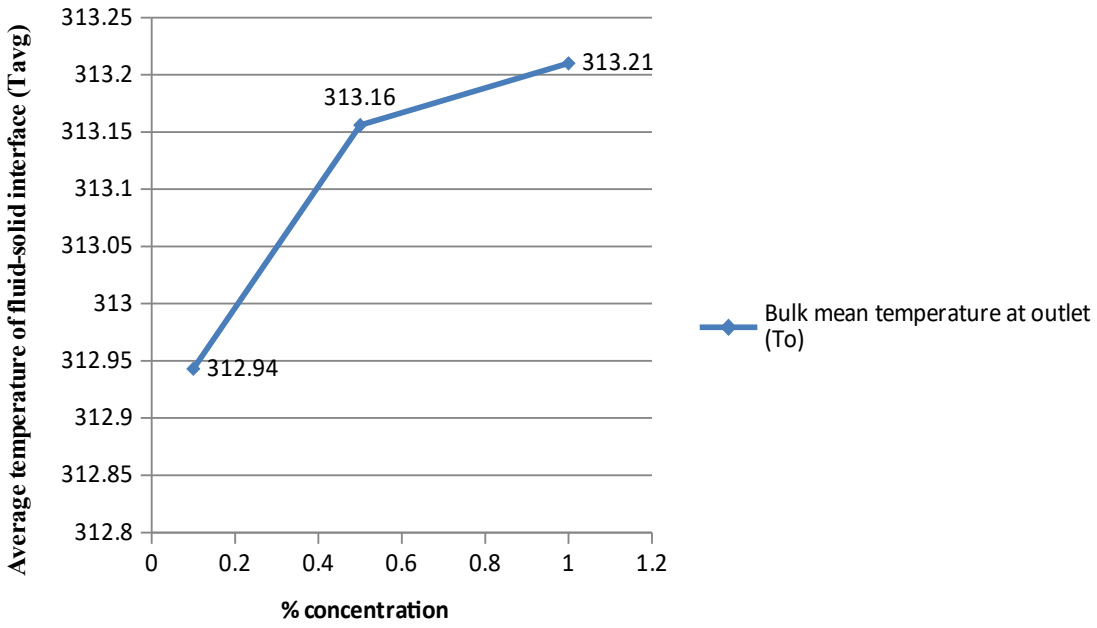


Figure 4.81: Variation of average temperature of fluid-solid interface ($T_{avg}$) with % concentration for $\acute{m}$ = 0.000182 kg/s for 6 jet (water + $TiO_2$)

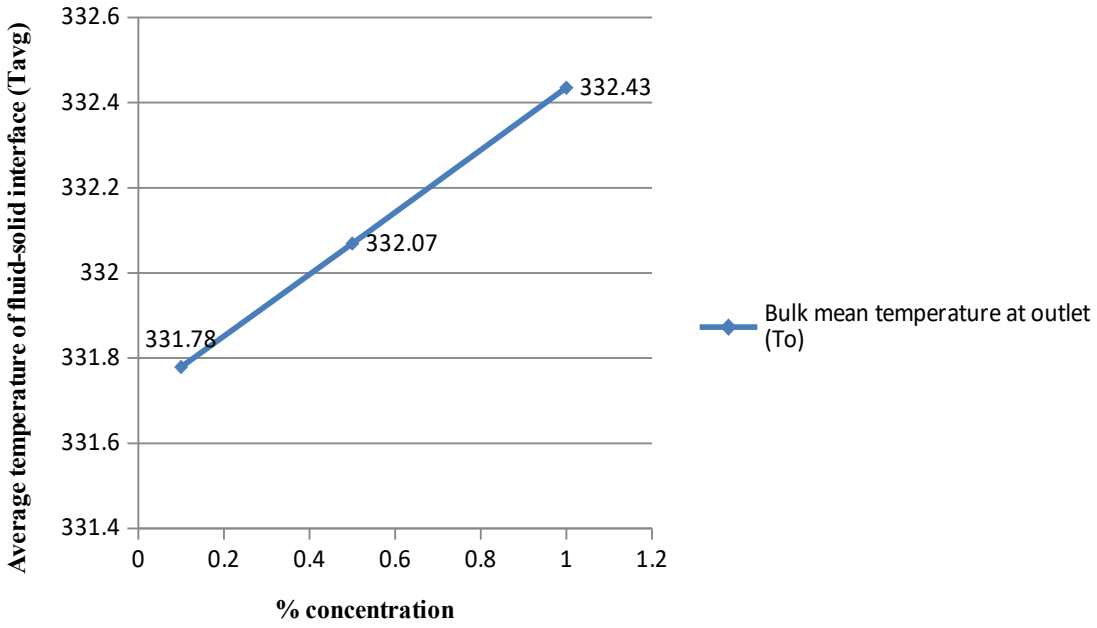


Figure 4.82: Variation of average temperature of fluid-solid interface ($T_{avg}$) with % concentration for $\acute{m}$ = 0.000062 kg/s for 6 jet (water + $Al_2O_3$)

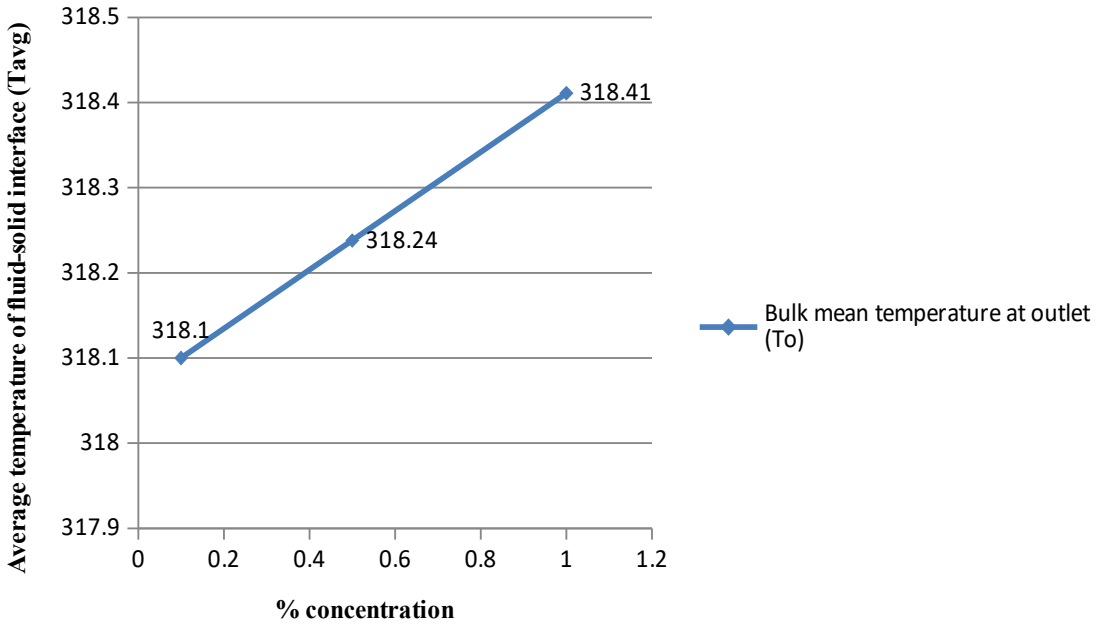


Figure 4.83: Variation of average temperature of fluid-solid interface ($T_{avg}$) with % concentration for $\acute{m}$ = 0.000122 kg/s for 6 jet (water + $Al_2O_3$)

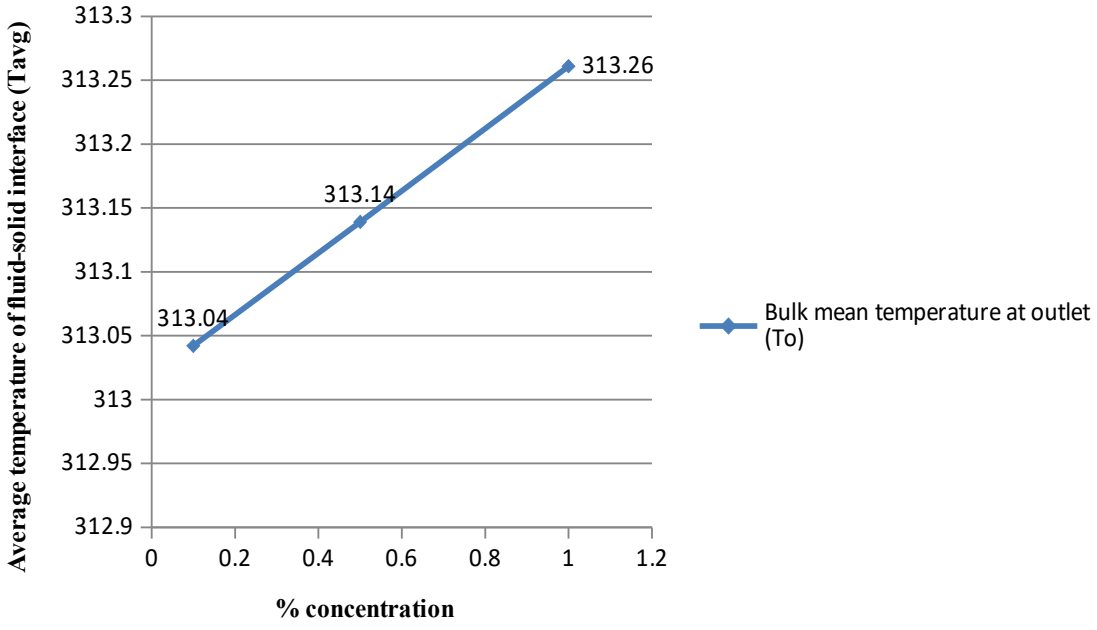

Figure 4.84: Variation of average temperature of fluid-solid interface ($T_{avg}$) with % concentration for $\dot{m}$ = 0.000182 kg/s for 6 jet (water + $Al_2O_3$)

Figure 4.85 shows variation of bulk mean temperature at outlet for 6 jet with concentration for $\dot{m}$ = 0.000062 kg/s. The bulk mean temperature of the nanofluid at the outlet for concentration of 0.1%, 0.5%, 1% $Al_2O_3$ was found to be 327.51 K, 327.874 K, 328.331 K and for concentration of 0.1%, 0.5%, 1% $TiO_2$ was found to be 327.515 K, 327.902 K, 328.423 K. It shows that bulk mean temperature of nanofluid containing $TiO_2$ is more than $Al_2O_3$ at every concentration taken into account. The values of bulk mean temperature at 0.1%, 0.5%, 1% concentration is given in the table 4.25. At 0.1% concentration, it shows little variation in bulk mean temperature between $TiO_2$ and $Al_2O_3$. This difference increases with increase in concentration and can be seen in figure 4.85.

**Table 4.25: Simulation result for 6 jet ($\dot{m}$ = 0.000062 kg/s)**

| **% Concentration** | **0.1** | **0.5** | **1** |
|---|---|---|---|
| **Bulk mean temperature at outlet for (water + $TiO_2$ )** | 327.515 | 327.902 | 328.423 |
| **Bulk mean temperature at outlet for (water + $Al_2O_3$ )** | 327.51 | 327.874 | 328.331 |

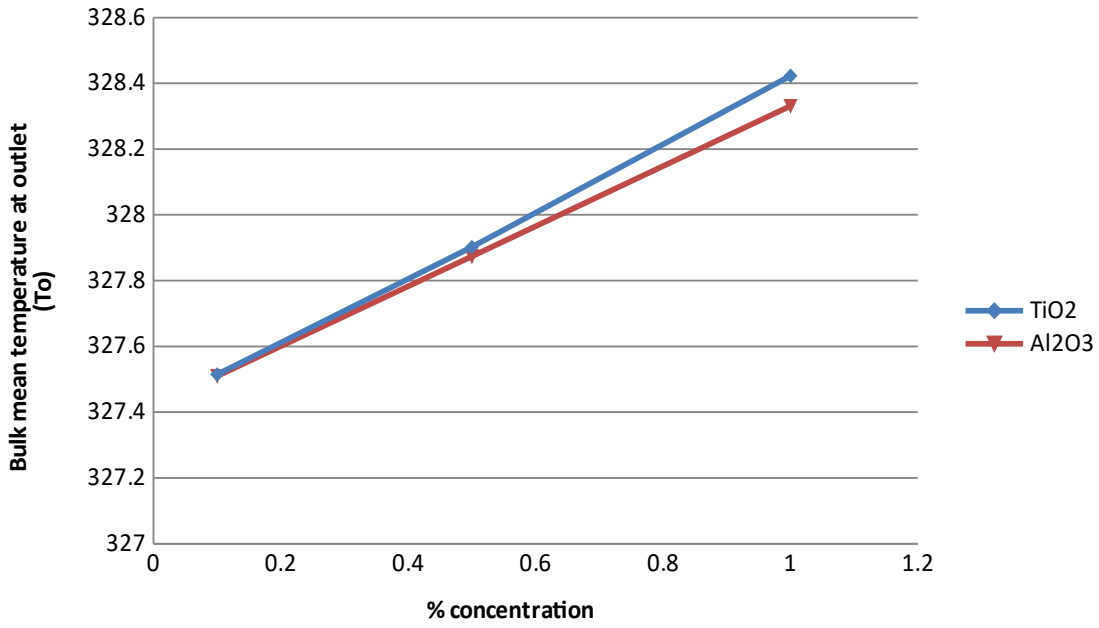


Figure 4.85: Variation of bulk mean temperature at outlet ($T_o$) with concentration for $\dot{m}$ = 0.000062 kg/s (6 jet)

Figure 4.86 shows variation of bulk mean temperature at outlet for 6 jet with concentration for $\dot{m}$ = 0.000122 kg/s. The bulk mean temperature of the nanofluid at the outlet for concentration of 0.1%, 0.5%, 1% $Al_2O_3$ was found to be 313.911 K, 314.095 K, 314.325 K and for concentration of 0.1%, 0.5%, 1% $TiO_2$ was found to be 313.914 K, 314.11 K, 314.376 K. It shows that bulk mean temperature of nanofluid containing $TiO_2$ is more than $Al_2O_3$ at every concentration taken into account. The values of bulk mean temperature at 0.1%, 0.5%, 1% concentration is given in the table 4.26. At 0.1% concentration, the difference in bulk mean temperature of $TiO_2$ and $Al_2O_3$ is less, the difference increases with increase in concentration and can be seen in figure 4.86.

**Table 4.26: Simulation result for 6 jet ($\dot{m}$ = 0.000122 kg/s)**

| **% Concentration** | **0.1** | **0.5** | **1** |
|---|---|---|---|
| **Bulk mean temperature at outlet for (water + $TiO_2$ )** | 313.914 | 314.11 | 314.376 |
| **Bulk mean temperature at outlet for (water + $Al_2O_3$ )** | 313.911 | 314.095 | 314.325 |

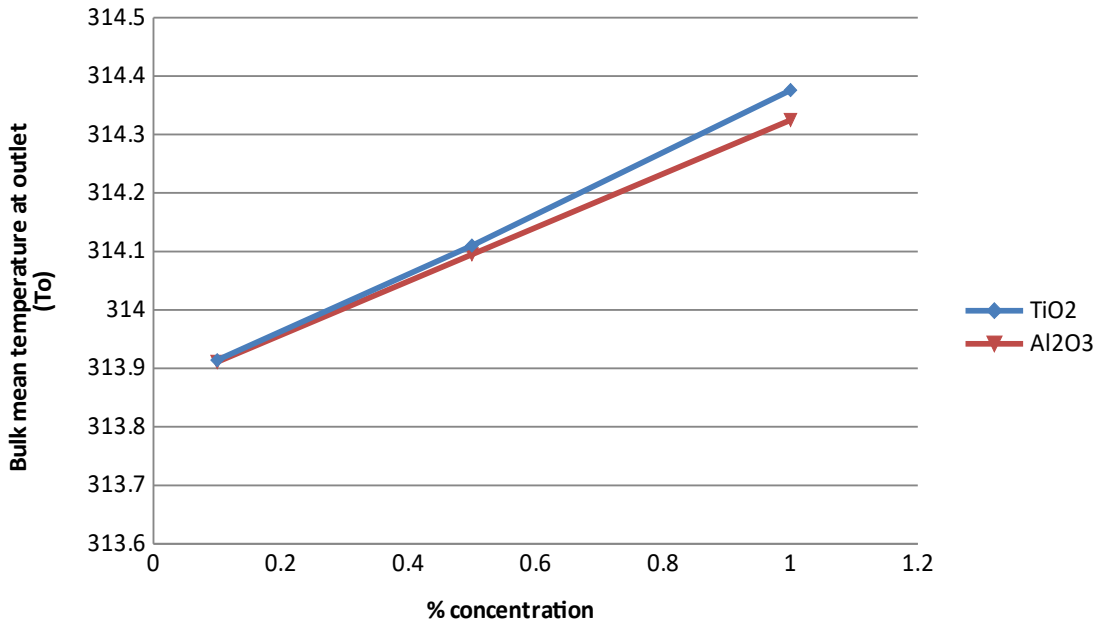


Figure 4.86: Variation of bulk mean temperature at outlet ($T_o$) with concentration for $\dot{m}$ = 0.000122 kg/s (6 jet)

Figure 4.87 shows variation of bulk mean temperature at outlet for 6 jet with concentration for $\dot{m}$ = 0.000182 kg/s. The bulk mean temperature of the nanofluid at the outlet for concentration of 0.1%, 0.5%, 1% $Al_2O_3$ was found to be 309.326 K, 309.447 K, 309.6 K and for concentration of 0.1%, 0.5%, 1% $TiO_2$ was found to be 309.342 K, 309.457 K, 309.633 K. It shows that bulk mean temperature of nanofluid containing $TiO_2$ is more than $Al_2O_3$ at every concentration taken into account. The values of bulk mean temperature at 0.1%, 0.5%, 1% concentration is given in the table 4.27. At 0.1% concentration, it shows little variation in bulk mean temperature between $TiO_2$ and $Al_2O_3$. This difference increases with increase in concentration and can be seen in figure 4.87.

**Table 4.27: Simulation result for 6 jet ($\dot{m}$ = 0.000182 kg/s)**

| **% Concentration** | **0.1** | **0.5** | **1** |
|---|---|---|---|
| **Bulk mean temperature at outlet for (water + $TiO_2$ )** | 309.342 | 309.457 | 309.633 |
| **Bulk mean temperature at outlet for (water + $Al_2O_3$ )** | 309.326 | 309.447 | 309.6 |

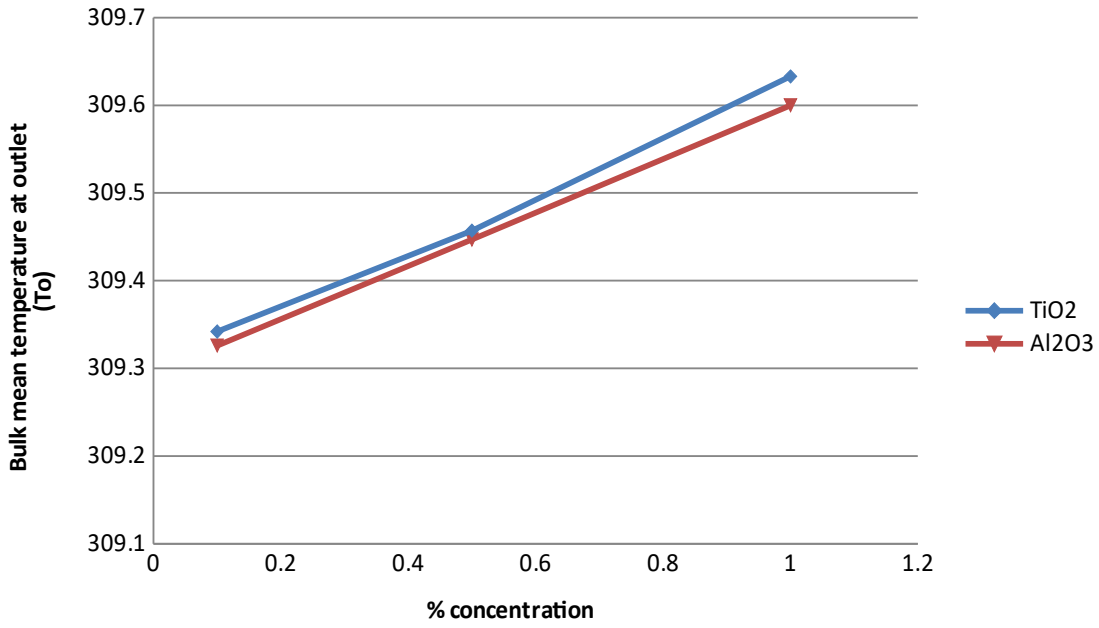


Figure 4.87: Variation of bulk mean temperature at outlet ($T_o$) with concentration for $\acute{m}$ = 0.000182 kg/s (6 jet)

Figure 4.88 shows variation of bulk mean temperature at outlet for 10 jet with concentration for $\acute{m}$ = 0.000062 kg/s. The bulk mean temperature of the nanofluid at the outlet for concentration of 0.1%, 0.5%, 1% $Al_2O_3$ was found to be 327.656 K, 328.019 K, 328.474 K and for concentration of 0.1%, 0.5%, 1% $TiO_2$ was found to be 327.662 K, 328.048 K, 328.531 K. It shows that bulk mean temperature of nanofluid containing $TiO_2$ is more than $Al_2O_3$ at every concentration taken into account. The values of bulk mean temperature at 0.1%, 0.5%, 1% concentration is given in the table 4.28. At 0.1% concentration, it shows little variation in bulk mean temperature between $TiO_2$ and $Al_2O_3$. This difference increases with increase in concentration and can be seen in figure 4.88.

**Table 4.28: Simulation result for 10 jet ($\acute{m}$ = 0.000062 kg/s)**

| **% Concentration** | **0.1** | **0.5** | **1** |
|---|---|---|---|
| **Bulk mean temperature at outlet for (water + $TiO_2$ )** | 327.662 | 328.048 | 328.531 |
| **Bulk mean temperature at outlet for (water + $Al_2O_3$ )** | 327.656 | 328.019 | 328.474 |

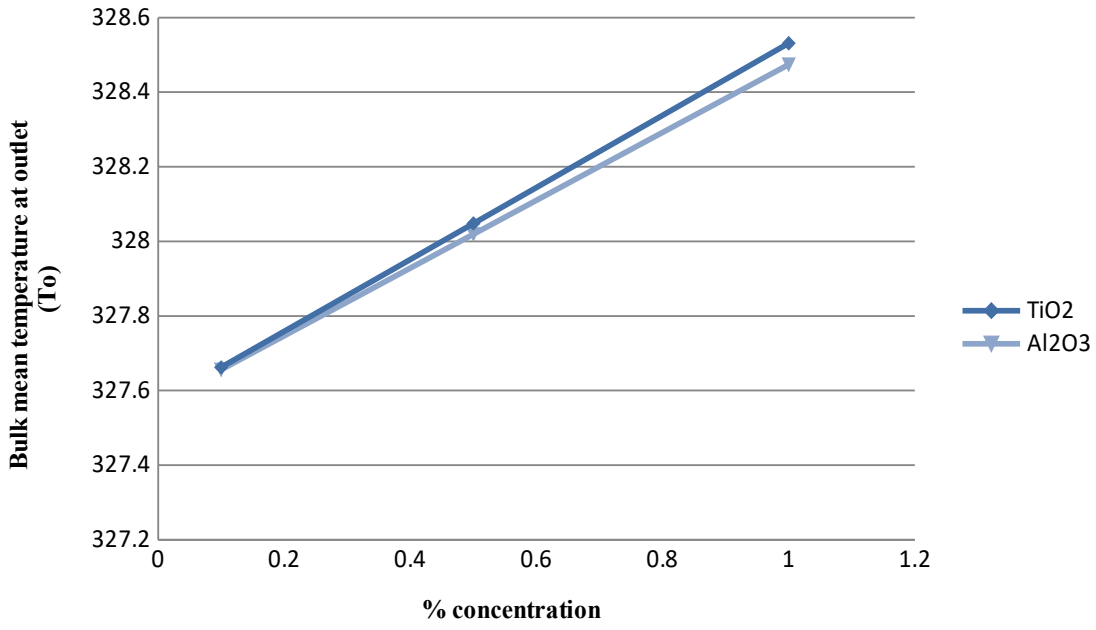


Figure 4.88: Variation of bulk mean temperature at outlet ($T_o$) with concentration for $\dot{m}$ = 0.000062 kg/s (10 jet)

Figure 4.89 shows variation of bulk mean temperature at outlet for 10 jet with concentration for $\dot{m}$ = 0.000122 kg/s. The bulk mean temperature of the nanofluid at the outlet for concentration of 0.1%, 0.5%, 1% $Al_2O_3$ was found to be 313.96 K, 314.145 K, 314.378 K and for concentration of 0.1%, 0.5%, 1% $TiO_2$ was found to be 313.963 K, 314.17 K, 314.407 K. It shows that bulk mean temperature of nanofluid containing $TiO_2$ is more than $Al_2O_3$ at every concentration taken into account. The values of bulk mean temperature at 0.1%, 0.5%, 1% concentration is given in the table 4.29. At 0.1% concentration, it shows little variation in bulk mean temperature between $TiO_2$ and $Al_2O_3$. This difference increases with increase in concentration and can be seen in figure 4.89.

**Table 4.29: Simulation result for 10 jet ($\dot{m}$ = 0.000122 kg/s)**

| % Concentration | 0.1 | 0.5 | 1 |
|---|---|---|---|
| **Bulk mean temperature at outlet for (water + $TiO_2$ )** | 313.963 | 314.17 | 314.407 |
| **Bulk mean temperature at outlet for (water + $Al_2O_3$ )** | 313.96 | 314.145 | 314.378 |

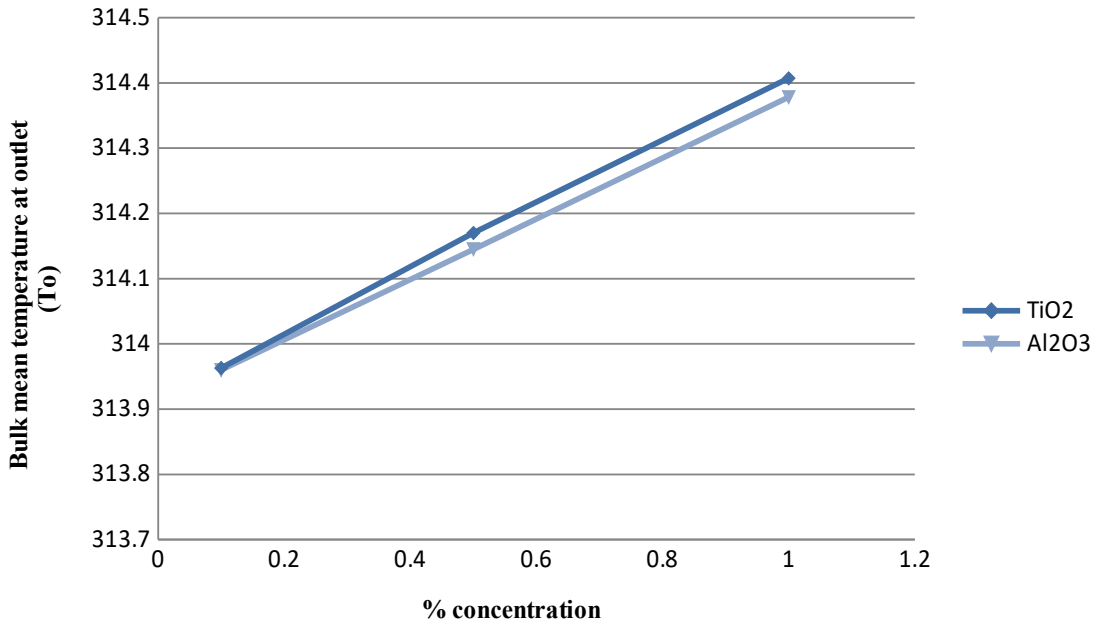


Figure 4.89: Variation of bulk mean temperature at outlet ($T_o$) with concentration for $\acute{m}$ = 0.000122 kg/s (10 jet)

Figure 4.90 shows variation of bulk mean temperature at outlet for 6 jet with concentration for $\acute{m}$ = 0.000182 kg/s. The bulk mean temperature of the nanofluid at the outlet for concentration of 0.1%, 0.5%, 1% $Al_2O_3$ was found to be 309.36 K, 309.471 K, 309.626 K and for concentration of 0.1%, 0.5%, 1% $TiO_2$ was found to be 309.375 K, 309.513 K, 309.678 K. It shows that bulk mean temperature of nanofluid containing $TiO_2$ is more than $Al_2O_3$ at every concentration taken into account. The values of bulk mean temperature at 0.1%, 0.5%, 1% concentration is given in the table 4.30. At 0.1% concentration, it shows little variation in bulk mean temperature between $TiO_2$ and $Al_2O_3$. This difference increases with increase in concentration and can be seen in figure 4.90.

**Table 4.30: Simulation result for 10 jet ($\acute{m}$ = 0.000182 kg/s)**

| % Concentration | 0.1 | 0.5 | 1 |
|---|---|---|---|
| **Bulk mean temperature at outlet for (water + $TiO_2$ )** | 309.375 | 309.513 | 309.678 |
| **Bulk mean temperature at outlet for (water + $Al_2O_3$ )** | 309.36 | 309.471 | 309.626 |

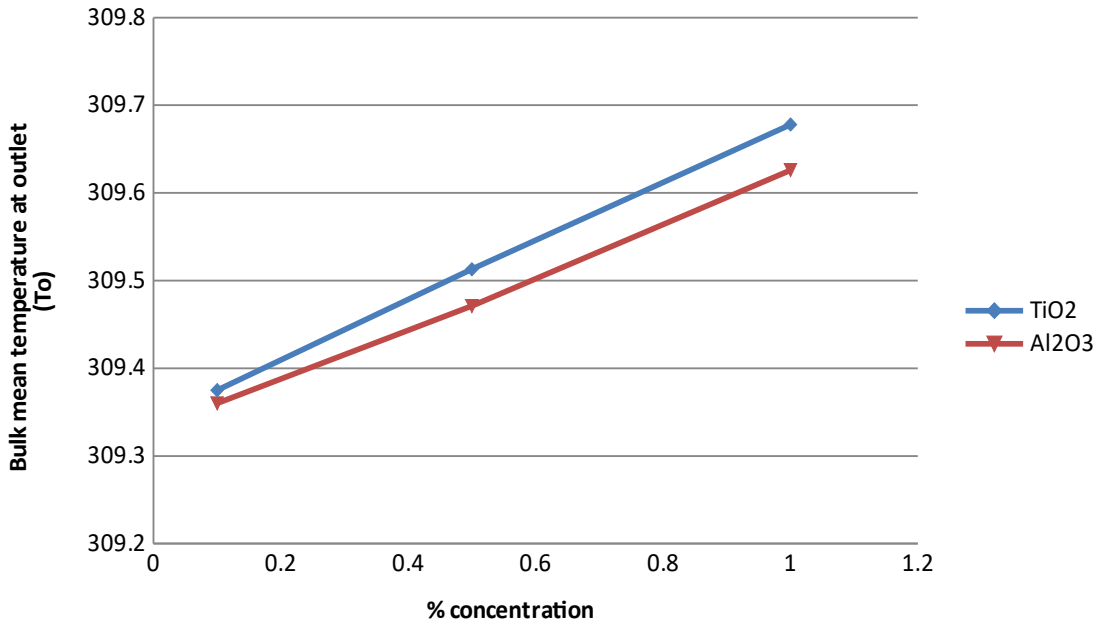


Figure 4.90: Variation of bulk mean temperature at outlet ($T_o$) with concentration for $\dot{m}$ = 0.000182 kg/s (10 jet)

Figure 4.91 shows variation of bulk mean temperature at outlet for 14 jet with concentration for $\dot{m}$ = 0.000062 kg/s. The bulk mean temperature of the nanofluid at the outlet for concentration of 0.1%, 0.5%, 1% $Al_2O_3$ was found to be 327.774 K, 328.134 K, 328.585 K and for concentration of 0.1%, 0.5%, 1% $TiO_2$ was found to be 327.779 K, 328.163 K, 328.643 K. It shows that bulk mean temperature of nanofluid containing $TiO_2$ is more than $Al_2O_3$ at every concentration taken into account. The values of bulk mean temperature at 0.1%, 0.5%, 1% concentration is given in the table 4.31. At 0.1% concentration, the difference in bulk mean temperature of $TiO_2$ and $Al_2O_3$ is less, the difference increases with increase in concentration and can be seen in figure 4.91.

**Table 4.31: Simulation result for 14 jet ($\dot{m}$ = 0.000062 kg/s)**

| **% Concentration** | **0.1** | **0.5** | **1** |
|---|---|---|---|
| **Bulk mean temperature at outlet for (water + $TiO_2$ )** | 327.779 | 328.163 | 328.643 |
| **Bulk mean temperature at outlet for (water + $Al_2O_3$ )** | 327.774 | 328.134 | 328.585 |

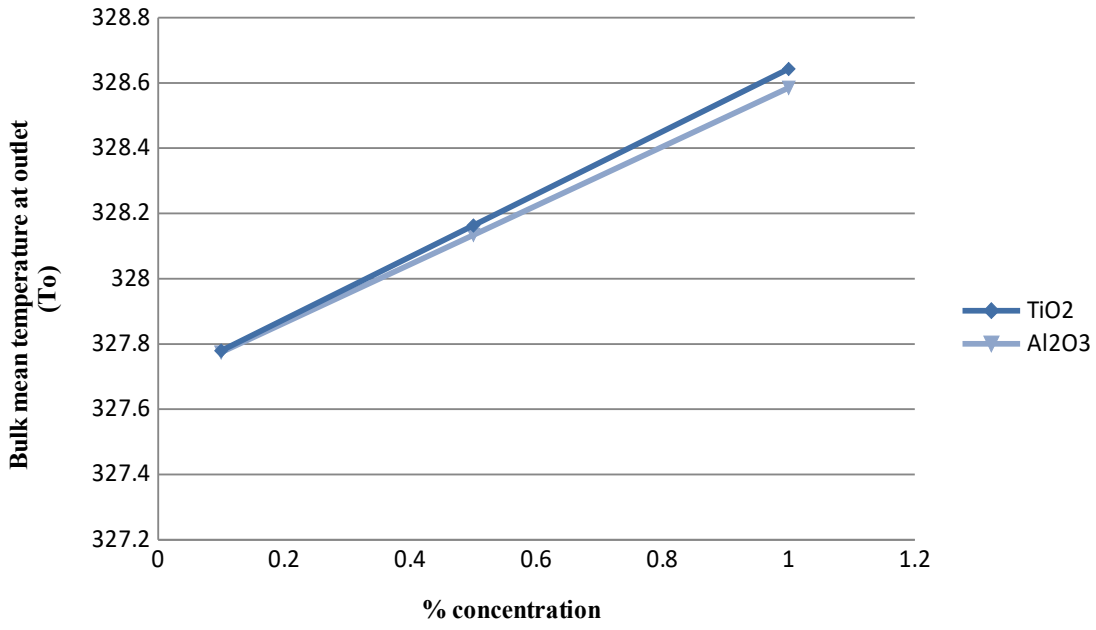


Figure 4.91: Variation of bulk mean temperature at outlet ($T_o$) with concentration for $\dot{m}$ = 0.000062 kg/s (14 jet)

Figure 4.92 shows variation of bulk mean temperature at outlet for 14 jet with concentration for $\dot{m}$ = 0.000122 kg/s. The bulk mean temperature of the nanofluid at the outlet for concentration of 0.1%, 0.5%, 1% $Al_2O_3$ was found to be 314.116 K, 314.3 K, 314.53 K and for concentration of 0.1%, 0.5%, 1% $TiO_2$ was found to be 314.119 K, 314.315K, 314.559 K. It shows that bulk mean temperature of nanofluid containing $TiO_2$ is more than $Al_2O_3$ at every concentration taken into account. The values of bulk mean temperature at 0.1%, 0.5%, 1% concentration is given in the table 4.32. At 0.1% concentration, the difference in bulk mean temperature of $TiO_2$ and $Al_2O_3$ is less, the difference increases with increase in concentration and can be seen in figure 4.92.

**Table 4.32: Simulation result for 14 jet ($\dot{m}$ = 0.000122 kg/s)**

| % Concentration | 0.1 | 0.5 | 1 |
|---|---|---|---|
| **Bulk mean temperature at outlet for (water + $TiO_2$ )** | 314.119 | 314.315 | 314.559 |
| **Bulk mean temperature at outlet for (water + $Al_2O_3$ )** | 314.116 | 314.3 | 314.53 |

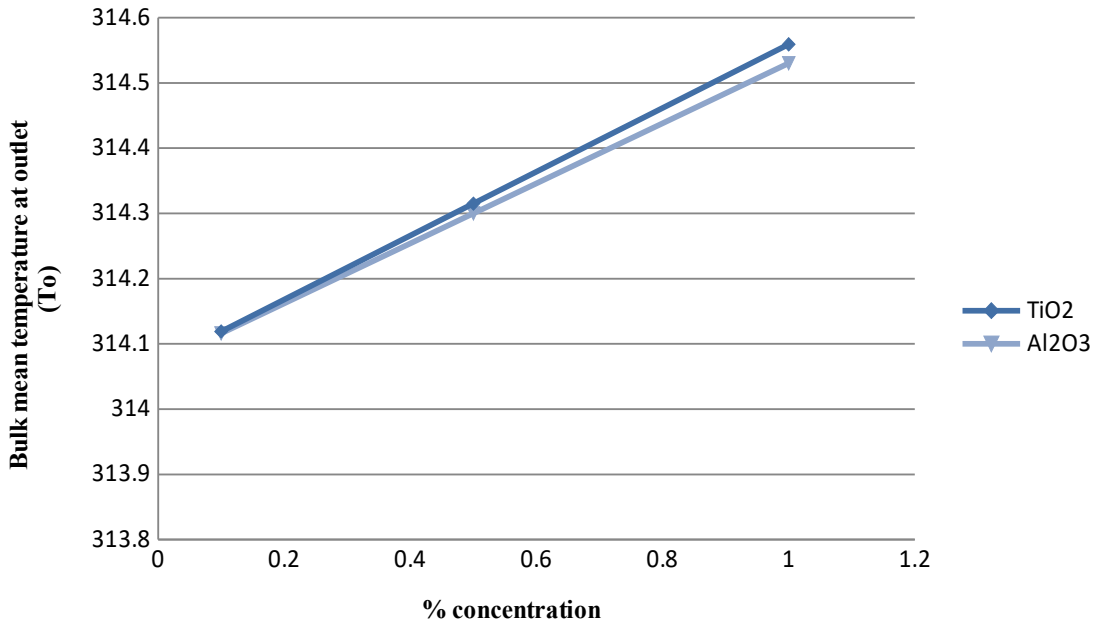


Figure 4.92: Variation of bulk mean temperature at outlet ($T_o$) with concentration for $\dot{m}$ = 0.000122 kg/s (14 jet)

Figure 4.93 shows variation of bulk mean temperature at outlet for 14 jet with concentration for $\dot{m}$ = 0.000182 kg/s. The bulk mean temperature of the nanofluid at the outlet for concentration of 0.1%, 0.5%, 1% $Al_2O_3$ was found to be 309.446 K, 309.57 K, 309.725 K and for concentration of 0.1%, 0.5%, 1% $TiO_2$ was found to be 309.448 K, 309.581 K, 309.744 K. It shows that bulk mean temperature of nanofluid containing $TiO_2$ is more than $Al_2O_3$ at every concentration taken into account. The values of bulk mean temperature at 0.1%, 0.5%, 1% concentration is given in the table 4.33. At 0.1% concentration, it shows little variation in bulk mean temperature between $TiO_2$ and $Al_2O_3$. This difference increases with increase in concentration and can be seen in figure 4.93.

**Table 4.33: Simulation result for 14 jet ($\dot{m}$ = 0.000182 kg/s)**

| % Concentration | 0.1 | 0.5 | 1 |
|---|---|---|---|
| **Bulk mean temperature at outlet for (water + $TiO_2$ )** | 309.448 | 309.581 | 309.744 |
| **Bulk mean temperature at outlet for (water + $Al_2O_3$ )** | 309.446 | 309.57 | 309.725 |

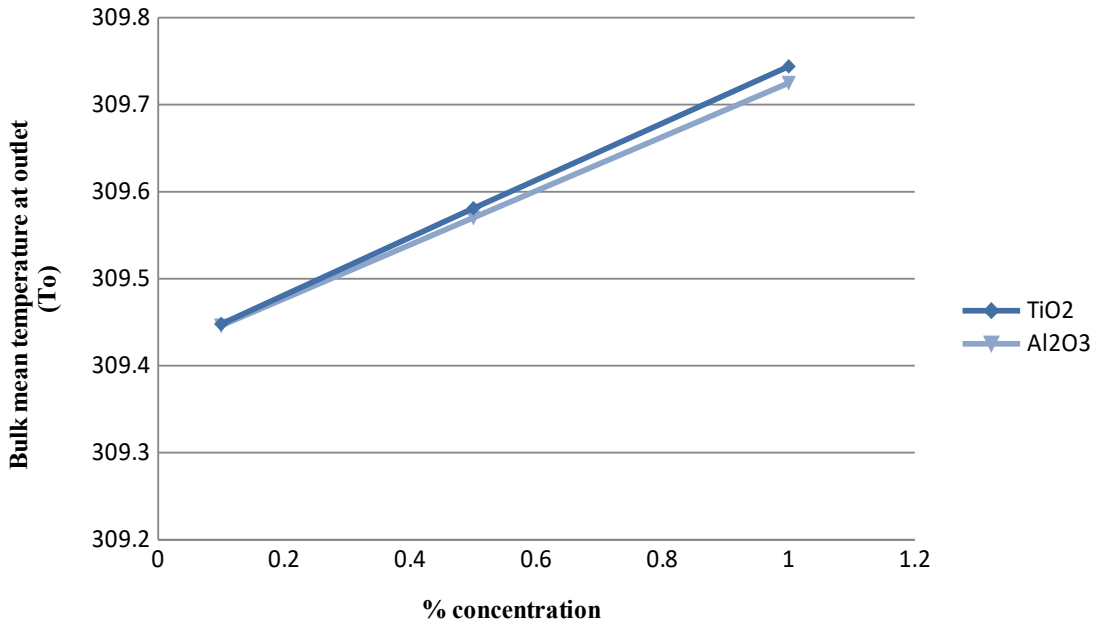


Figure 4.93: Variation of bulk mean temperature at outlet ($T_o$) with concentration for $\dot{m}$ = 0.000182 kg/s (14 jet)

Figure 4.94 shows variation of bulk mean temperature at outlet for 18 jet with concentration for $\dot{m}$ = 0.000062 kg/s. The bulk mean temperature of the nanofluid at the outlet for concentration of 0.1%, 0.5%, 1% $Al_2O_3$ was found to be 328.011 K, 328.371 K, 328.822 K and for concentration of 0.1%, 0.5%, 1% $TiO_2$ was found to be 328.017 K, 328.401 K, 328.881 K. It shows that bulk mean temperature of nanofluid containing $TiO_2$ is more than $Al_2O_3$ at every concentration taken into account. The values of bulk mean temperature at 0.1%, 0.5%, 1% concentration is given in the table 4.34. At 0.1% concentration, it shows little variation in bulk mean temperature between $TiO_2$ and $Al_2O_3$. This difference increases with increase in concentration and can be seen in figure 4.94.

**Table 4.34: Simulation result for 18 jet ($\dot{m}$ = 0.000062 kg/s)**

| % Concentration | 0.1 | 0.5 | 1 |
|---|---|---|---|
| **Bulk mean temperature at outlet for (water + $TiO_2$ )** | 328.017 | 328.401 | 328.881 |
| **Bulk mean temperature at outlet for (water + $Al_2O_3$ )** | 328.011 | 328.371 | 328.822 |

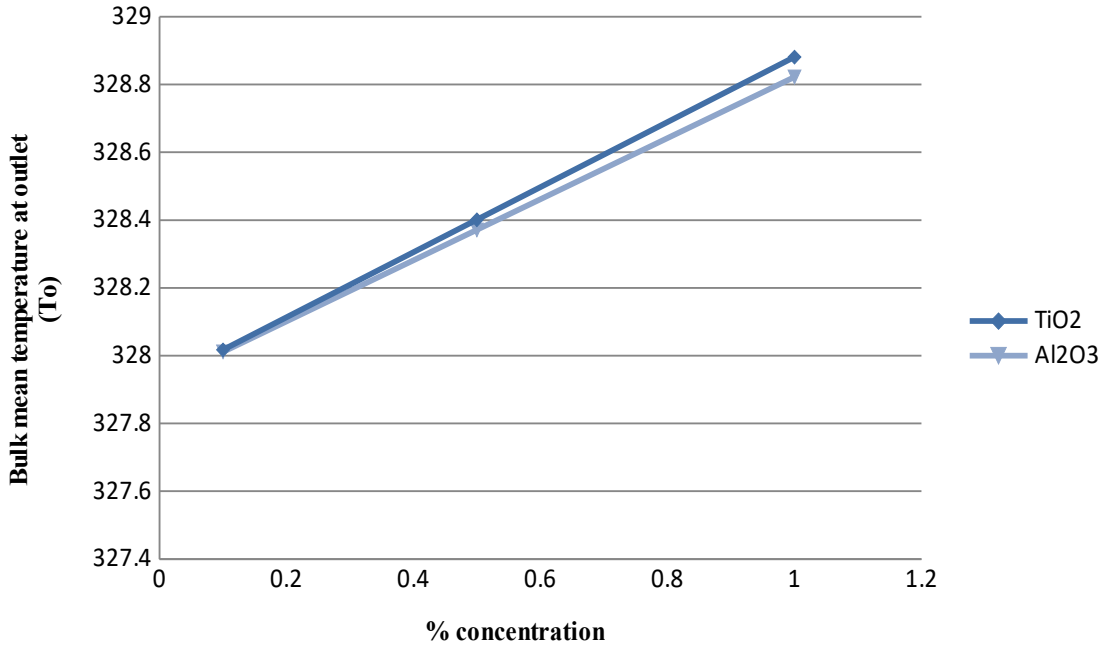


Figure 4.94: Variation of bulk mean temperature at outlet ($T_o$) with concentration for $\dot{m}$ = 0.000062 kg/s (18 jet)

Figure 4.95 shows variation of bulk mean temperature at outlet for 18 jet with concentration for $\dot{m}$ = 0.000122 kg/s. The bulk mean temperature of the nanofluid at the outlet for concentration of 0.1%, 0.5%, 1% $Al_2O_3$ was found to be 314.285 K, 314.468 K, 314.699 K and for concentration of 0.1%, 0.5%, 1% $TiO_2$ was found to be 314.288 K, 314.484 K, 314.73 K. It shows that bulk mean temperature of nanofluid containing $TiO_2$ is more than $Al_2O_3$ at every concentration taken into account. The values of bulk mean temperature at 0.1%, 0.5%, 1% concentration is given in the table 4.35. At 0.1% concentration, it shows little variation in bulk mean temperature between $TiO_2$ and $Al_2O_3$. This difference increases with increase in concentration and can be seen in figure 4.95.

**Table 4.35: Simulation result for 18 jet ($\dot{m}$ = 0.000122 kg/s)**

| % Concentration | 0.1 | 0.5 | 1 |
|---|---|---|---|
| **Bulk mean temperature at outlet for (water + $TiO_2$ )** | 314.288 | 314.484 | 314.73 |
| **Bulk mean temperature at outlet for (water + $Al_2O_3$ )** | 314.285 | 314.468 | 314.699 |

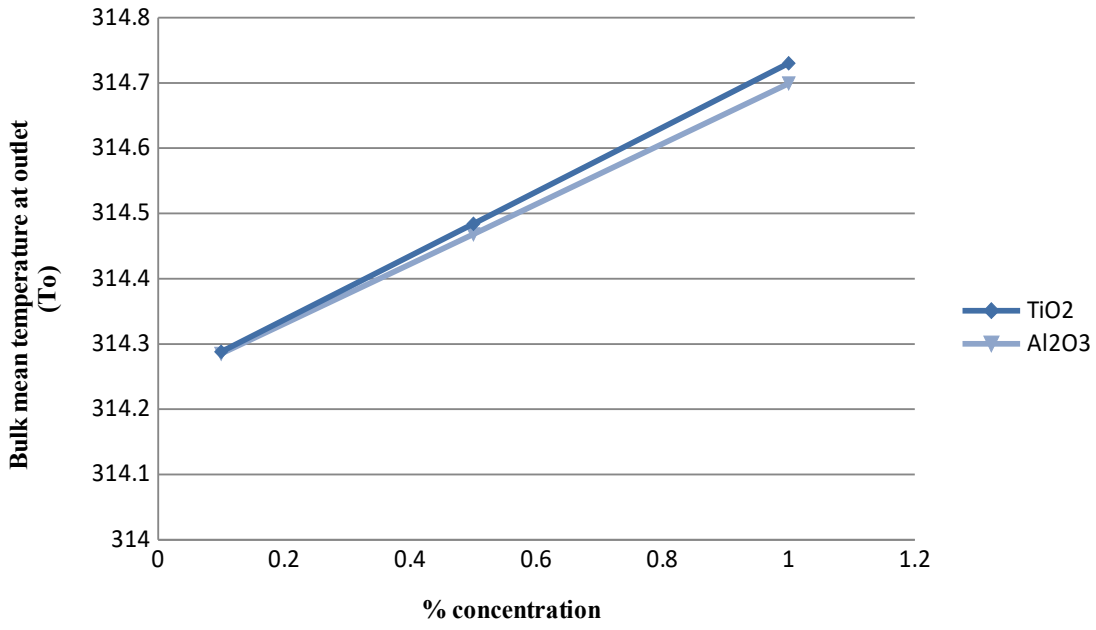


Figure 4.95: Variation of bulk mean temperature at outlet ($T_o$) with concentration for $\dot{m}$ = 0.000122 kg/s (18 jet)

Figure 4.96 shows variation of bulk mean temperature at outlet for 18 jet with concentration for $\dot{m}$ = 0.000182 kg/s. The bulk mean temperature of the nanofluid at the outlet for concentration of 0.1%, 0.5%, 1% $Al_2O_3$ was found to be 309.566 K, 309.691 K, 309.848 K and for concentration of 0.1%, 0.5%, 1% $TiO_2$ was found to be 309.568 K, 309.701 K, 309.867 K. It shows that bulk mean temperature of nanofluid containing $TiO_2$ is more than $Al_2O_3$ at every concentration taken into account. The values of bulk mean temperature at 0.1%, 0.5%, 1% concentration is given in the table 4.36. At 0.1% concentration, it shows little variation in bulk mean temperature between $TiO_2$ and $Al_2O_3$. This difference increases with increase in concentration and can be seen in figure 4.96.

**Table 4.36: Simulation result for 18 jet ($\dot{m}$ = 0.000182 kg/s)**

| % Concentration | 0.1 | 0.5 | 1 |
|---|---|---|---|
| **Bulk mean temperature at outlet for (water + $TiO_2$ )** | 309.568 | 309.701 | 309.867 |
| **Bulk mean temperature at outlet for (water + $Al_2O_3$ )** | 309.566 | 309.691 | 309.848 |

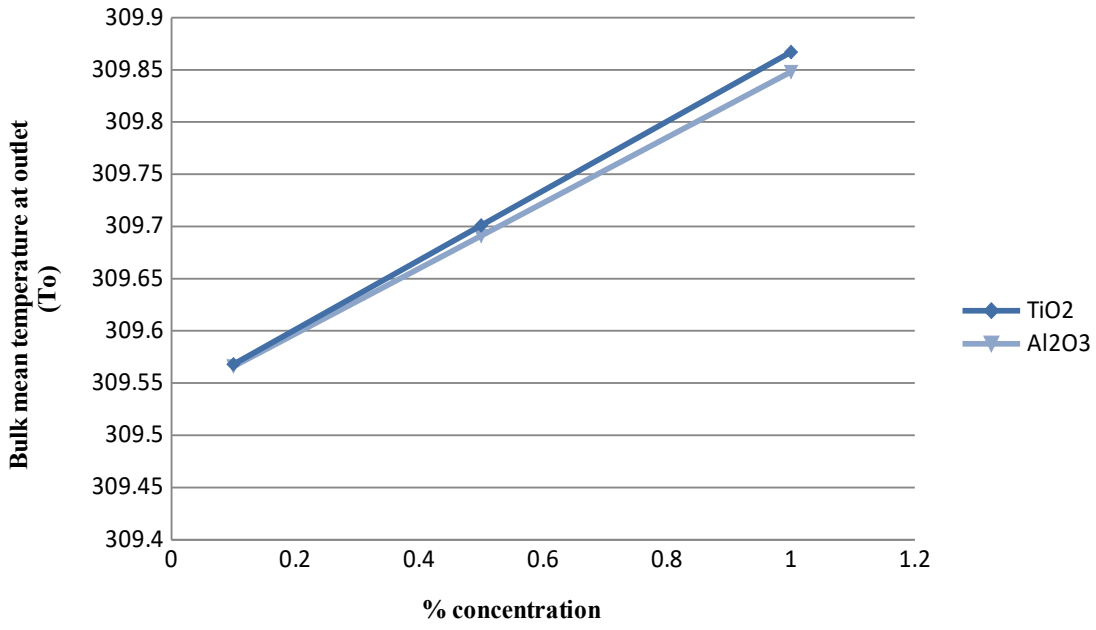


Figure 4.96: Variation of bulk mean temperature at outlet ($T_o$) with concentration for $\dot{m}$ = 0.000182 kg/s (18 jet)

Figure 4.97 shows variation of bulk mean temperature at outlet with 6, 10, 14, 18 jets for $\dot{m}$ = 0.000062 kg/s. As, the number of jets are increased, the bulk mean temperature (outlet) of the arrangement also increases. Table 4.37 and Figure 4.97 shows that bulk mean temperature of nanofluid containing $TiO_2$ is more than $Al_2O_3$ at every concentration taken into account.

The bulk mean temperature at outlet for nanofluid is more than that of water. Water shows the least temperature ($T_o$) for all the jet arrangement used in the simulation. The 18 jet arrangement used during simulation shows maximum bulk mean temperature at the outlet.

**Table 4.37: Simulation result of bulk mean temperature for different jets ($\dot{m}$ = 0.000062 kg/s)**

| Number of jets | 6 | 10 | 14 | 18 |
|---|---|---|---|---|
| **Bulk mean temperature at outlet for (water + 0.1% $TiO_2$ )** | 327.515 | 327.662 | 327.779 | 328.017 |
| **Bulk mean temperature at outlet for (water + 0.1% $Al_2O_3$ )** | 327.51 | 327.656 | 327.774 | 328.011 |
| **Bulk mean temperature at outlet for (water + 0.5% $TiO_2$ )** | 327.902 | 328.048 | 328.163 | 328.401 |

| | | | | |
|---|---|---|---|---|
| **Bulk mean temperature at outlet for (water + 0.5% $Al_2O_3$ )** | 327.874 | 328.019 | 328.134 | 328.371 |
| **Bulk mean temperature at outlet for (water + 1% $TiO_2$ )** | 328.423 | 328.531 | 328.643 | 328.881 |
| **Bulk mean temperature at outlet for (water + 1% $Al_2O_3$ )** | 328.331 | 328.474 | 328.585 | 328.822 |
| **Bulk mean temperature at outlet for water** | 327.423 | 327.58 | 327.693 | 327.935 |

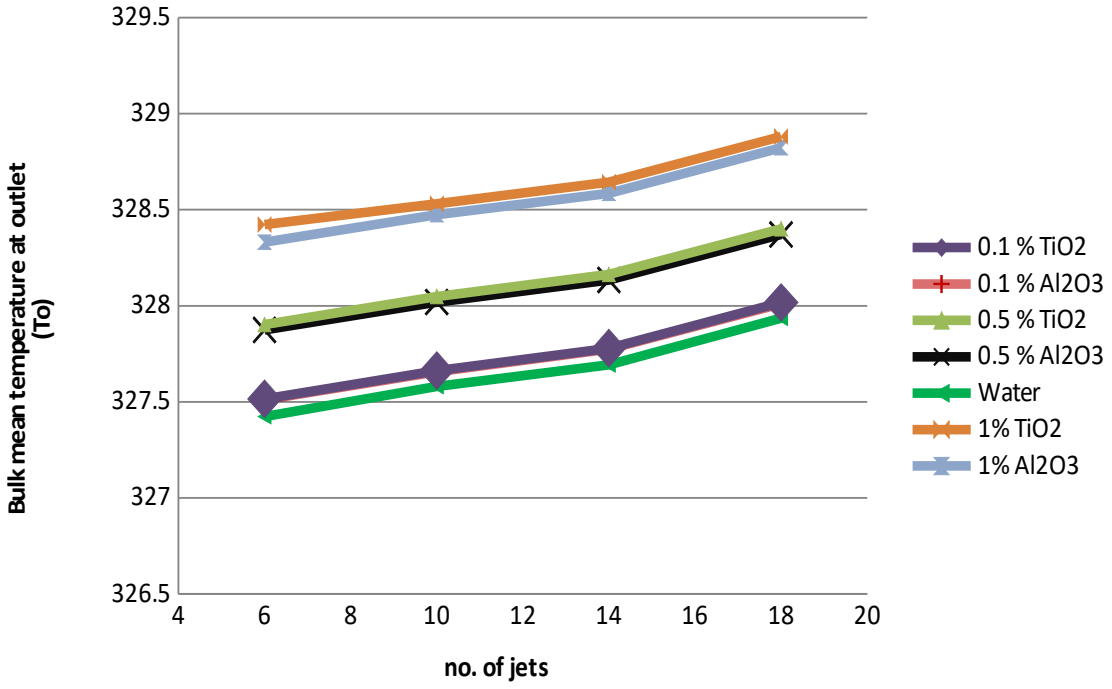


Figure 4.97: Variation of bulk mean temperature at outlet ($T_o$) with number of jets for $\dot{m}$ = 0.000062 kg/s

# CHAPTER 5

# CONCLUSION

Numerical simulation has been presented in this study on heat transfer characteristics, maximum temperature drop of nanofluid containing $Al_2O_3$ nanoparticles and water as base fluid, $TiO_2$ nanoparticles and water as base fluid. The study has been conducted under steady laminar flow for micro-channel geometry. The nanofluid has been considered homogenous with modified thermo physical properties. These modified properties are taken into account while simulating both the nanofluids.

The CFD results were compared against the available literature correlations. The following conclusions can be drawn from the present study.

- CFD predictions for nanofluid showed an increase in the heat transfer, with respect to the base fluid.
- Results showed that as mass flow rate of nanofluid was increased, the bulk mean temperature at outlet and average surface temperature decreased.
- It was observed that bulk mean temperature of nanofluid at the outlet increased with increase in % concentration of the nanoparticles and the number of jets.

- It was observed that the bulk mean temperature of nanofluid containing $TiO_2$ is more than $Al_2O_3$ at all the concentration taken into account.
- When mass flow rate was increased keeping number of jets constant than bulk mean temperature at outlet decreased thus decreasing the heat transfer rate.
- The 18 jet arrangement used during the simulation showed maximum bulk mean temperature at the outlet for all the arrangements keeping mass flow rate constant.

# REFERENCES


[1] Tuckerman, D.B. and Pease, R.F.W., 1981. High-performance heat sinking for VLSI.
IEEE Electron device letters, 2(5), pp.126-129.

[2] Knight, R.W., Hall, D.J., Goodling, J.S. and Jaeger, R.C., 1992. Heat sink optimization with application to micro-channels. IEEE Transactions on Components, Hybrids, and Manufacturing Technology, 15(5), pp.832-842.

[3] Yeh, L.T., 1995. Review of heat transfer technologies in electronic equipment. Transactions of the ASME-P-Journal of Electronic Packaging, 117(4), pp.333-339.

[4] B.W. and Ma, C.F., 1995. Single-phase liquid jet impingement heat transfer. Advances in heat transfer, 26, pp.105-217.

[5] Garimella, S.V. and Rice, R.A., 1995. Confined and submerged liquid jet impingement heat transfer. Transactions-ASME-P-Journal of Heat Transfer, 117, pp.871-877.

[6] Peng, X. F., and G. P. Peterson. "Convective heat transfer and flow friction for water flow in microchannel structures." International Journal of Heat and Mass Transfer 39, no. 12 (1996): 2599-2608.

[7] Mala, G.M., Li, D. and Dale, J.D., 1997. Heat transfer and fluid flow in microchannels. International Journal of Heat and Mass Transfer, 40(13), pp.3079-3088.

[8] Wu, S., Mai, J., Tai, Y.C. and Ho, C.M., 1999, January. Micro heat exchanger by using MEMS impinging jets. In Micro Electro Mechanical Systems, 1999. MEMS'99. Twelfth IEEE International Conference on (pp. 171-176). IEEE.

[9] Lee, D.Y. and Vafai, K., 1999. Comparative analysis of jet impingement and microchannel cooling for high heat flux applications. International Journal of Heat and Mass Transfer, 42(9), pp.1555-1568.

[10] Fedorov, A.G. and Viskanta, R., 2000. Three-dimensional conjugate heat transfer in the microchannel heat sink for electronic packaging. International Journal of Heat and Mass Transfer, 43(3), pp.399-415.

[11] Ambatipudi, K.K. and Rahman, M.M., 2000. Analysis of conjugate heat transfer in micro channel heat sinks. Numerical Heat Transfer: Part A: Applications, 37(7), pp.711-731.

[12] Qu, W. and Mudawar, I., 2002. Analysis of three-dimensional heat transfer in micro-channel heat sinks. International Journal of heat and mass transfer, 45(19), pp.3973-3985.

[13] Qu, W. and Mudawar, I., 2002. Experimental and numerical study of pressure drop and heat transfer in a single-phase micro-channel heat sink. International Journal of Heat and Mass Transfer, 45(12), pp.2549-2565.

[14] Toh, K.C., Chen, X.Y. and Chai, J.C., 2002. Numerical computation of fluid flow and heat transfer in microchannels. International Journal of Heat and Mass Transfer, 45(26), pp.51335141.

[15] Garimella, S.V. and Sobhan, C.B., 2003. Transport in microchannels-a critical review. Annual review of heat transfer, 13(13) pp. 460-478

[16] Liu, D. and Garimella, S.V., 2005. Analysis and optimization of the thermal performance of microchannel heat sinks. International Journal of Numerical Methods for Heat & Fluid Flow, 15(1), pp.7-26.

[17] Liu, D. and Garimella, S.V., 2005. Analysis and optimization of the thermal performance of microchannel heat sinks. International Journal of Numerical Methods for Heat & Fluid Flow, 15(1), pp.7-26.

[18] Fabbri, M. and Dhir, V.K., 2005. Optimized heat transfer for high power electronic cooling using arrays of microjets. Journal of heat transfer, 127(7), pp.760-769.

[19] Foli, K., Okabe, T., Olhofer, M., Jin, Y. and Sendhoff, B., 2006. Optimization of micro heat exchanger: CFD, analytical approach and multi -objective evolutionary algorithms. International Journal of Heat and Mass Transfer, 49(5), pp.1090-1099.

[20] Sung, M.K. and Mudawar, I., 2006. Experimental and numerical investigation of single -phase heat transfer using a hybrid jet-impingement/micro-channel cooling scheme. International journal of heat and mass transfer, 49(3), pp.682-694.

[21] Luo, X., Chen, W., Sun, R. and Liu, S., 2008. Experimental and numerical investigation of a microjet-based cooling system for high power LEDs. Heat Transfer Engineering, 29(9), pp.774-781.

[22] Husain, A. and Kim, K.Y., 2008. Shape optimization of micro-channel heat sink for micro-electronic cooling. IEEE Transactions on Components and PackagingTechnologies, 31(2), pp.322-330.

[23] Samad, A., Lee, K.D. and Kim, K.Y., 2008. Multi-objective optimization of a dimpled channel for heat transfer augmentation. Heat and Mass Transfer, 45(2), pp.207.

[24] Michna, G.J., Browne, E.A., Peles, Y. and Jensen, M.K., 2009. Single-phase micro scale jet stagnation point heat transfer. Journal of Heat Transfer, 131(11), pp.111-402.

[25] Husain, A. and Kim, K.Y., 2010. Enhanced multi-objective optimization of a micro channel heat sink through evolutionary algorithm coupled with multiple surrogate models. Applied Thermal Engineering, 30(13), pp.1683-1691.

[26] De Paz, M.L. and Jubran, B.A., 2011. Numerical modelling of multi micro jet impingement cooling of a three dimensional turbine vane. Heat and mass transfer, 47(12), pp.1561-1579.

[27] Heo, M.W., Lee, K.D. and Kim, K.Y., 2011. Optimization of an inclined elliptic impinging jet with cross flow for enhancing heat transfer. Heat and Mass Transfer, 47(6), pp.731-742.

[28] Husain, A. and Kim, K.Y., 2011. Thermal transport and performance analysis of pressure -and electrosmotically-driven liquid flow micro channel heat sink with wavy wall. Heat and Mass Transfer, 47(1), pp.93-105.

[29] Husain, A., Kim, S.M. and Kim, K.Y., 2013. Performance analysis and design optimization of micro-jet impingement heat sink. Heat and Mass Transfer, 49(11), pp.1613-1624.

[30] Peterson G.P and Li C.H.., 2006, Experimental Investigation of Temperature and Volume Fraction Variations on The Effective Thermal Conductivity of Nanoparticle Suspensions Nanofluids), Applied Physics, Vol. 99, Issue. 08314, PP. 1-8.

[31] Kondaraju Sasidhar, Jin E.K. and Lee Joon Sang, 2010, Direct numerical simulation of thermal conductivity of nanofluids: The effect of temperature two-way coupling and coagulation of particles, International Journal of Heat and Mass Transfer 53, 862–869.

[32] Wang Wei, Lin Lin, XiaoFeng Zhou and Wang Shengyue, 2012, A Comprehensive Model for the Enhanced Thermal Conductivity of Nanofluids, Journal of Advanced Research in Physics 3(2), 021209.

[33] R.L. Hamilton, O.K. Crosser, Thermal conductivity of heterogeneous two-component system, I EC Fundam. (1962) 182–191.

[34] H.C. Brinkman, The viscosity of concentrated suspensions and solutions, J. Chem. Phys. 20 (1952) 571–581.

[35] Y. Xuan, W. Roetzel, Conceptions for heat transfer correlation of nanofluids, Int. J. Heat Mass Transfer 43 (2000) 3701–3707.

[36] S.E.B. Maliga, S.M. Palm, C.T. Nguyen, G. Roy, N. Galanis, Heat transfer enhancement using nanofluid in forced convection flow, Int. J. Heat Fluid Flow 26 (2005) 530–546.

[37] K. Khanafer, K. Vafai, M. Lightstone, Buoyancy-driven heat transfer enhancement in a two-dimensional enclosure utilizing nanofluids, Int. J. Heat Mass Transfer 46 (2003) 3639–3663.

[38] J.C. Maxwell, A Treatise on Electricity and Magnetism, second ed., Oxford University Press, Cambridge, 1904.

[39] D. Wen, Y. Ding, Experimental investigation on convective heat transfer of nanofluids at the entrance region under laminar flow conditions, Int. J. Heat Mass Transfer 47 (2004) 5181-5188.

[40] Yang, Y., Zhang, Z. G., Grulke, E. A., Anderson, W. B., & Wu, G. (2005). Heat transfer properties of nanoparticle-in-fluid dispersions (nanofluids) in laminar flow. International Journal of Heat and Mass Transfer, 48(6), 1107–1116.

[41] Chein, R., & Chen, J. (2009). Numerical study of the inlet/outlet arrangement effect on microchannel heat sink performance. International Journal of Thermal Sciences, 48(8), 1627–1638.